Supporting information for

$Pd_{12}M_nL_{24}$ (for n= 6, 8, 12) nanospheres by post-modification of $Pd_{12}L_{24}$ spheres

Eduard. O. Bobylev,[a] Leonardo Passerini,[b] Felix J. de Zwart,[a] David A. Poole III,[a] Simon Mathew,[a] Martina Huber,[b] Bas de Bruin[a] and Joost N. H. Reek*[a]

[a] van 't Hoff Institute for Molecular Sciences, University of Amsterdam, Science Park 904, 1098 XH Amsterdam, the Netherlands.

[b]Department of Physics, Huygens-Kamerlingh Onnes Laboratory, Leiden University, Niels Bohrweg 2, 2333 CA Leiden, The Netherlands

Materials and methods

General procedures: All synthetic procedures were carried out under a nitrogen atmosphere using standard Schlenk techniques. All commercially available chemicals were used as received without further purification. Solvents used for synthesis were dried, distilled and degassed with the most suitable method. Column chromatography was performed open to air using solvents as received.

Eletronspray-ionization MS (ESI-MS): Mass spectra were collected on a HR-ToF Bruker Daltonik GmbH (Bremen, Germany) Impact II, an ESI-ToF MS capable of resolution of at least 40000 FWHM. Detection was in positive-ion mode and the source voltage was between 4 and 6 kV. The sample was introduced with a syringe pump at a flow rate of 18 ul/hr. The drying gas (N_2) was held at 40°C and the spray gas was held at 60°C. The machine was calibrated prior to every experiment via direct infusion of a TFA-Na solution, which provided a m/z range of singly charged peaks up to 3500 Da in both ion modes. Software acquisition Compass 2.0 for Otof series. Software processing m- mass.

EPR measurements: EPR measurements were performed in air-tight J-Young quartz tubes in an atmosphere of purified argon. Frozen solution EPR spectra were recorded on a Bruker EMX-plus CW X-band spectrometer equipped with a Bruker ER 4112HV-CF100 helium cryostat. The spectra were obtained on freshly prepared solutions of 1–10 mM compound and simulated using EasySpin[1]via the cwEPR GUI.[2]

Synthesis of building blocks (SI1)

Synthesis of **L^{DMAP}**

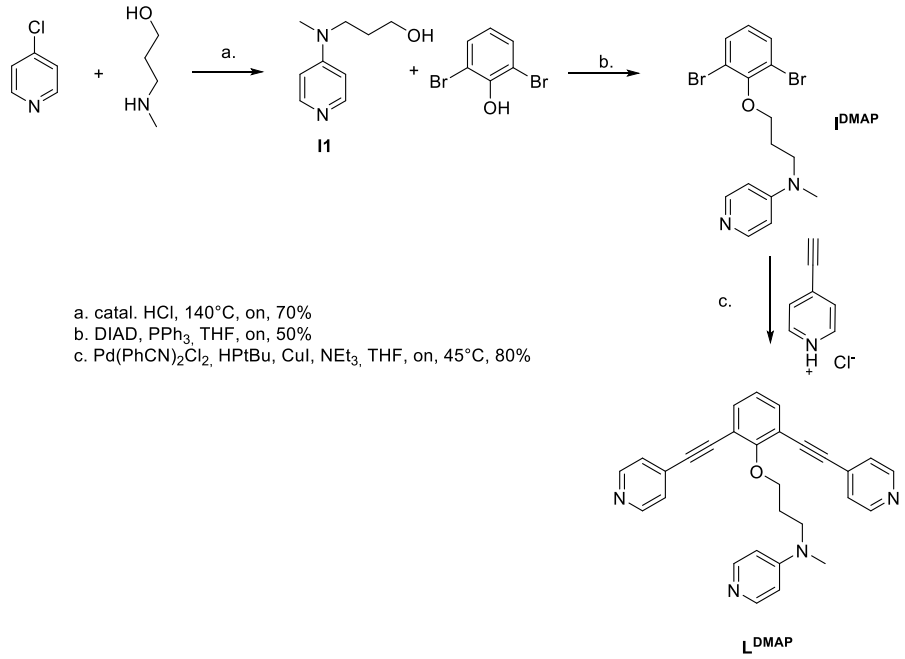

Scheme S1. Synthetic route for the DMAP containing building block **L^{DMAP}**.

I1 was synthesized according to literature procedure.[3] Briefly: To a solution of 1.42 g 4-chloropyridine and 3.21g 3-(methylamino)propan-1-ol, 6 drops of HCl·Et_2O were added. The resulting mix was stirred at 140°C overnight. 200 mL sat. $NaHCO_3$ aq. was added and the product was extracted into EtOAc. The solvent was evaporated *in vacuo* and the resulting oil was used as such for the consecutive steps. ^{1}H NMR (400 MHz, Chloroform-*d*) δ 8.22 – 8.15 (m, 1H), 6.57 – 6.50 (m, 1H), 3.73 (t, *J* = 5.9 Hz, 1H), 3.52 (t, *J* = 7.1 Hz, 1H), 3.00 (d, *J* = 0.8 Hz, 1H), 1.92 – 1.82 (m, 1H).

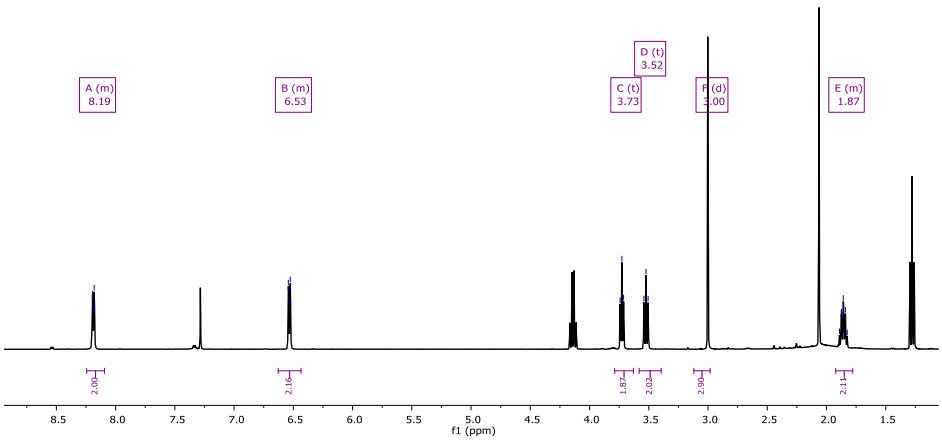

Figure S1. I1 precursor, ^{1}H NMR in $CDCl_3$.

I^{DMAP}: To a solution of 760 mg (3 mmol, 1 eq.) 2,6-dibromo-phenol, 500 mg (3 mmol, 1 eq.) I1 and 780 mg (3 mmol, 1 eq.) PPh3 in 10 mL THF, 0.7 mL (666 mg, 3.3 mmol, 1.1 eq.) DIAD was added. The solution was stirred overnight. The solvent was evaporated *in vacuo* and the crude material was purified by column chromatography (SiO2, MeOH:DCM 1:99 to 10:90) to afford 0.6 g (50%) of IDMAP as an orange oil. ESI-MS: calc for $[C_{15}H_{16}Br_2N_2O]H^+$ 400.968, obtained 400.9. ^{1}H NMR (400 MHz, Chloroform-*d*) δ 8.29 – 8.11 (m, 2H), 7.53 (d, *J* = 8.0 Hz, 2H), 6.91 (t, *J* = 8.0 Hz, 1H), 6.77 – 6.60 (m, 2H), 4.11 (t, *J* = 5.6 Hz, 2H), 3.85 – 3.75 (m, 2H), 3.16 (s, 3H), 2.27 – 2.08 (m, 2H). ^{13}C NMR (126 MHz, $CDCl_3$) δ 154.69, 153.05, 145.79, 135.15, 132.85, 126.60, 118.33, 106.70, 77.30, 77.04, 76.79, 70.38, 50.76, 49.06, 38.04, 27.29.

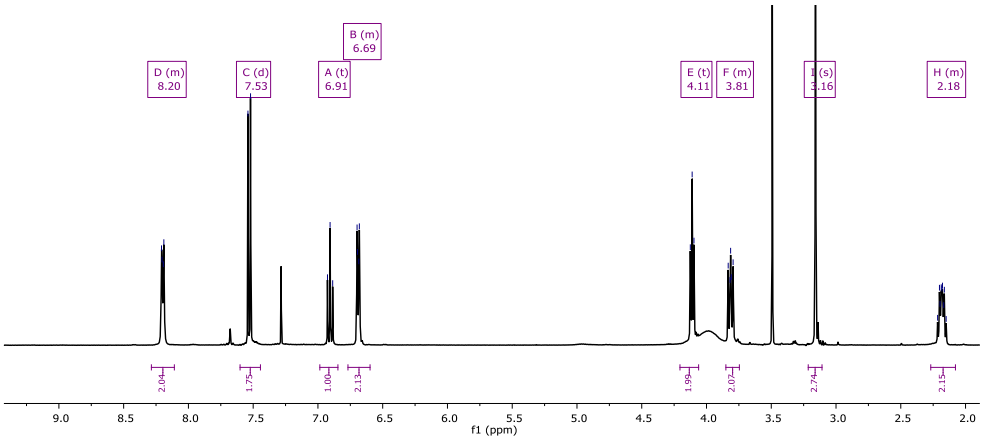

Figure S2. I^{DMAP} precursor, ^{1}H NMR in $CDCl_3$.

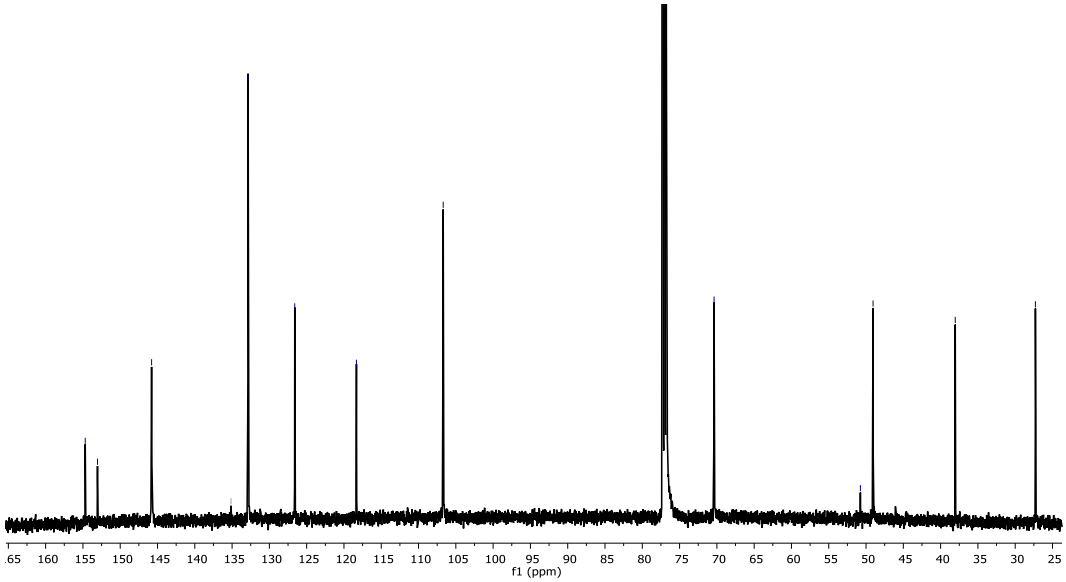

Figure S3. I^{DMAP} precursor, ^{13}C NMR in $CDCl_3$.

L^{DMAP}: To a degassed solution containing 53 mg (138 µmol, 0.06 eq.) [Pd(PhCN)$_2$Cl$_2$] and 80 mg (276 µmol, 0.12 eq.) HP^{t}BuBF$_4$ in 20 mL THF and 20 mL NEt$_3$, 1g (2.3 mmol, 1 eq.) **I^{DMAP}** and 805 mg (5.75 mmol, 2.5 eq.) 4-ethynylpyridine hydrochloride were added. The resulting suspension was stirred 15 min at room temperature before the mixture was heated to 50°C. 20 mg (0.04 eq.) CuI was added and the mixture stirred at 50°C overnight. The solution was then poured into 400 mL EtOAc, filtered over a pad of sand and concentrated *in vacuo*. The crude material was purified by column chromatography (SiO$_2$, MeOH:DCM, 5:95 to 25:75) to afford 810 mg of **L^{DMAP}** as a beige solid. ESI-MS: calc for [C$_{29}$H$_{24}$N$_4$O]H$^+$ 445.202, obtained 445.4. ^{1}H NMR (300 MHz, Chloroform-*d*) δ 8.76 – 8.54 (m, 4H), 8.17 (d, *J* = 5.8 Hz, 2H), 7.58 (d, *J* = 7.7 Hz, 2H), 7.41 – 7.31 (m, 4H), 7.16 (t, *J* = 7.7 Hz, 1H), 6.57 (d, *J* = 5.9 Hz, 2H), 4.43 (t, *J* = 5.7 Hz, 2H), 3.75 (dd, *J* = 8.0, 6.4 Hz, 2H), 3.00 (s, 3H), 2.28 – 2.06 (m, 2H).

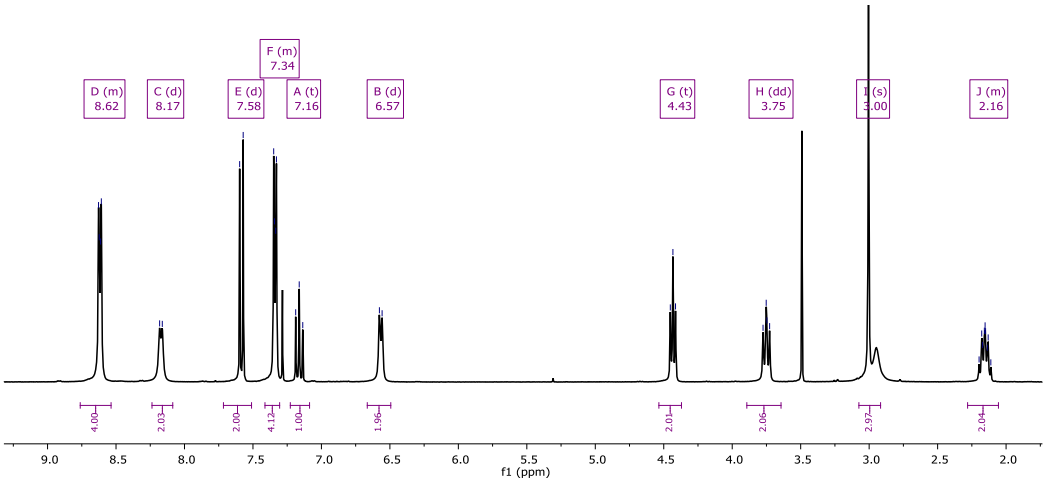

Figure S4. L^{DMAP} building block, ^{1}H NMR in CDCl$_3$.

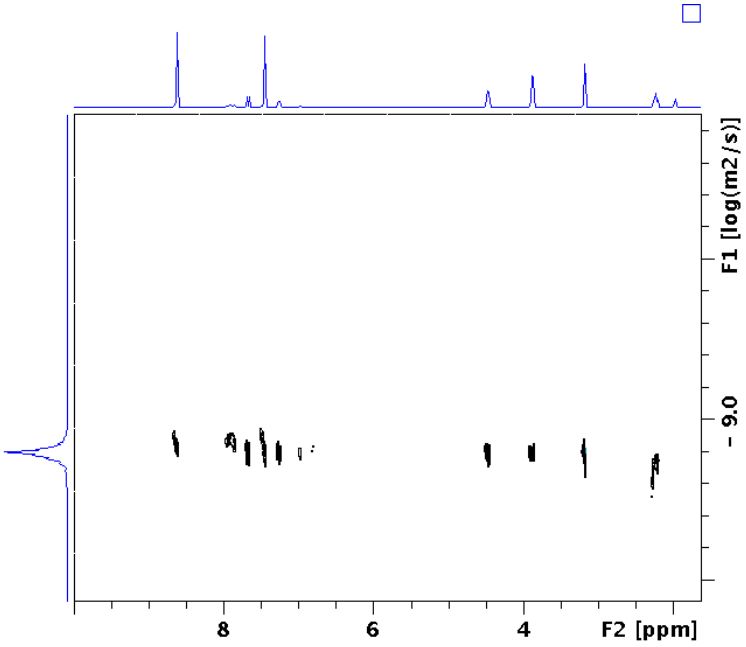

Figure S5. L^{DMAP} building block, DOSY NMR in MeCN-d$_3$ at 300 K.

L^{DMAPH}: To a solution containing 13.3 mg (30 μmol, 1 eq.) **L^{DMAP}** in 3 mL MeCN, 5.51 mg (33 μmol, 1.1 eq.) pyridinium tetrafluoroborate was added. The resulting solution was stirred 15 min at room before the solvent was removed under reduced pressure to yield quantitatively **L^{DMAPH}**. ^{1}H NMR (300 MHz, Acetonitrile-d_3) δ 11.08 (s, 1H), 8.76 – 8.50 (m, 4H), 7.89 (d, J = 13.0 Hz, 2H), 7.68 (d, J = 7.7 Hz, 2H), 7.52 – 7.38 (m, 4H), 7.26 (t, J = 7.8 Hz, 1H), 6.98 (s, 1H), 6.81 (s, 1H), 4.47 (t, J = 5.9 Hz, 2H), 4.03 – 3.76 (m, 2H), 3.18 (s, 3H), 2.31 – 2.13 (m, 2H). ^{13}C NMR (75 MHz, CD_3CN) δ 161.08, 157.25, 149.94, 135.04, 130.54, 125.26, 124.38, 116.43, 106.97, 91.13, 89.17, 71.64, 49.37, 38.30, 27.30. HR-ESI-MS, calculated for C29H25N4O 445.2023, obtained 445.1298.

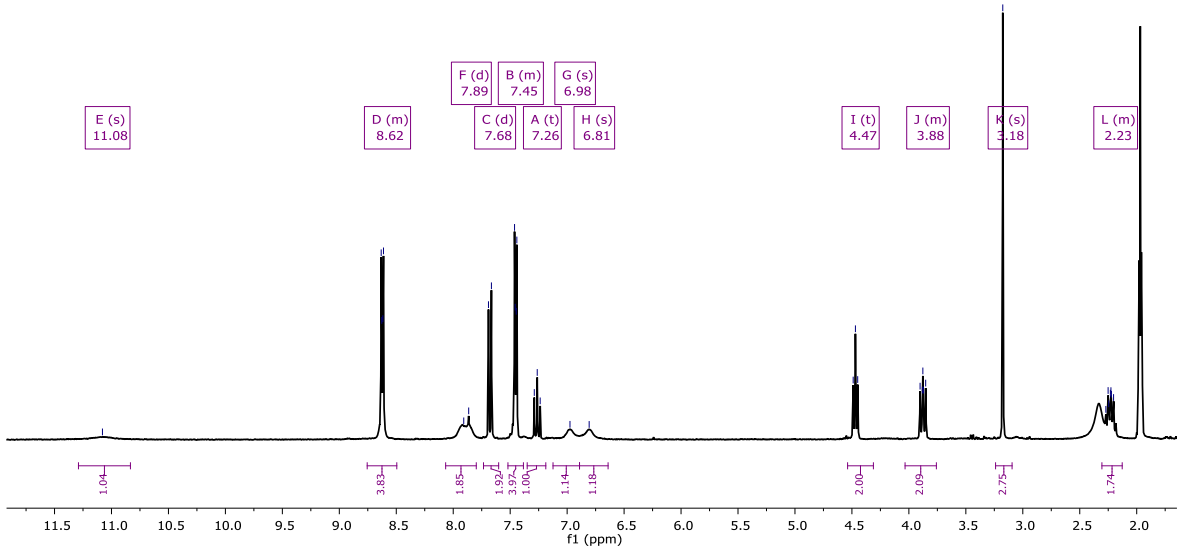

Figure S6. L^{DMAPH} building block, ^{1}H NMR in MeCN-d_3.

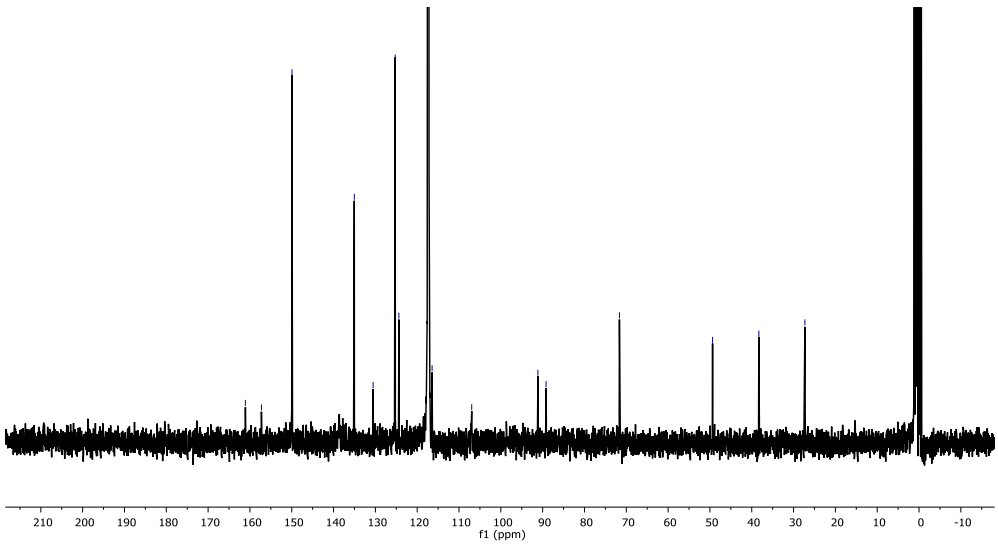

Figure S7. L^{DMAPH} building block, ^{13}C NMR in MeCN-d_3.

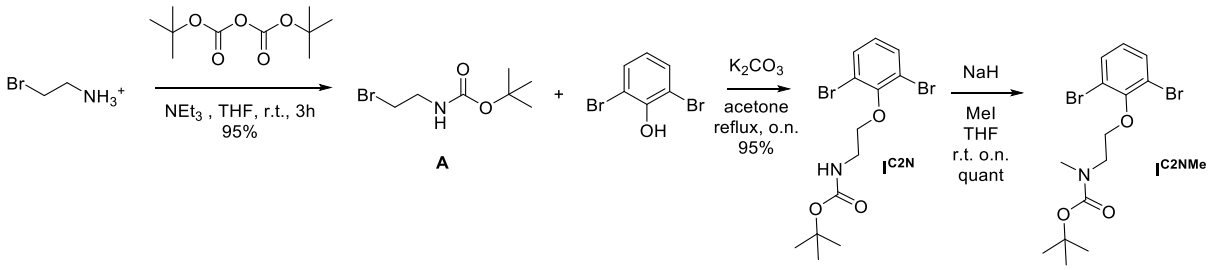

Scheme S2. Synthetic route for the precursors $\mathbf{I^{C2N}}$ and $\mathbf{I^{C2NMe}}$ required for the preparation of $\mathbf{L^{NMe}}$, $\mathbf{L^{Pro}}$ and $\mathbf{L^{His}}$.

A [4] and $\mathbf{I^{C2N}}$ [5] and $\mathbf{L^{C2N}}$ [5] were synthesized according to literature procedure.

$\mathbf{I^{C2Me}}$: To a solution of 2g $\mathbf{I^{C2N}}$ (5 mmol, 1 eq.) in 100 mL dry THF, 303 mg (7.59mmol, 1.5 eq.) 60% NaH in mineral oil was added portion wise. The resulting suspension was stirred 15 min at room temperature before 3.6 g (25 mmol, 5 eq.) Iodomethane was added. The solution was stirred over night at room temperature. The solvent was evaporated *in vacuo*. The product was extracted into Et_2O and the organic phase was washed three times with brine. After evaporation of the solvent 2g of $\mathbf{I^{C2NMe}}$ was obtained as a colorless oil.^{1}H NMR (400 MHz, Chloroform-*d*) δ 7.52 (d, *J* = 8.0 Hz, 2H), 6.89 (t, *J* = 8.0 Hz, 1H), 4.23 – 4.04 (m, 2H), 3.67 (d, *J* = 6.2 Hz, 2H), 3.09 (s, 3H), 1.49 (d, *J* = 3.9 Hz, 9H). ^{13}C NMR (101 MHz, $CDCl_3$) δ 132.74, 126.43, 118.51, 77.34, 77.03, 76.71, 49.07, 28.52.

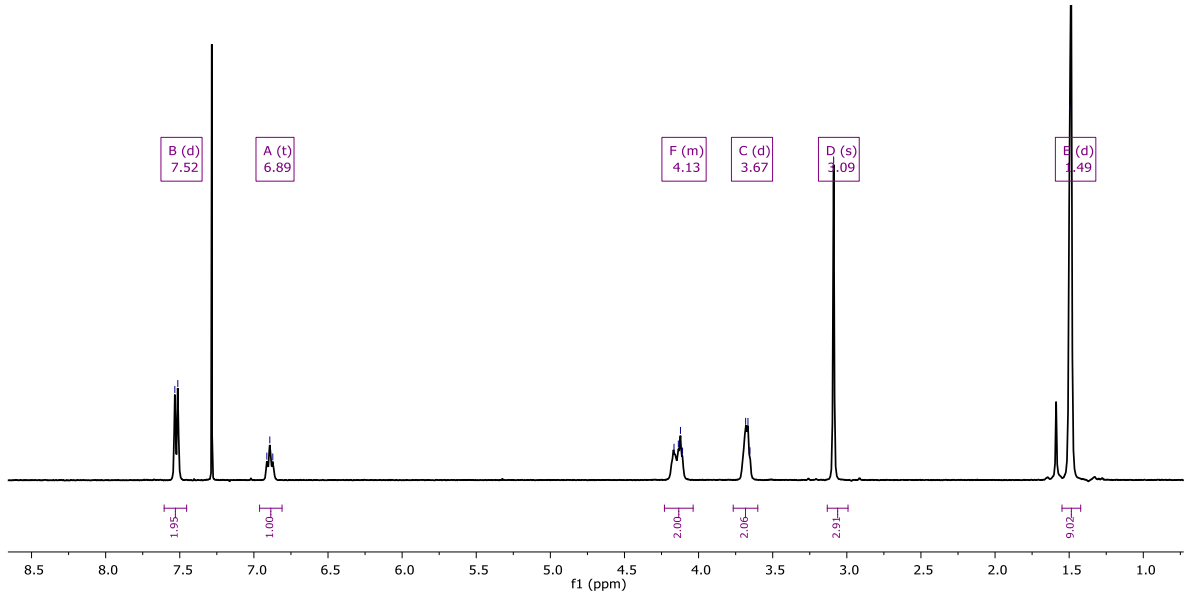

Figure S8. $\mathbf{I^{C2NMe}}$ intermediate, ^{1}H NMR in $CDCl_3$.

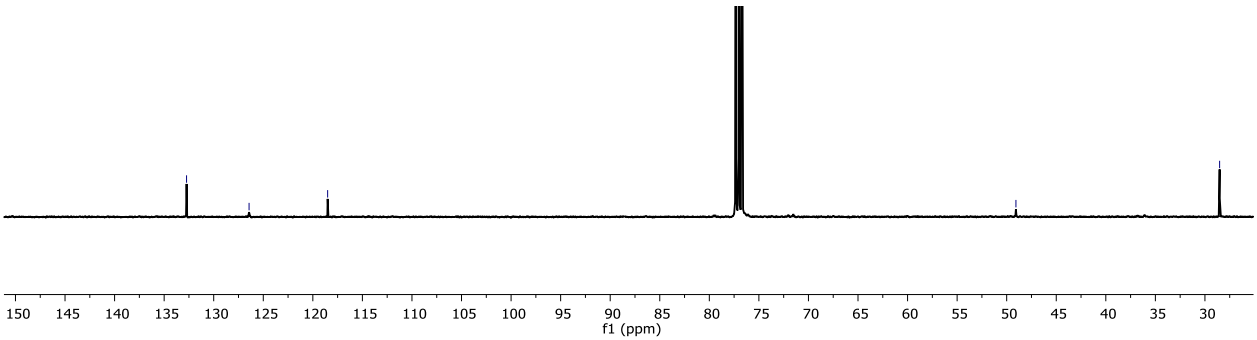

Figure S9. I^{C2NMe} intermediate, ^{13}C NMR in $CDCl_3$.

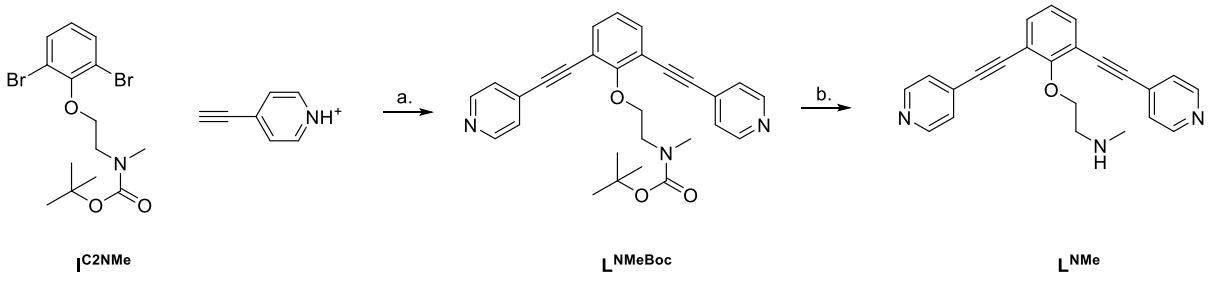

a. $[Pd(PhCN)_2Cl_2]$, CuI, HP^tBuBF_4, NEt_3, THF, 50°C, 43%
b. TFA, DCM, r.t., 1h, quant.

Scheme S3. Synthetic route for the building block $\mathbf{L^{NMe}}$.

$\mathbf{L^{NMeBoc}}$: To a degassed solution containing 53 mg (138 µmol, 0.06 eq.) $[Pd(PhCN)_2Cl_2]$ and 80 mg (276 µmol, 0.12 eq.) HP^tBuBF_4 in 20 mL THF and 20 mL NEt_3, 1g (2.4 mmol, 1 eq.) $\mathbf{I^{C2NMe}}$ and 805 mg (5.75 mmol, 2.5 eq.) 4-ethynylpyridine hydrochloride were added. The resulting suspension was stirred 15 min at room temperature before the mixture was heated to 50°C. 20 mg (0.04 eq.) CuI was added and the mixture stirred at 50°C overnight. The solution was then poured into 400 mL EtOAc, filtered over a pad of sand and concentrated *in vacuo*. The crude material was purified by column chromatography (SiO_2, MeOH:DCM, 5:95 to 25:75) to afford 470 mg of $\mathbf{L^{NMeBoc}}$ as a beige solid. ESI-MS: calc for $[C_{28}H_{27}N_3O_3]Na^+$ 476.1925, obtained 475.9. ^1H NMR (300 MHz, Chloroform-*d*) δ 8.61 (ddd, *J* = 8.8, 5.2, 3.0 Hz, 6H), 7.54 (d, *J* = 7.8 Hz, 2H), 7.46 – 7.33 (m, 4H), 7.10 (d, *J* = 7.4 Hz, 1H), 4.51 – 4.27 (m, 2H), 3.70 (t, *J* = 7.9 Hz, 3H), 3.03 (d, *J* = 2.0 Hz, 3H), 1.48 – 1.28 (m, 10H). ^{13}C NMR (75 MHz, $CDCl_3$) δ 150.44, 149.94, 149.89, 149.84, 142.75, 140.39, 134.77, 130.85, 126.03, 125.39, 123.92, 120.51, 116.71, 111.99, 92.00, 91.33, 90.95, 79.59, 77.53, 77.10, 76.68, 73.01, 53.45, 49.06, 36.01, 35.65, 28.34, 25.70.

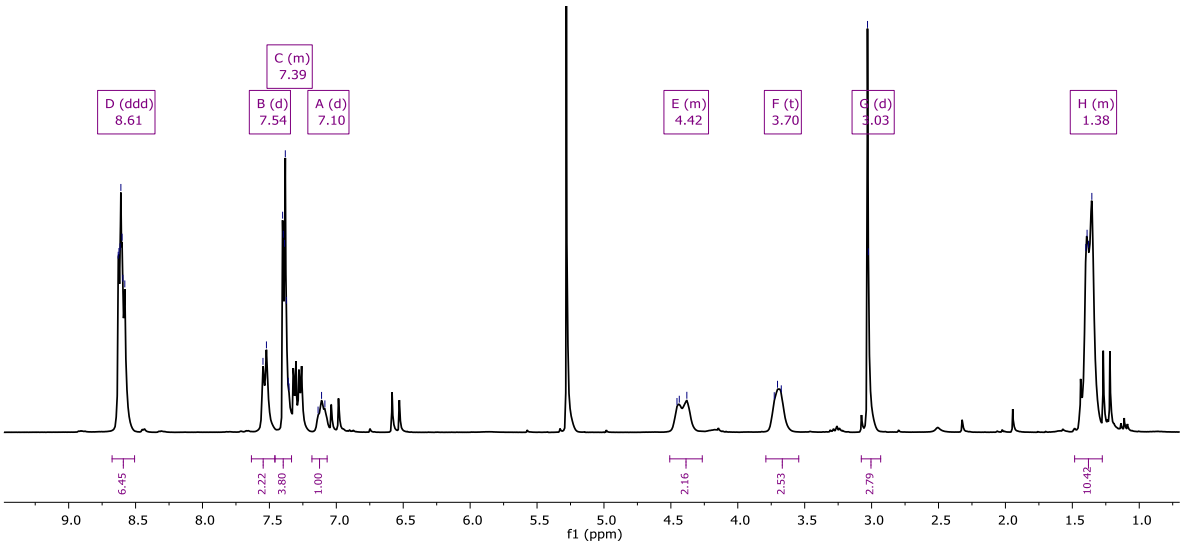

Figure S10. L^{NMeBoc} building block, ^{1}H NMR in $CDCl_3$.

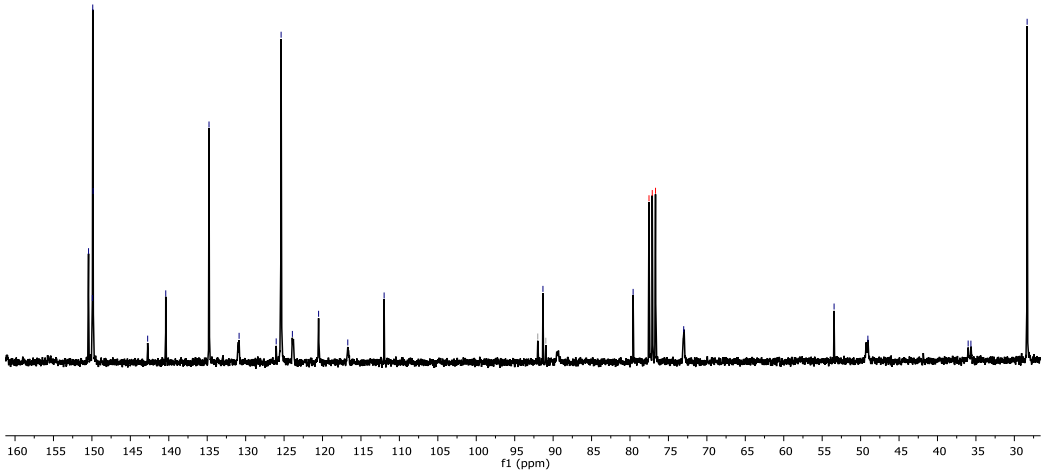

Figure S11. L^{NMeBoc} building block, ^{13}C NMR in $CDCl_3$.

L^{NMe}: To a solution of 470 mg (1 mmol) of **L^{NMeBoc}** in 100 mL DCM, 5 mL TFA was added and the resulting solution was stirred for 1h at room temperature. The volatiles were removed *in vacuo*. The resulting oil was suspended in 500 mL sat. NaHCO3 and the product was extracted with DCM (3x 100 mL). After removal of the solvent under educed pressure **L^{NMe}** was obtained as a colorless oil. ESI-MS: calc for $[C_{23}H_{19}N_3O]H^+$ 354.1601, obtained 353.9. ^{1}H NMR (300 MHz, Chloroform-*d*) δ 8.70 – 8.56 (m, 4H), 7.57 (d, *J* = 7.7 Hz, 2H), 7.50 – 7.39 (m, 4H), 7.15 (t, *J* = 7.7 Hz, 1H), 4.56 – 4.41 (m, 2H), 3.11 – 2.97 (m, 2H), 2.49 (s, 3H). ^{13}C NMR (75 MHz, $CDCl_3$) δ 161.25, 149.87, 134.78, 131.04, 125.41, 123.89, 116.74, 91.38, 89.52, 77.45, 77.03, 76.60, 73.74, 51.70, 50.80, 36.24. HR-ESI-MS, calculated for C23H20N3O 354.1601, obtained 354.2611.

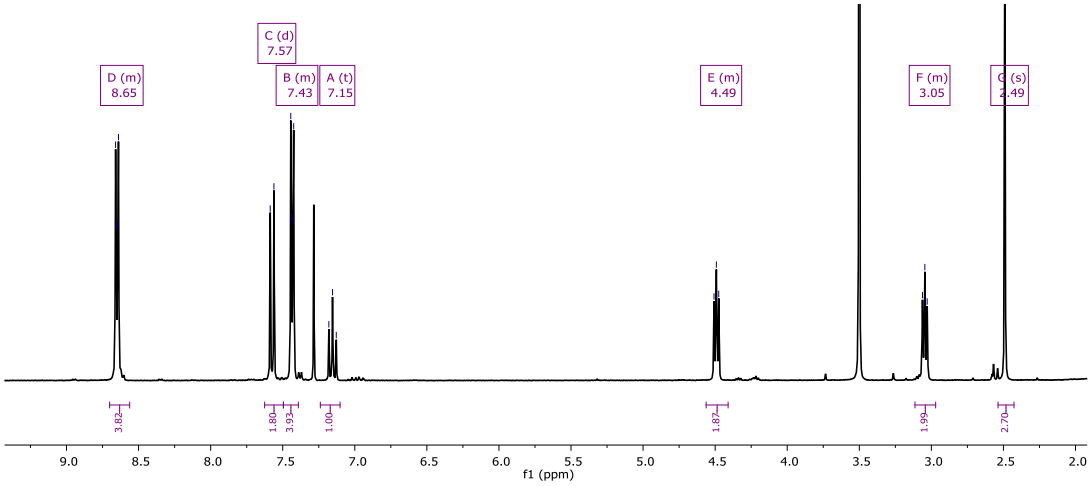

Figure S12. L^{NMe} building block, ^{1}H NMR in $CDCl_3$.

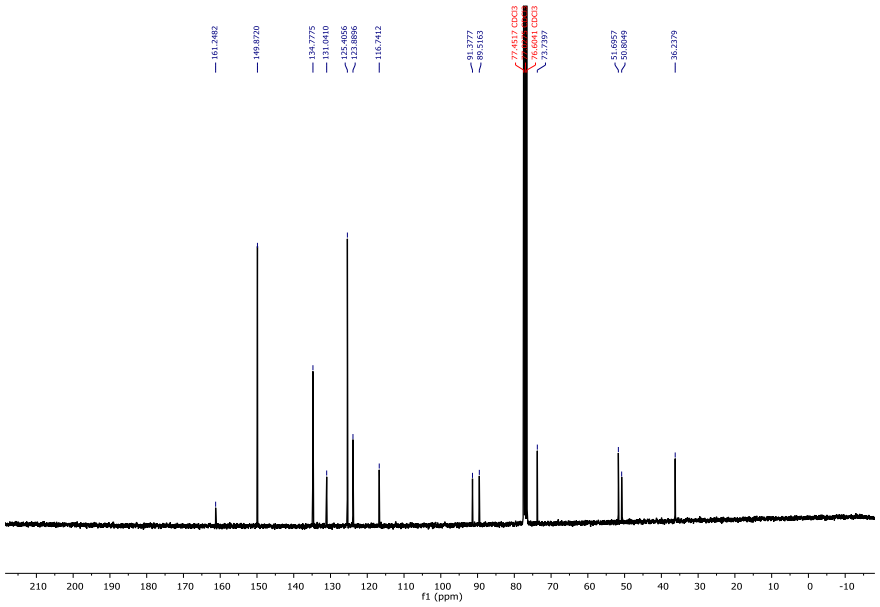

Figure S13. L^{NMe} building block, ^{13}C NMR in $CDCl_3$.

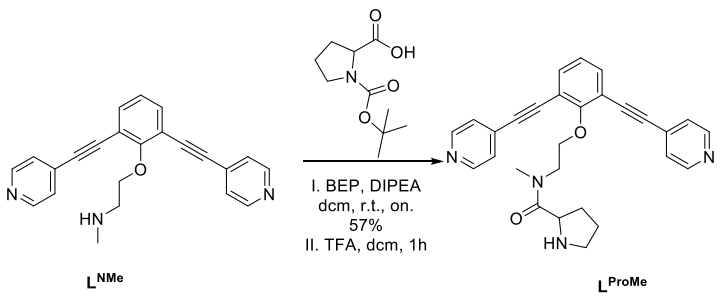

Scheme S4. Synthetic route for the building block L^{ProMe}.

L^{ProMe}: To a solution of 250 mg (0.7 mmol, 1eq.) **L^{NMe}** and 170 mg (0.78 mmol, 1.1 eq.) Boc-Pro-OH in 10 mL dcm, 420 mg (0.78 mmol, 1.1 eq.) BEP and 0.6 mL (2.1 mmol, 3 eq.) DIPEA were added. The solution was stirred over night at room temperature. All volatiles were removed under reduced pressure and the crude material was purified by column

chromatography (SiO_2, DCM:MeOH, 98:2) to afford $\mathbf{L^{BocProMe}}$ as an orange oil. This intermediate was treated with TFA (3 mL) in 10 mL dcm at room temperature for 1 h. The volatiles were removed *in vacuo*. The resulting oil was suspended in 500 mL sat. $NaHCO_3$ and the product was extracted with DCM (3x 100 mL). After removal of the solvent under educed pressure $\mathbf{L^{ProMe}}$ was obtained as a colorless oil (180 mg, 57%). The product exists as two rotamers (*cis* and *trans* across the peptide bond) which interconvert at elevated temperature. ^{1}H NMR (300 MHz, Acetonitrile-d_3) δ 8.69 – 8.60 (m, 4H), 7.66 (dd, *J* = 7.8, 6.2 Hz, 2H), 7.51 (dt, *J* = 4.0, 2.0 Hz, 4H), 7.25 (dt, *J* = 9.6, 7.8 Hz, 1H), 4.58 – 4.37 (m, 2H), 4.02 – 3.74 (m, 3H), 3.15 (s, 2H), 3.10 – 2.98 (m, 2H), 2.61 (ddt, *J* = 24.5, 10.6, 6.8 Hz, 1H), 1.75 – 1.45 (m, 2H). ^{13}C NMR (75 MHz, CD_3CN) δ 174.40, 150.03, 134.90, 130.52, 125.34, 125.28, 124.21, 91.22, 88.91, 71.88, 58.32, 48.68, 48.26, 47.40, 35.56, 30.62, 30.16, 26.38. HR-ESI-MS, calculated for C28H27N4O2 451.2129, obtained 451.2179.

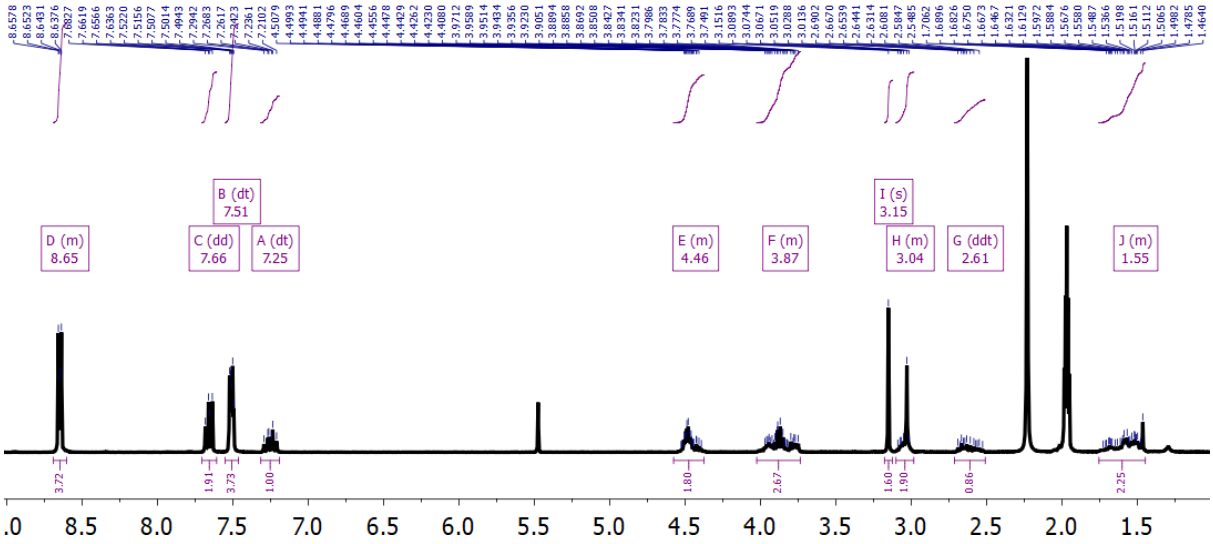

Figure S14. $\mathbf{L^{ProMe}}$ building block, ^{1}H NMR in MeCN-d_3.

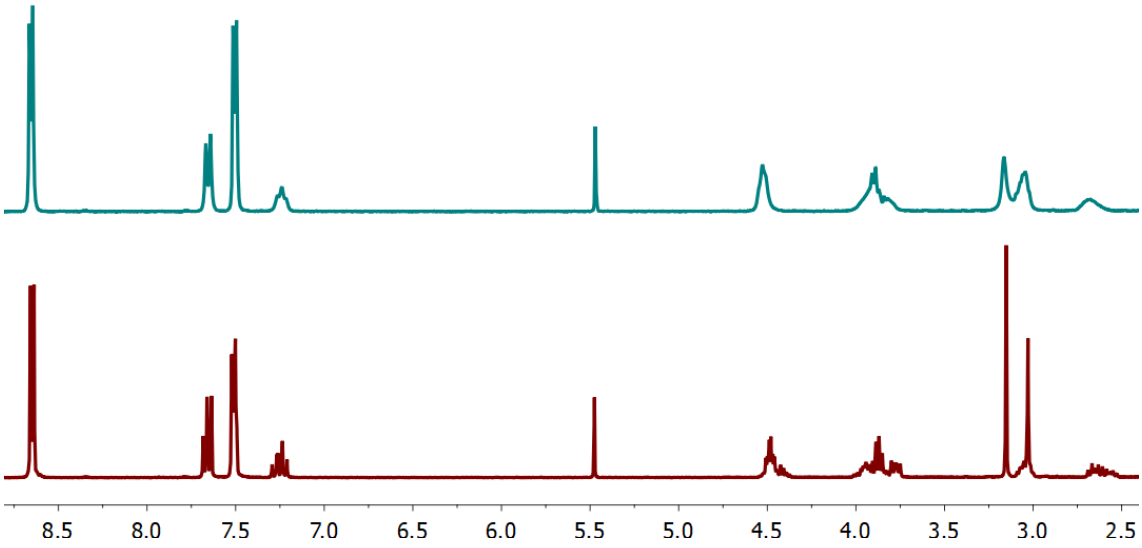

Figure S15. $\mathbf{L^{ProMe}}$ building block, ^{1}H NMR in MeCN-d_3; (top) 50°C; (bottom) 25°C.

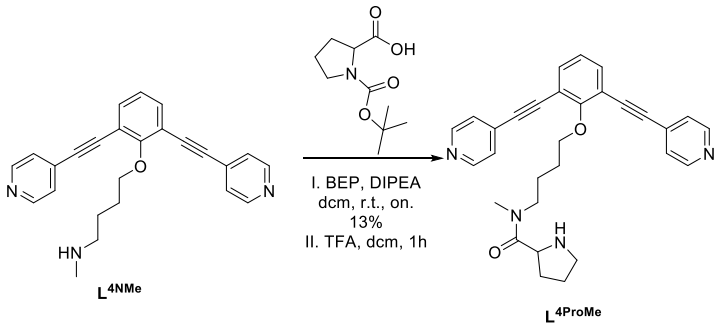

Scheme S5. Synthetic route for the building block **L^{4ProMe}**.

L^{4ProMe}: Was synthesized in analogy to **L^{ProMe}**. Briefly, to a solution of 500 mg (1 mmol, 1eq.) **L^{4NMe}** and 240 mg (1.1 mmol, 1.1 eq.) Boc-Pro-OH in 20 mL dcm, 305 mg (1.1 mmol, 1.1 eq.) BEP and 0.6 mL (3 mmol, 3 eq.) DIPEA were added. The solution was stirred over night at room temperature. All volatiles were removed under reduced pressure and the crude material was purified by column chromatography (SiO_2, DCM:MeOH, 98:2) to afford **L^{4BocProMe}** as an orange oil. This intermediate was treated with TFA (3 mL) in 10 mL dcm at room temperature for 1 h. The volatiles were removed *in vacuo*. The resulting oil was suspended in 500 mL sat. $NaHCO_3$ and the product was extracted with DCM (3x 100 mL). After removal of the solvent under educed pressure **L^{4ProMe}** was obtained as a colorless oil (60 mg, 13%). The product exists as two rotamers (*cis* and *trans* across the peptide bond) which interconvert at elevated temperature. ^{1}H NMR (300 MHz, Acetonitrile-d_3) δ 8.64 (dt, *J* = 4.4, 1.5 Hz, 4H), 7.63 (dd, *J* = 7.7, 2.5 Hz, 2H), 7.46 (td, *J* = 4.3, 1.6 Hz, 4H), 7.21 (td, *J* = 7.8, 3.7 Hz, 1H), 4.41 – 4.33 (m, 2H), 3.78 (td, *J* = 6.3, 3.4 Hz, 1H), 3.40 (dtd, *J* = 26.2, 13.0, 8.3 Hz, 2H), 3.07 (ddd, *J* = 11.4, 7.0, 4.9 Hz, 1H), 2.92 (s, 2H), 2.81 (s, 1H), 2.76 – 2.61 (m, 3H), 1.93 – 1.42 (m, 4H). ^{13}C NMR (75 MHz, CD_3CN) δ 173.64, 173.50, 161.52, 150.08, 150.05, 134.85, 130.58, 125.24, 125.20, 124.17, 124.03, 90.99, 90.96, 89.19, 89.11, 74.49, 74.45, 58.23, 57.98, 54.33, 48.39, 47.37, 47.10, 33.90, 32.54, 30.74, 30.26, 27.43, 27.33, 26.44, 26.38, 25.30, 23.76. HR-ESI-MS, calculated for C30H31N4O2 479.2442, obtained 479.2540.

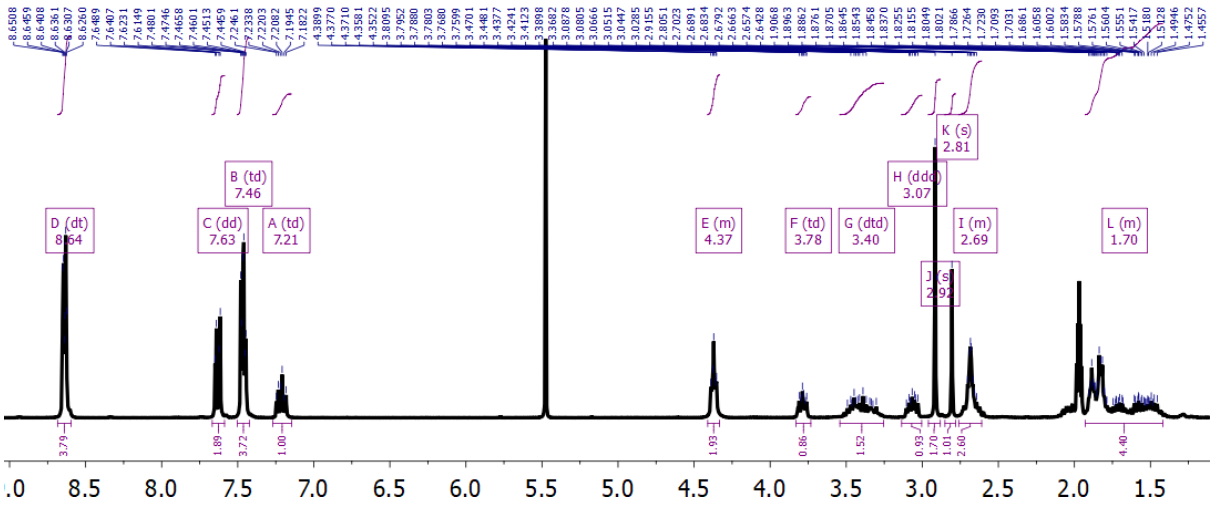

Figure S16. L^{4ProMe} building block, ^{1}H NMR in MeCN-d_3.

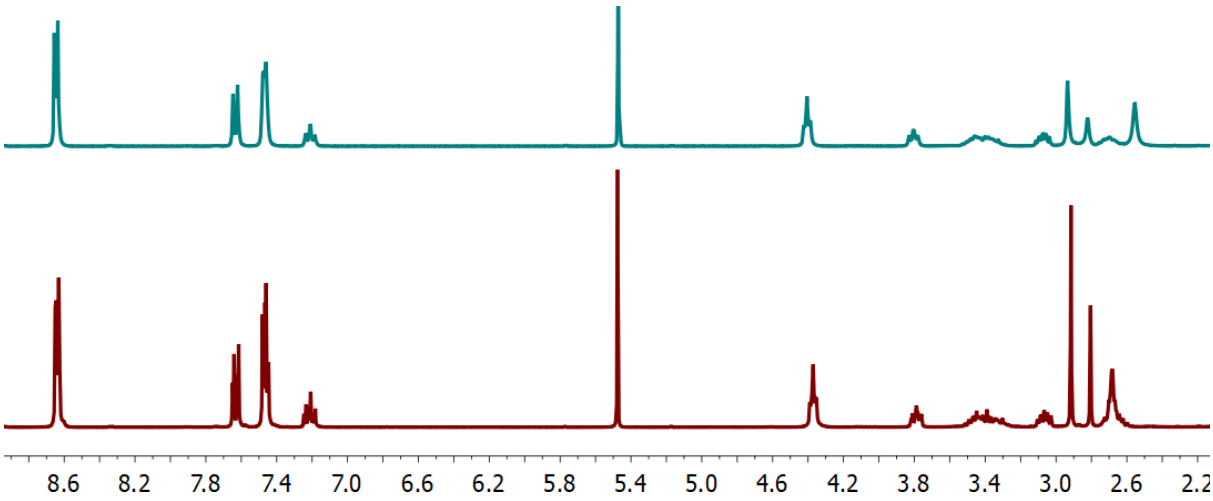

Figure S17. L^{4ProMe} building block, ^{1}H NMR in MeCN-d$_3$; (top) 50°C; (bottom) 25°C.

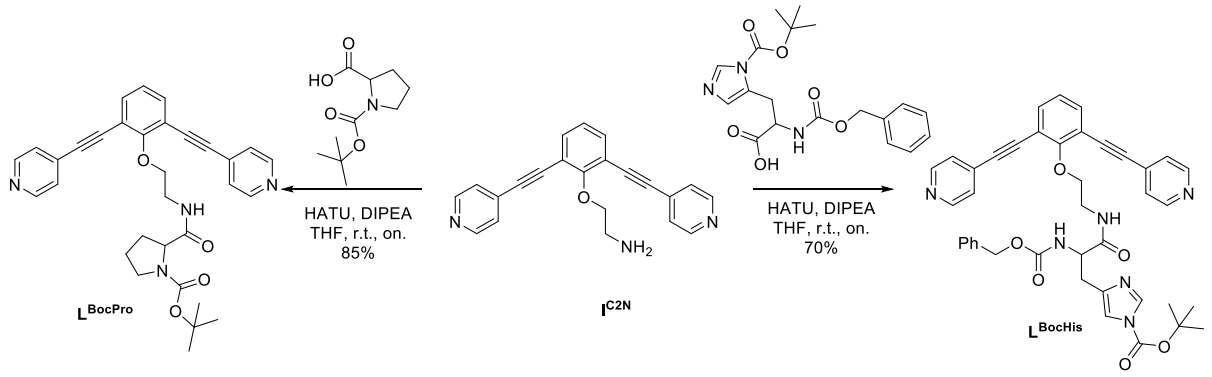

Scheme S6. Synthetic route for the building block **L^{BocPro}** and **L^{BocHis}**.

L^{BocHis}: To a solution of 457 mg (1.17 mmol, 1eq.) Boc-His(Z)-OH in 40 mL dry THF, 491 mg (1.3 mmol, 1.1 eq.) HATU and 840 mg (6.46 mmol, 5.5 eq.) DIPEA were added. The resulting solution was stirred for 1 h at room temperature. Then, 800 mg (1.17 mmol, 1 eq.) **I^{C2N}** was added. The resulting solution was stirred at room temperature overnight. The volatiles were removed under reduced pressure and the crude material was purified by column chromatography (SiO_2, DCM:MeOH, 98:2) to afford **L^{BocHis}** as an orange oil. ESI-MS: calc for $[C_{41}H_{38}N_6O_6]Na^+$ 733.27, obtained 733.5. ^{1}H NMR (400 MHz, Acetonitrile-d_3) δ 8.68 – 8.54 (m, 4H), 7.90 (d, J = 1.3 Hz, 1H), 7.62 (d, J = 7.8 Hz, 2H), 7.54 – 7.44 (m, 4H), 7.32 (q, J = 6.4 Hz, 4H), 7.21 (t, J = 7.8 Hz, 1H), 5.47 (s, 2H), 4.36 (dt, J = 17.9, 6.6 Hz, 3H), 3.67 (q, J = 6.0 Hz, 2H), 2.89 (q, J = 8.5, 7.9 Hz, 2H), 2.27 (s, 2H), 1.97 (p, J = 2.5 Hz, 1H), 1.53 (s, 10H). ^{13}C NMR (101 MHz, CD_3CN) δ 171.33, 161.20, 156.00, 149.99, 146.90, 138.97, 137.00, 136.90, 134.91, 130.45, 128.42, 127.90, 127.71, 125.33, 124.23, 117.32, 116.57, 116.41, 114.64, 91.35, 88.92, 85.35, 72.73, 66.22, 54.81, 54.35, 39.60, 30.07, 26.98.

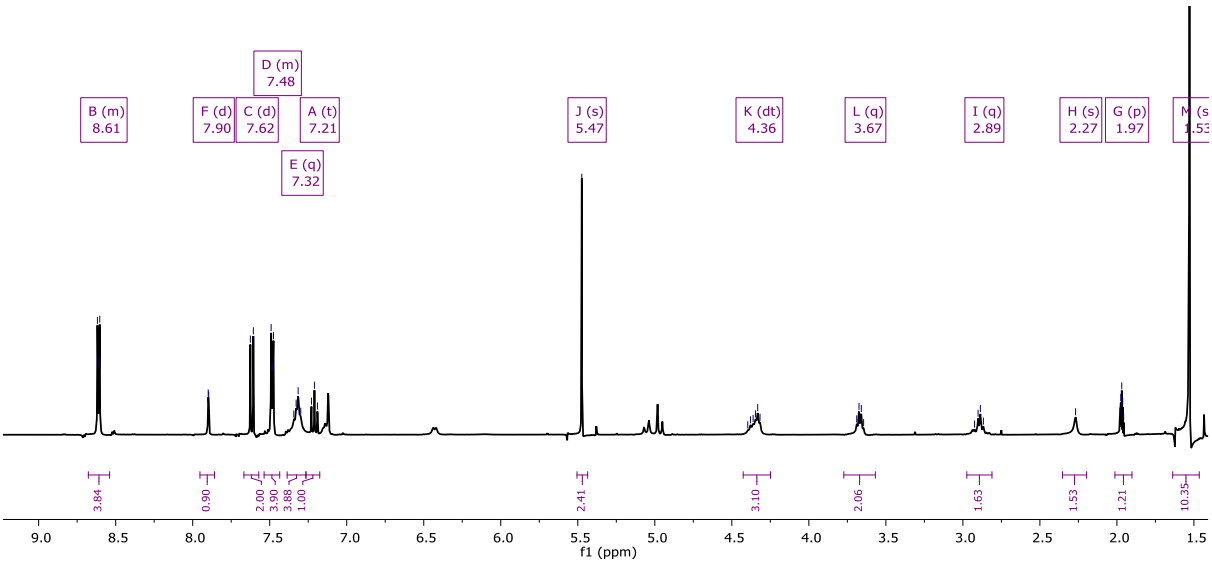

Figure S18. L^{BocHis} building block, ^{1}H NMR in MeCN-d$_3$.

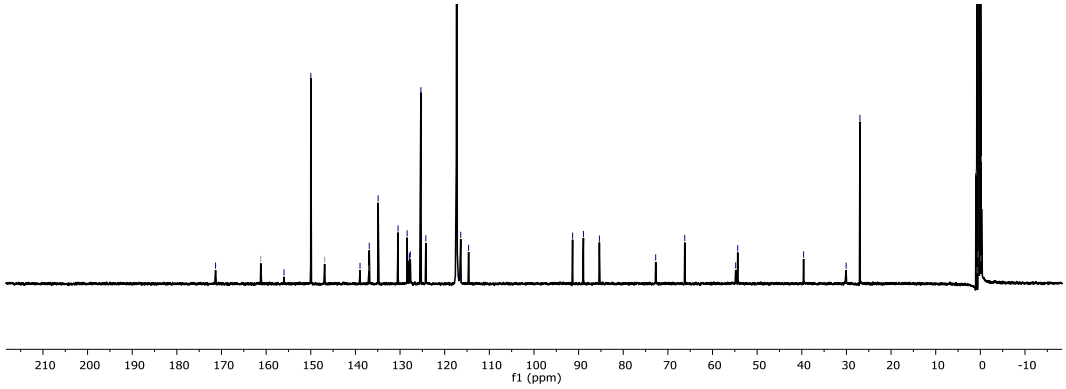

Figure S19. L^{BocHis} building block, ^{13}C NMR in MeCN-d$_3$.

L^{BocPro}: To a solution of 252 mg (1.17 mmol, 1eq.) Boc-Pro-OH in 40 mL dry THF, 491 mg (1.3 mmol, 1.1 eq.) HATU and 840 mg (6.46 mmol, 5.5 eq.) DIPEA were added. The resulting solution was stirred for 1 h at room temperature. Then, 800 mg (1.17 mmol, 1 eq.) **I^{C2N}** was added. The resulting solution was stirred at room temperature overnight. The volatiles were removed under reduced pressure and the crude material was purified by column chromatography (SiO_2, DCM:MeOH, 98:2) to afford **L^{BocPro}** as an orange oil. ESI-MS: calc for $[C_{32}H_{32}N_4O_4]Na^+$ 559.23, obtained 560.1. ^{1}H NMR (300 MHz, Methylene Chloride-d_2) δ 8.70 – 8.57 (m, 4H), 7.62 (d, J = 7.7 Hz, 2H), 7.52 – 7.40 (m, 4H), 7.19 (t, J = 7.7 Hz, 1H), 4.48 (dd, J = 6.4, 5.0 Hz, 2H), 4.09 (s, 1H), 3.77 (dq, J = 5.6, 2.8 Hz, 2H), 3.29 (t, J = 5.8 Hz, 1H), 1.80 (d, J = 29.1 Hz, 5H), 1.54 – 1.26 (m, 12H). ^{13}C NMR (75 MHz, CD_2Cl2) δ 161.28, 149.94, 149.86, 134.79, 130.67, 125.32, 123.90, 116.51, 91.47, 89.13, 79.92, 73.45, 47.03, 39.99, 28.00, 26.91, 18.46.

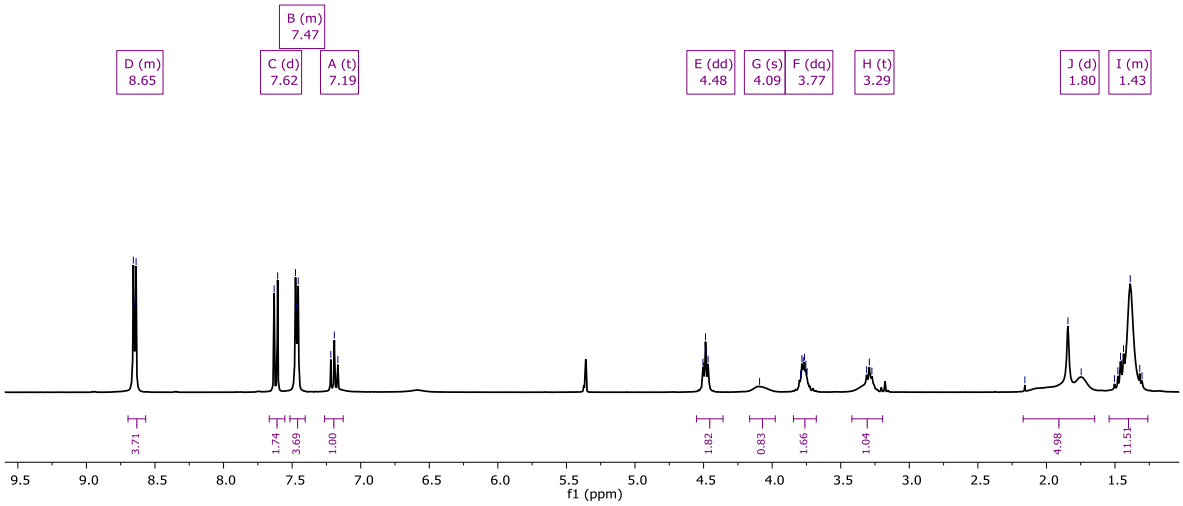

Figure S20. L^{BocPro} building block, ^{1}H NMR in methylenechloride-d$_2$.

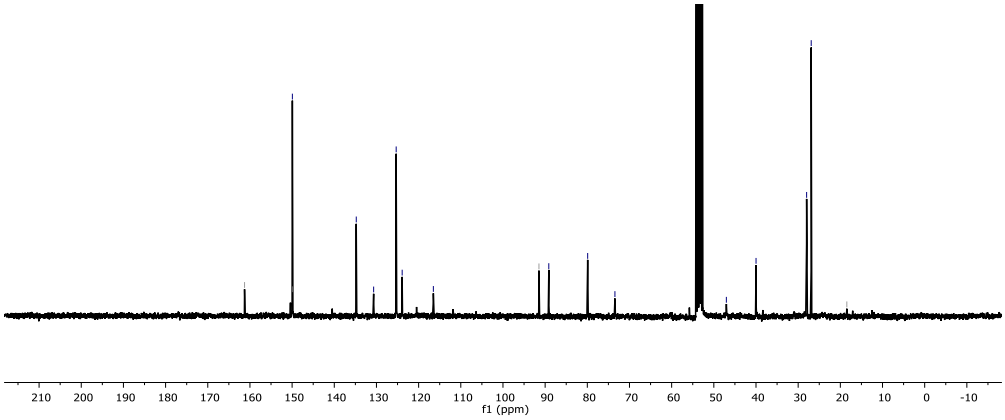

Figure S21. L^{BocPro} building block, ^{13}C NMR in methylenechloride-d$_2$.

L^{His}: To a solution of 426 mg (0.6 mmol) of **L^{BocHis}** in 100 mL DCM, 5 mL TFA was added and the resulting solution was stirred for 1h at room temperature. The volatiles were removed *in vacuo*. The resulting oil was suspended in 500 mL sat. $NaHCO_3$ and the product was extracted with DCM (3x 100 mL). After removal of the solvent under educed pressure **L^{His}** was obtained as a colorless solid (350 mg, 96%). ESI-MS: calc for $[C_{36}H_{30}N_6O_4]H^+$ 611.24, obtained 611.1. ^{1}H NMR (400 MHz, Acetonitrile-d_3) δ 10.06 (s, 1H), 8.69 – 8.55 (m, 4H), 7.65 (d, J = 7.8 Hz, 2H), 7.58 – 7.47 (m, 4H), 7.37 (d, J = 26.7 Hz, 5H), 7.23 (t, J = 7.8 Hz, 1H), 7.14 (s, 1H), 6.73 (s, 1H), 6.12 (s, 2H), 5.15 – 4.90 (m, 2H), 4.45 – 4.14 (m, 3H), 3.65 (d, J = 6.3 Hz, 2H), 2.88 (d, J = 13.7 Hz, 2H).

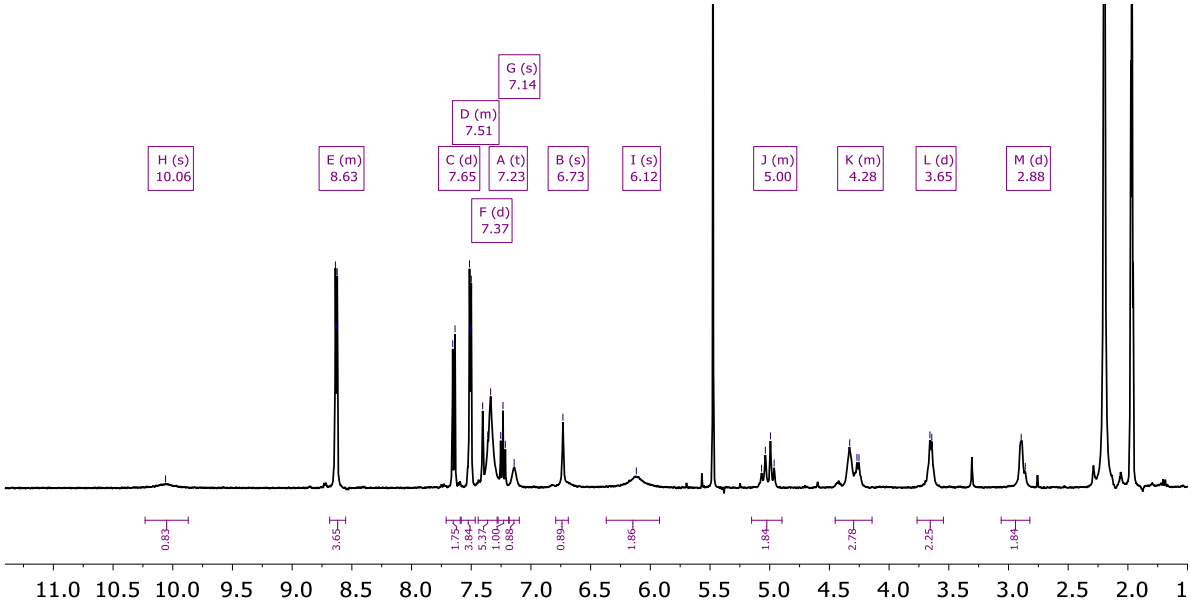

Figure S22. L^{His} building block, ^{1}H NMR in MeCN-d_3.

L^{ProH}: To a solution of 426 mg (0.6 mmol) of **L^{BocPro}** in 100 mL DCM, 5 mL TFA was added and the resulting solution was stirred for 1h at room temperature. The volatiles were removed *in vacuo*. The resulting oil was suspended in 500 mL sat. $NaHCO_3$ and the product was extracted with DCM (3x 100 mL). After removal of the solvent under educed pressure **L^{Pro}** was obtained as an orange oil (330 mg, 95%). To a solution containing 13.1 mg (30 µmol, 1 eq.) **L^{Pro}** in 3 mL MeCN, 5.51 mg (33 µmol, 1.1 eq.) pyridinium tetrafluoroborate was added. The resulting solution was stirred 15 min at room before the solvent was removed under reduced pressure to yield quantitatively **L^{ProH}**. ESI-MS: calc for $[C_{27}H_{24}N_4O_2]H^+$ 437.52, obtained 436.9. ^{1}H NMR (300 MHz, DMSO-d_6) δ 8.76 (t, *J* = 5.6 Hz, 1H), 8.73 – 8.62 (m, 4H), 7.73 (d, *J* = 7.7 Hz, 2H), 7.64 – 7.50 (m, 4H), 7.30 (t, *J* = 7.7 Hz, 1H), 4.47 – 4.29 (m, 2H), 4.20 – 4.01 (m, 1H), 3.77 (dq, *J* = 11.9, 5.9 Hz, 1H), 3.64 (p, *J* = 6.1 Hz, 1H), 3.16 (dt, *J* = 7.2, 3.3 Hz, 2H), 2.18 (q, *J* = 7.2, 6.6 Hz, 1H), 1.88 – 1.66 (m, 3H). ^{13}C NMR (75 MHz, DMSO) δ 168.97, 161.23, 150.55, 135.49, 130.33, 125.74, 125.17, 116.45, 91.75, 89.47, 72.86, 65.39, 59.52, 46.19, 29.90, 23.91, 15.63. HR-ESI-MS, calculated for C27H24N4O2 437.1973, obtained 437.1825.

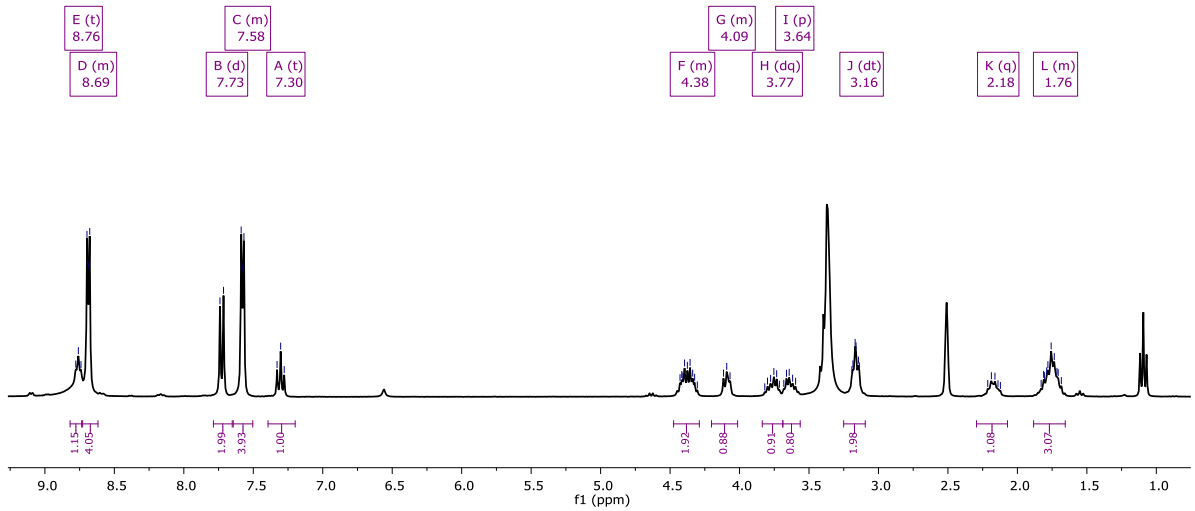

Figure S23. L^{ProH} building block, ^{1}H NMR in MeCN-d$_3$.

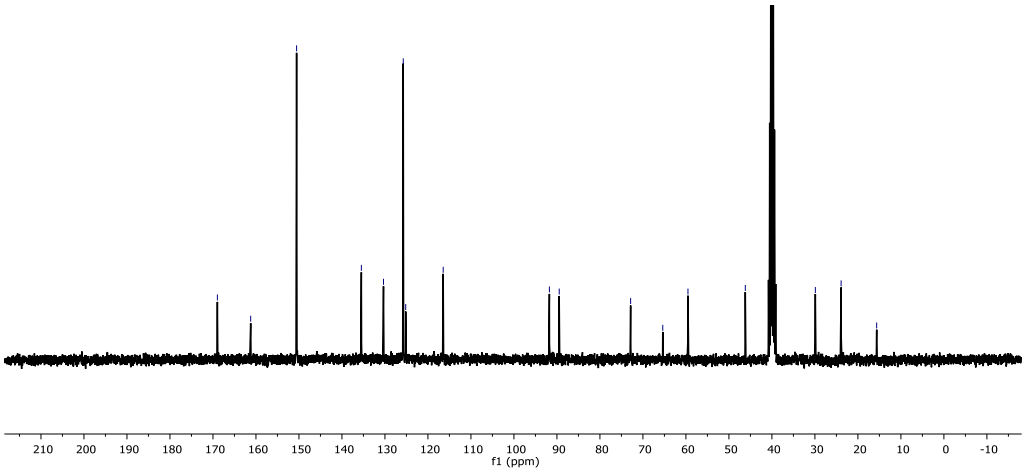

Figure S24. L^{ProH} building block, ^{1}H NMR in MeCN-d$_3$.

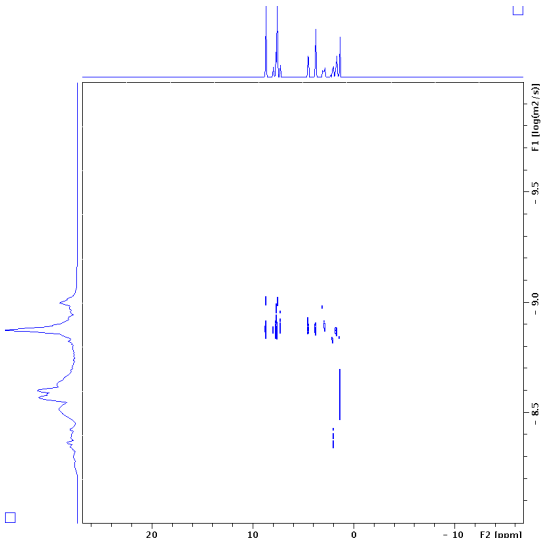

Figure S25. L^{ProH} building block, DOSY NMR in MeCN-d$_3$ at 300K.

Sphere preparation (SI2)

All self-assemblies were prepared according to the following procedure: 10 µmol of the corresponding ligand and 10.5 µmol pyridinium salt (either BF_4^- or OTf^- salt) were dissolved in 0.5 mL MeCN. The solution was stirred 20 min at room temperature before all volatiles were removed at room temperature under reduced pressure. The resulting solids were dissolved in 1 mL MeCN-d_3 and 5.5 µmol solid $[Pd(X)_2(MeCN)_4]$ was added. The resulting solutions were stirred overnight at room temperature. Thereafter, the samples were analyzed *via* different techniques. The final solutions contain the desired spheres and a small quantity of the excess of pyridinium salt which was used during the preparation (see Fig. S26). **Note:** The pyridinium BF_4 salt decomposes slowly to a non-identified pink product. Once this product is present, sphere formation is hampered. Therefore, we recommend to prepare pyridinium BF_4 fresh or use pyridinium OTf.

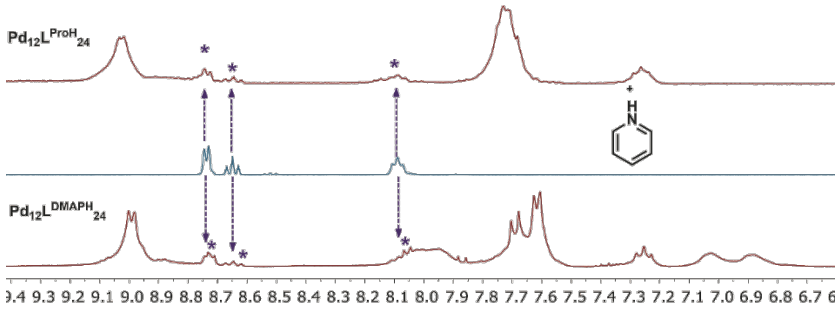

Figure S26. $[Pd_{12}\mathbf{L}^{\mathbf{DMAPH}}{}_{24}]$, $[Pd_{12}\mathbf{L}^{\mathbf{ProH}}{}_{24}]$ assembly and pure pyridinium salt, ^{1}H NMR in MeCN-d_3 showing the trace amount of the pyridinium salt in some final samples.

The hydrodynamic radius of the analytes was calculated using the Stokes-Einstein equation (1)

(1) $r = \frac{k_b T}{6\pi\eta D}$ with η = viscosity; D = diffusion coefficient; k_b = Boltzmann constant

(2) $d = 2r$

Nanocage formation without prior protonation: When nanosphere formation is performed using any of the described building blocks with interior nitrogen-donor, only ill-defined species are obtained (likely due to random coordination of interior nitrogen-donor and framework pyridines).

Exemplary: 4.44 mg (10 mmol, 1 eq.) $\mathbf{L}^{\mathbf{DMAP}}$ and 2.44 mg (5.5 mmol, 0.55 eq.) $[Pd(BF_4)_2(MeCN)_4]$ were mixed in 1 mL acetonitrile-d_3 at room temperature. Immediately, a color change to light brown is observed. ^{1}H-NMR displays a non-symmetrical construct with many framework pyridines not coordinated to palladium. ESI-MS displays only single and double charged species with the absence of any nanosphere (indicative of random oligomer formation, exemplary Fig. S27-28). Similar results are also obtained with the other building blocks.

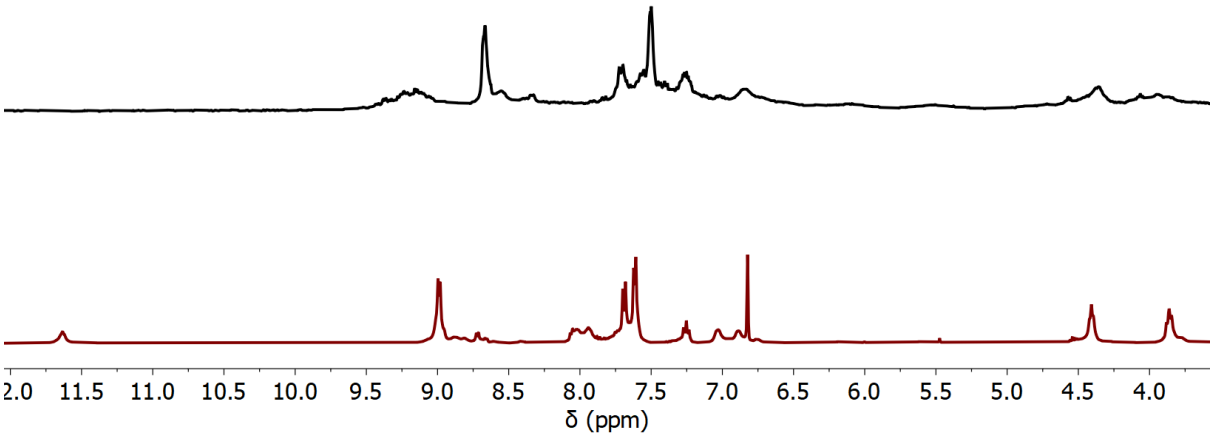

Figure S27. [Pd_{12}**L**$^{\mathbf{DMAPH}}{}_{24}$] assembly (bottom, using protonated building block **L**$^{\mathbf{DMAP}}$), attempted nanosphere assembly using non-protonated **L**$^{\mathbf{DMAP}}$ (top) showing no presence of nanosphere, ^{1}H NMR in MeCN-d_3.

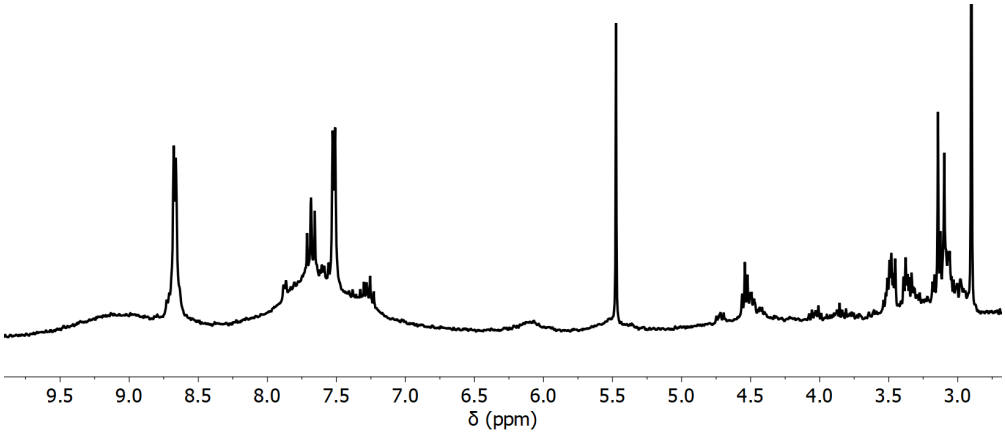

Figure S28. Attempted nanosphere assembly using non-protonated **L**$^{\mathbf{ProMe}}$ showing no presence of nanosphere, ^{1}H NMR in MeCN-d_3.

$\underline{Pd_{12}\mathbf{L}^{\mathbf{DMAPH}}{}_{24}}$

According to the general procedure, 4.44 mg (10 mmol, 1 eq.) **L**$^{\mathbf{DMAP}}$, 1.83 mg (11 mmol, 1.1 eq.) pyridinium tetrafluoroborate and 2.44 mg (5.5 mmol, 0.55 eq.) $[Pd(BF_4)_2(MeCN)_4]$ were utilized for the preparation of the self-assembly. ^{1}H NMR (300 MHz, Acetonitrile-d_3) δ 11.62 (s, 1H), 8.98 (m, 4H), 7.96 (m , 2H), 7.61 (d, 2H), 7.60 (m, 4H), 7.25 (t, 1H), 7.03(s_{br}, 1H), 6.89 (s_{br}, 1H), 4.41 (s_{br}, 2H), 3.85 (s_{br}, 2H), 3.17 (s_{br}, 3H). *log D* (300 K; Acetonitrile-d_3) = -9.58; *d* = 5.0 nm.

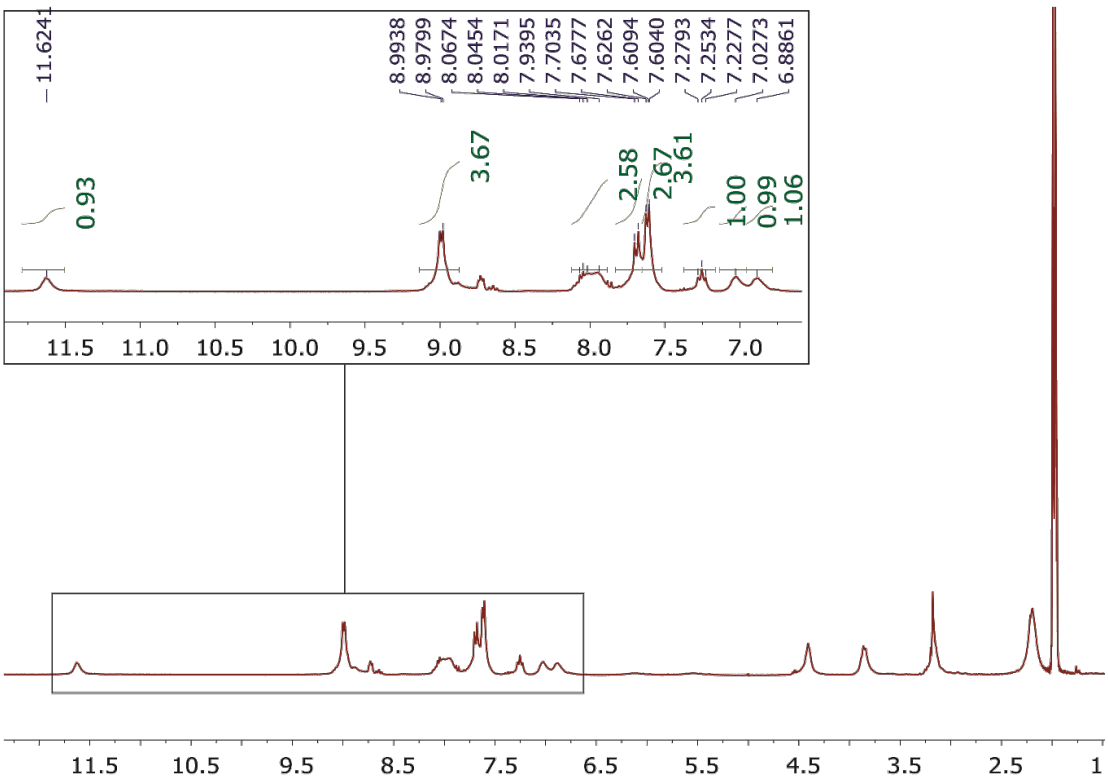

Figure S29. [$Pd_{12}\mathbf{L}^{\mathbf{DMAPH}}{}_{24}$] assembly, ^{1}H NMR in MeCN-d_3.

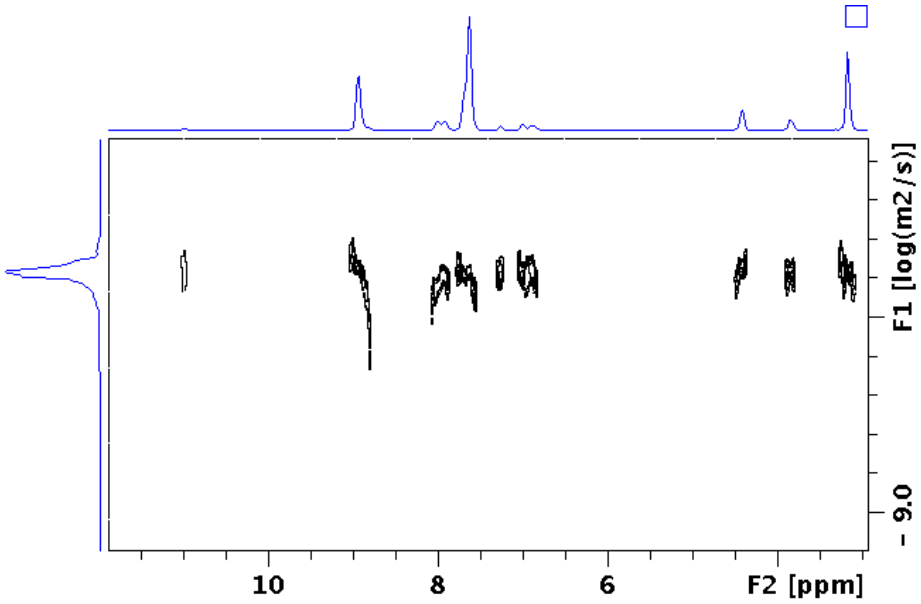

Figure S30. [$Pd_{12}\mathbf{L}^{\mathbf{DMAPH}}{}_{24}$] assembly, DOSY NMR in MeCN-d_3 at 300K.

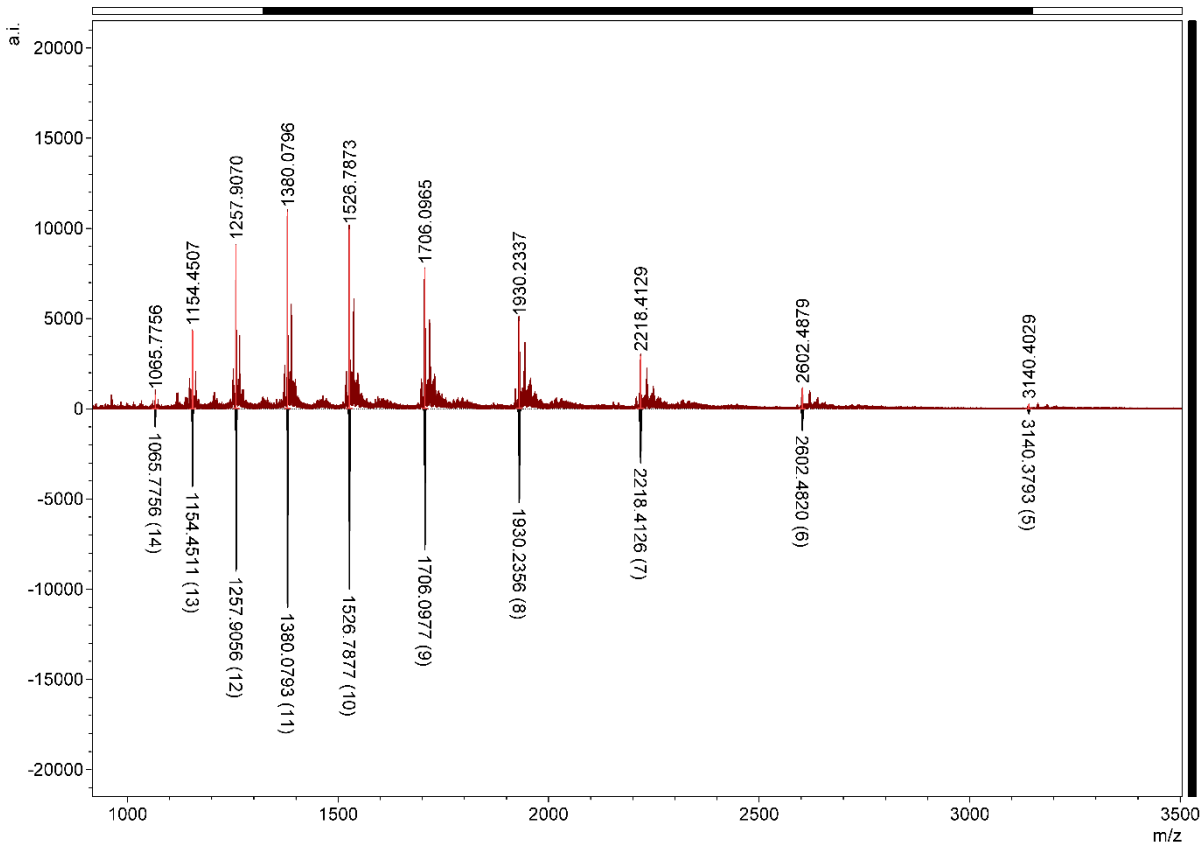

Figure S31. $[Pd_{12}\mathbf{L}^{\mathbf{DMAPH}}{}_{24}]$ assembly, full HR-ESI MS spectrum, top measured; bottom, simulated spectra of different charged states of the self-assembly.

Table S1. Calculated and observed species of the $[Pd_{12}(\mathbf{L}^{\mathbf{DMAPH}})_{24}]^{48+}$ assembly.

Composition	Calculated	Observed
$[Pd_{12}(\mathbf{L}^{\mathbf{DMAPH}})_{24}(BF_4)_{43}]^{5+}$	3140.3793	3140.4029
$[Pd_{12}(\mathbf{L}^{\mathbf{DMAPH}})_{24}(BF_4)_{42}]^{6+}$	2602.4820	2602.4879
$[Pd_{12}(\mathbf{L}^{\mathbf{DMAPH}})_{24}(BF_4)_{41}]^{7+}$	2218.4126	2218.4129
$[Pd_{12}(\mathbf{L}^{\mathbf{DMAPH}})_{24}(BF_4)_{40}]^{8+}$	1930.2356	1930.2337
$[Pd_{12}(\mathbf{L}^{\mathbf{DMAPH}})_{24}(BF_4)_{39}]^{9+}$	1706.0977	1706.0965
$[Pd_{12}(\mathbf{L}^{\mathbf{DMAPH}})_{24}(BF_4)_{38}]^{10+}$	1526.7877	1526.7873
$[Pd_{12}(\mathbf{L}^{\mathbf{DMAPH}})_{24}(BF_4)_{37}]^{11+}$	1380.0793	1380.0796
$[Pd_{12}(\mathbf{L}^{\mathbf{DMAPH}})_{24}(BF_4)_{36}]^{12+}$	1257.9056	1257.9070
$[Pd_{12}(\mathbf{L}^{\mathbf{DMAPH}})_{24}(BF_4)_{35}]^{13+}$	1154.4511	1154.4507
$[Pd_{12}(\mathbf{L}^{\mathbf{DMAPH}})_{24}(BF_4)_{34}]^{14+}$	1065.7756	1065.7756

Table S2. Zoom into different charged species of $[Pd_{12}(\mathbf{L}^{\mathbf{DMAPH}})_{24}]^{n+}$ assembly.

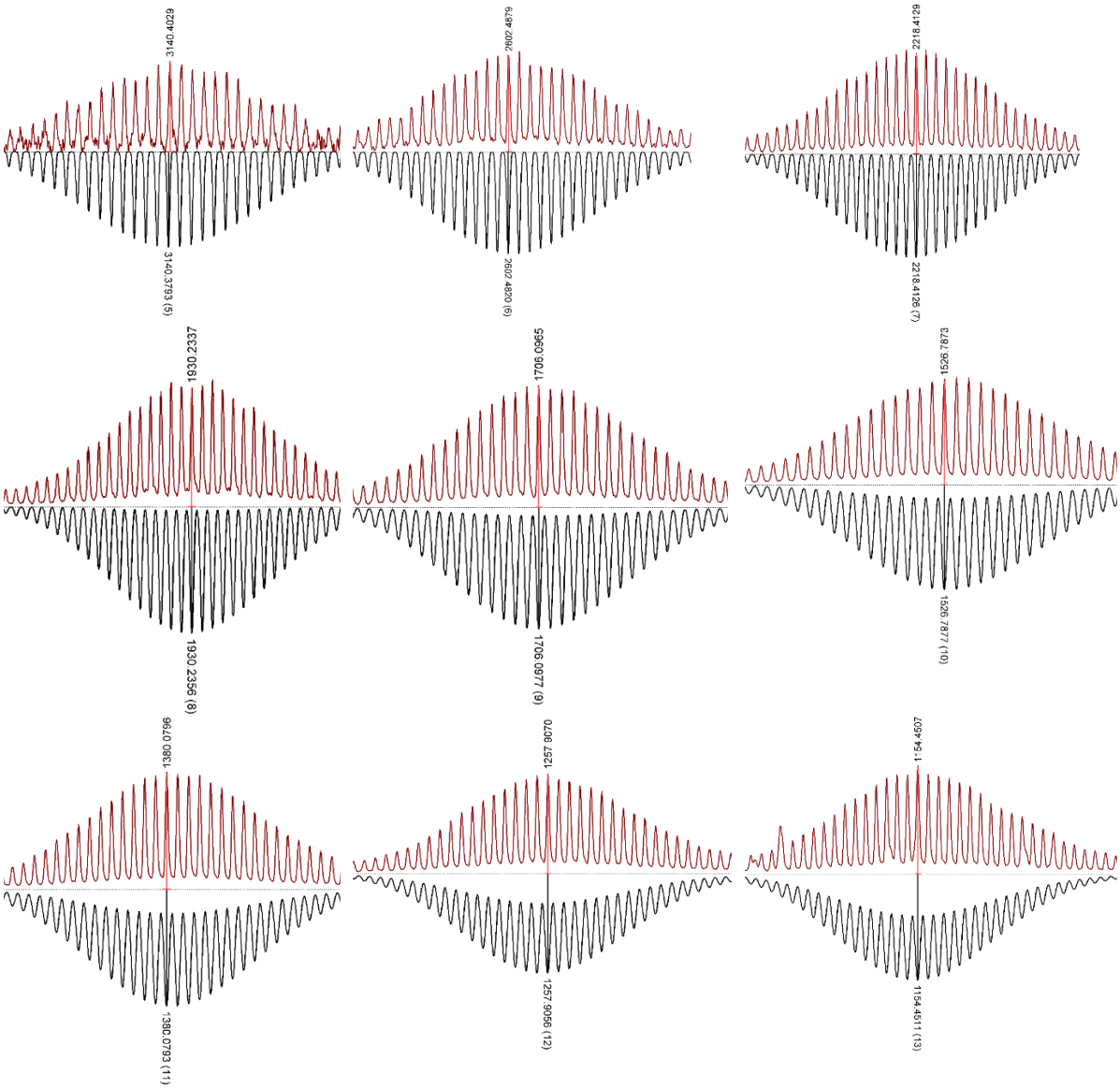

<u>$Pd_{12}\mathbf{L}^{\mathbf{ProMeH}}{}_{24}$</u>

According to the general procedure, 4.5 mg (10 mmol, 1 eq.) $\mathbf{L}^{\mathbf{ProMe}}$, 1.83 mg (11 mmol, 1.1 eq.) pyridinium tetrafluoroborate and 2.44 mg (5.5 mmol, 0.55 eq.) $[Pd(BF_4)_2(MeCN)_4]$ were utilized for the preparation of the self-assembly. ^{1}H NMR (300 MHz, Acetonitrile-d_3) δ 9.11 (m, 4H), 8.05 (s_{br}, 1H), 7.69 (m, 8H), 7.26 (m, 1H), 4.72 (s, 1H), 4.46 (m, 2H), 3.91 (s, 2H), 3.47 (s, 2H), 3.14 (m, 3H), 2.52 (s, 1H). *log D* (300 K; Acetonitrile-d_3) = -9.34; *d* = 2.9 nm.

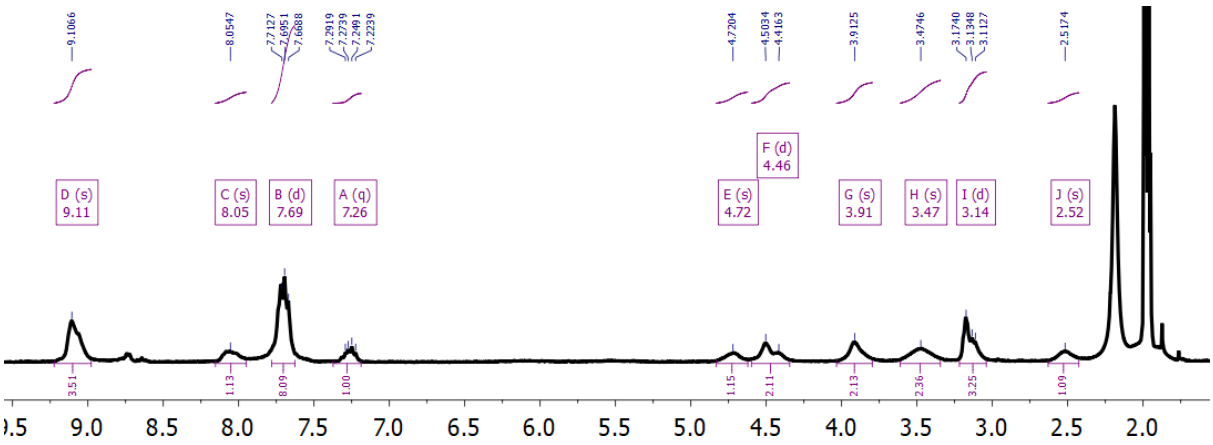

Figure S32. [$Pd_{12}\mathbf{L}^{\mathbf{ProMeH}}{}_{24}$] assembly, ^{1}H NMR in MeCN-d_3.

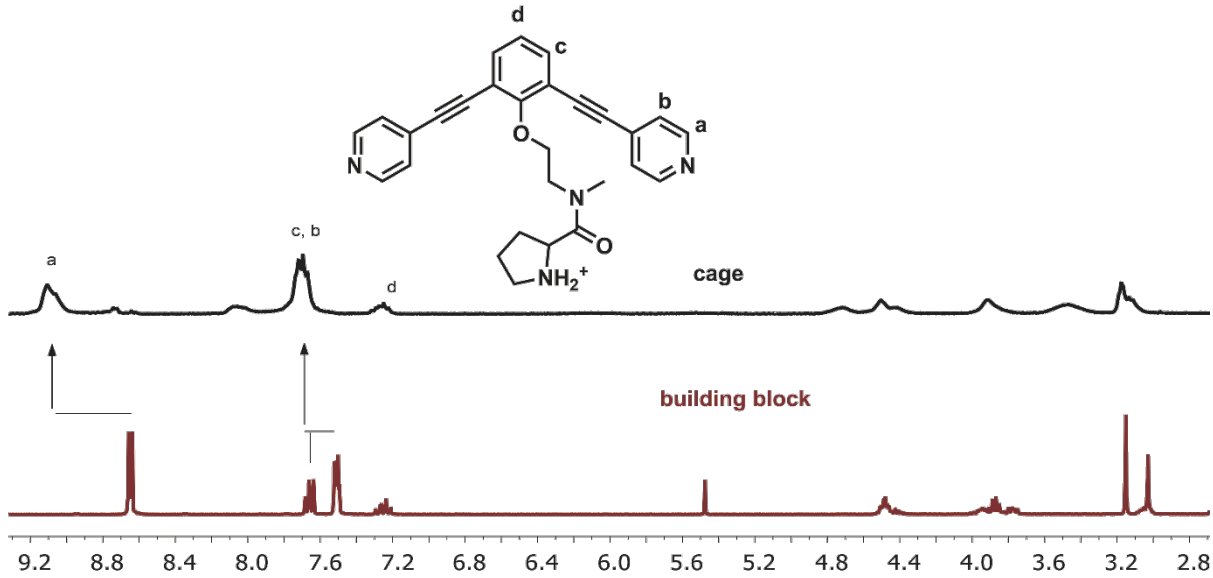

Figure S33. [$Pd_{12}\mathbf{L}^{\mathbf{ProMeH}}{}_{24}$] assembly (top) and free building block $\mathbf{L}^{\mathbf{ProMe}}$ (bottom), ^{1}H NMR in MeCN-d_3.

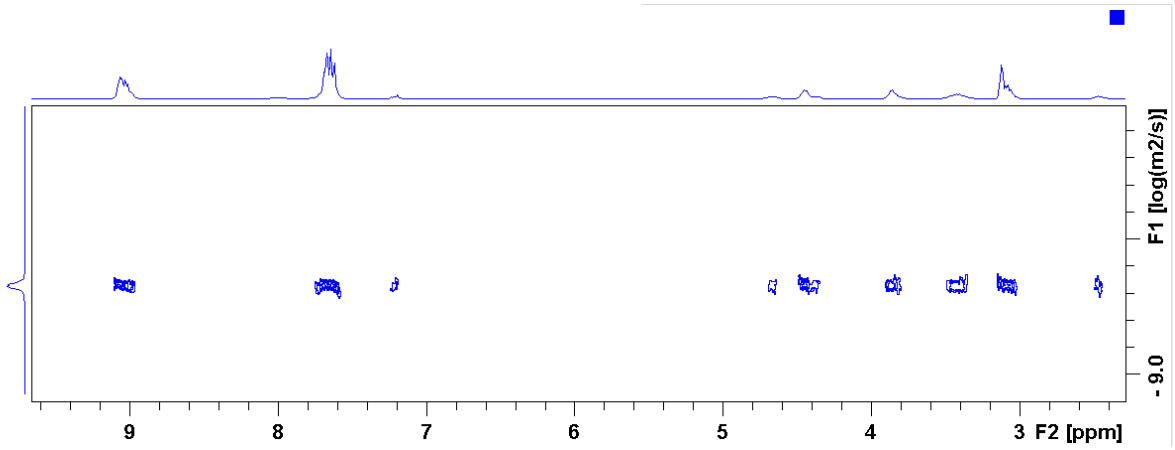

Figure S34. [$Pd_{12}\mathbf{L}^{\mathbf{ProMeH}}{}_{24}$] assembly, DOSY NMR in MeCN-d_3 at 300K.

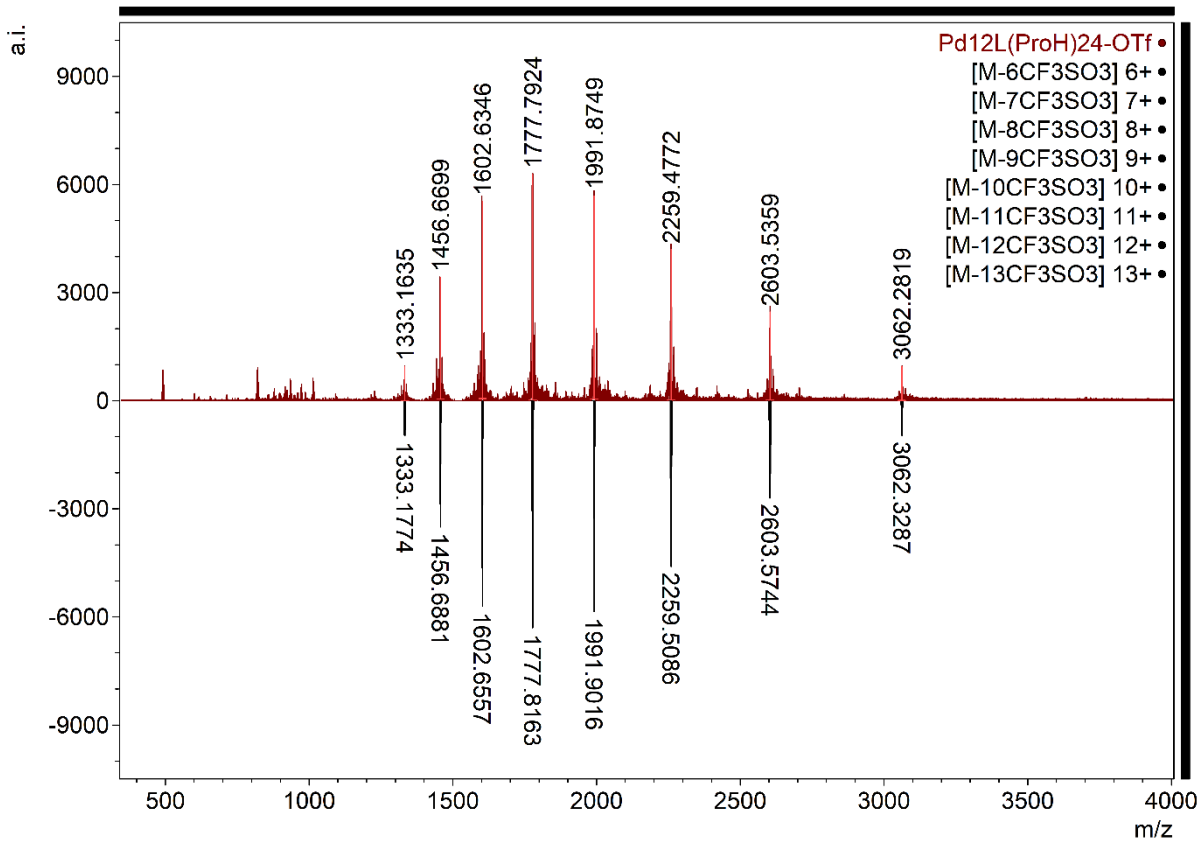

Figure S35. $[Pd_{12}\mathbf{L}^{\mathbf{ProMeH}}{}_{24}]$ assembly, full HR-ESI MS spectrum, top measured; bottom, simulated spectra of different charged states of the self-assembly.

Table S3. Calculated and observed species of the $[Pd_{12}(\mathbf{L}^{\mathbf{ProMeH}})_{24}]^{48+}$ assembly.

Composition	Calculated	Observed
$[Pd_{12}(\mathbf{L}^{\mathbf{ProMeH}})_{24}(OTf)_{42}]^{6+}$	3062.3287	3140.4029
$[Pd_{12}(\mathbf{L}^{\mathbf{ProMeH}})_{24}(OTf)_{41}]^{7+}$	2603.5744	2602.4879
$[Pd_{12}(\mathbf{L}^{\mathbf{ProMeH}})_{24}(OTf)_{40}]^{8+}$	2259.5086	2218.4129
$[Pd_{12}(\mathbf{L}^{\mathbf{ProMeH}})_{24}(OTf)_{39}]^{9+}$	1991.9016	1930.2337
$[Pd_{12}(\mathbf{L}^{\mathbf{ProMeH}})_{24}(OTf)_{38}]^{10+}$	1777.8163	1706.0965
$[Pd_{12}(\mathbf{L}^{\mathbf{ProMeH}})_{24}(OTf)_{37}]^{11+}$	1602.6557	1526.7873
$[Pd_{12}(\mathbf{L}^{\mathbf{ProMeH}})_{24}(OTf)_{36}]^{12+}$	1456.6881	1380.0796
$[Pd_{12}(\mathbf{L}^{\mathbf{ProMeH}})_{24}(OTf)_{35}]^{13+}$	1333.1774	1257.9070

Table S4. Zoom into different charged species of $[Pd_{12}(\mathbf{L}^{\mathbf{ProMeH}})_{24}]^{n+}$ assembly.

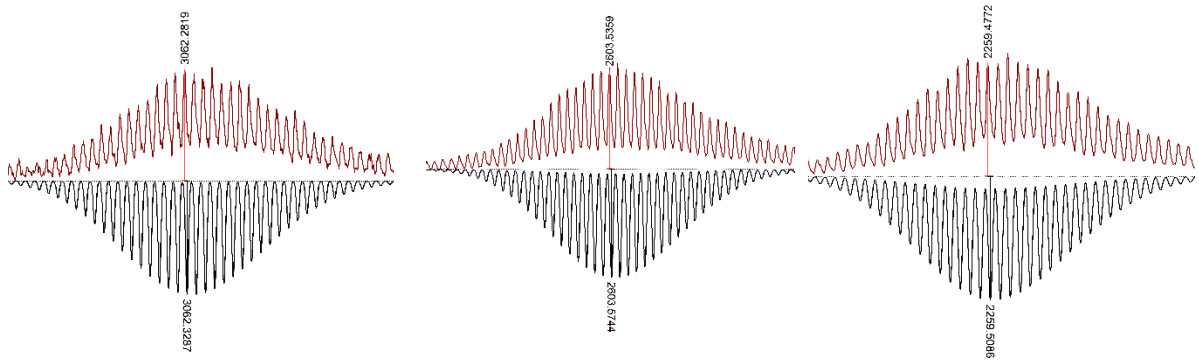

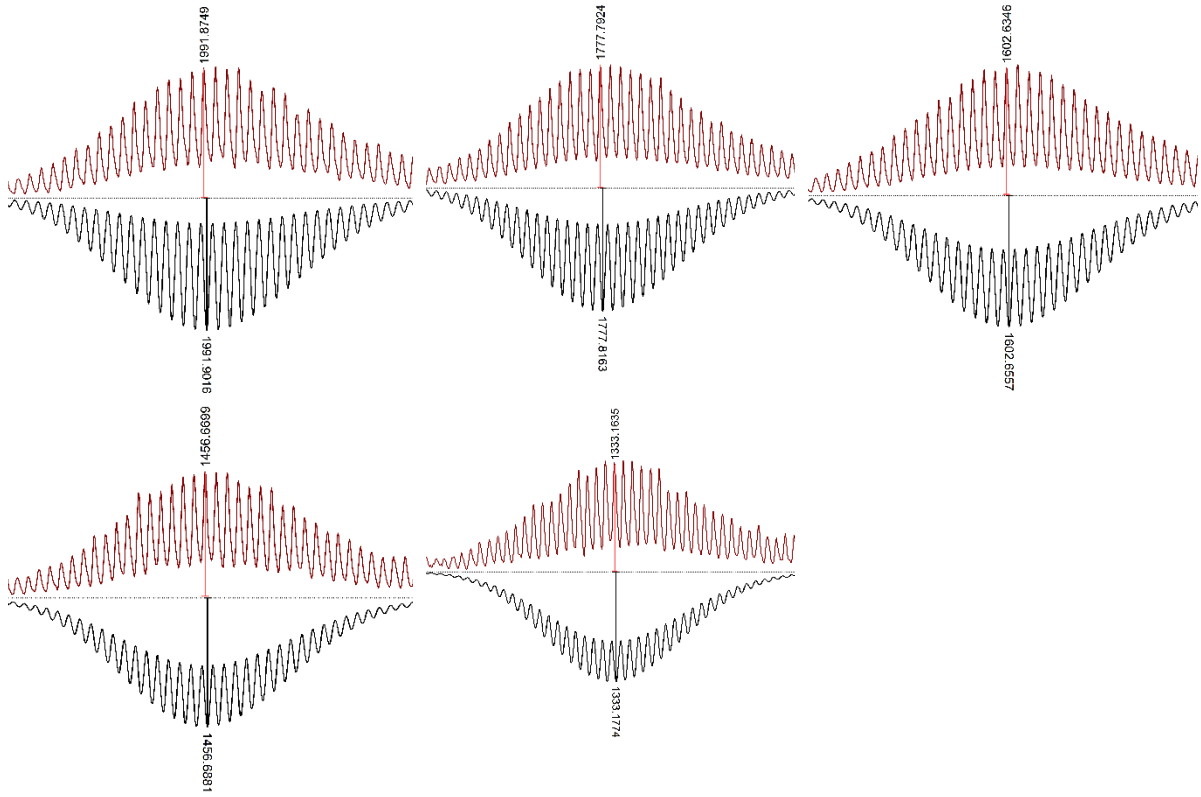

$\underline{Pd_{12}\mathbf{L^{4ProMeH}}_{24}}$

According to the general procedure, 4.8 mg (10 mmol, 1 eq.) $\mathbf{L^{4ProMe}}$, 1.83 mg (11 mmol, 1.1 eq.) pyridinium tetrafluoroborate and 2.44 mg (5.5 mmol, 0.55 eq.) $[Pd(BF_4)_2(MeCN)_4]$ were utilized for the preparation of the self-assembly. ^{1}H NMR (300 MHz, Acetonitrile-d_3) δ 9.08 (s, 4H), 7.68 (m, 6H), 7.25 (s_{br}, 1H), 4.69 (s, 1H), 4.34 (s, 2H), 3.48 (s, 4H), 2.99 (m, 1H), 2.78 (s, 1H), 2.54 (s, 1H). *log D* (300 K; Acetonitrile-d_3) = -9.42; d = 3.5 nm.

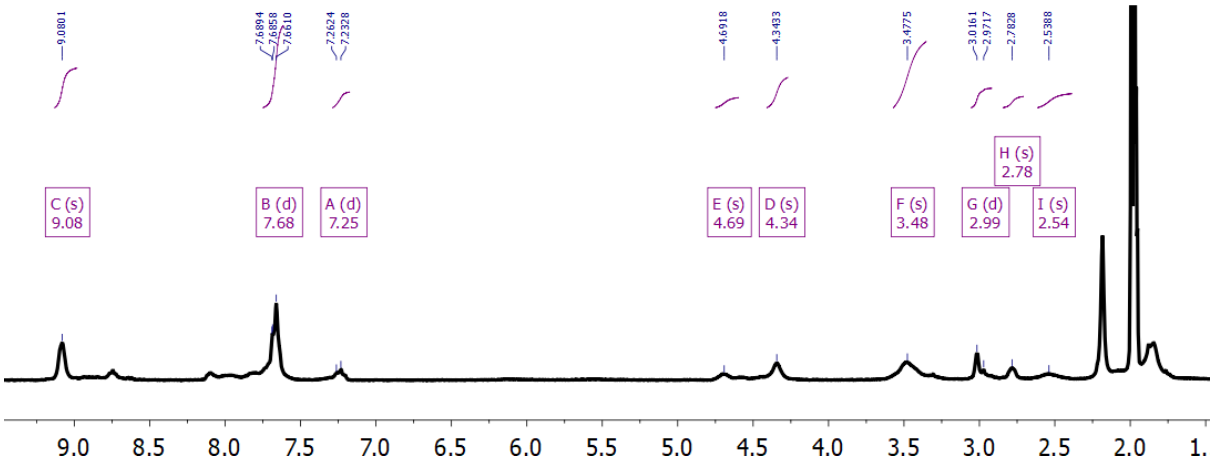

Figure S36. $[Pd_{12}\mathbf{L^{4ProMeH}}_{24}]$ assembly, ^{1}H NMR in MeCN-d_3 at 300K.

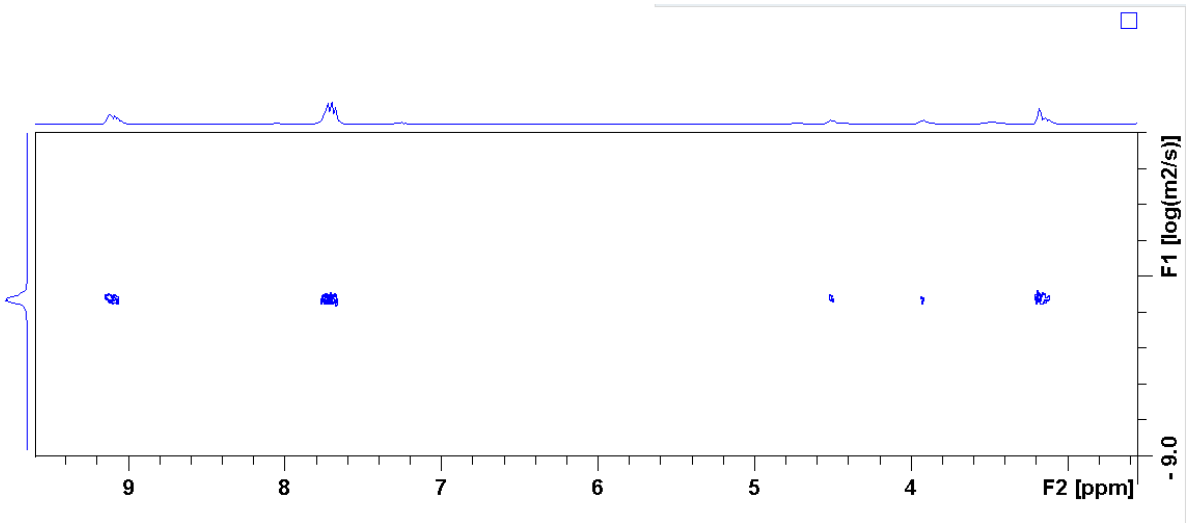

Figure S37. [Pd_{12}**L**$^{\mathbf{4ProMeH}}{}_{24}$] assembly, DOSY NMR in MeCN-d_3 at 300K.

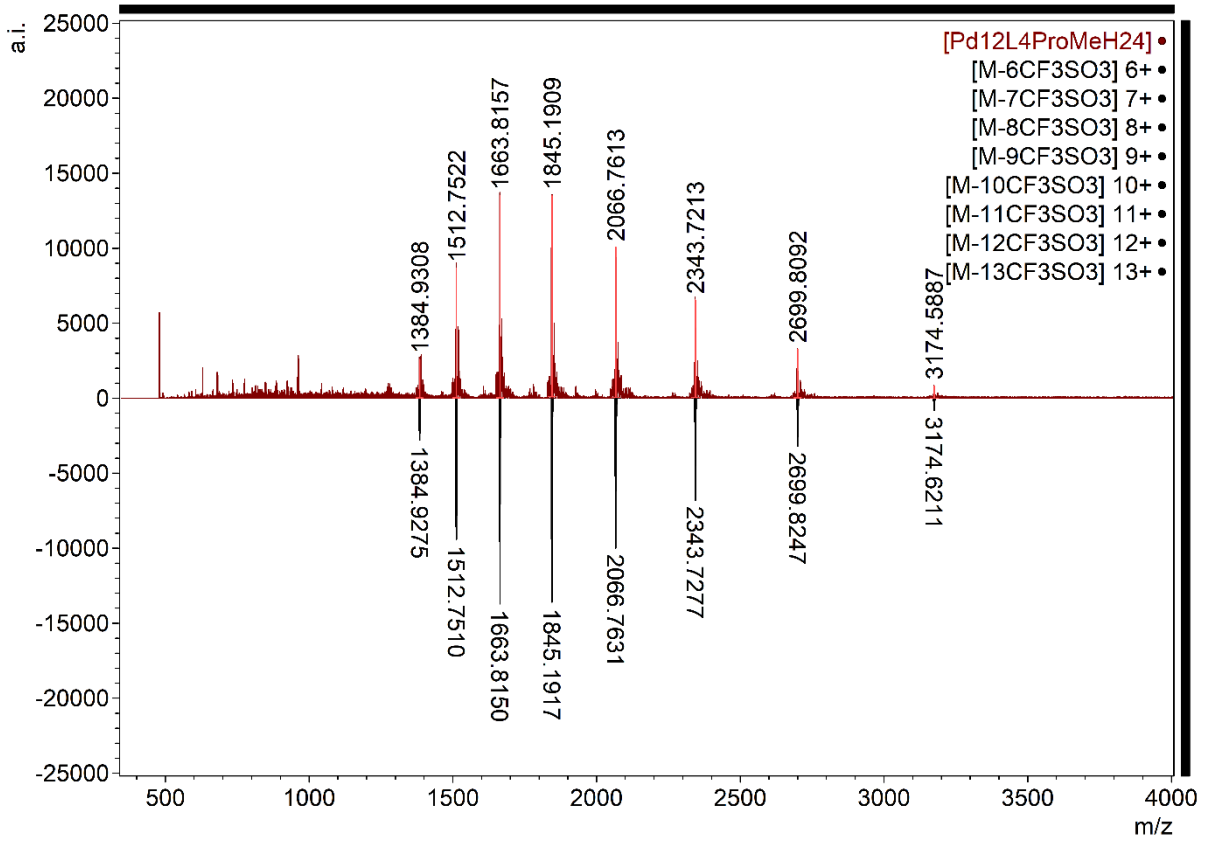

Figure S38. [Pd_{12}**L**$^{\mathbf{4ProMeH}}{}_{24}$] assembly, full HR-ESI MS spectrum, top measured; bottom, simulated spectra of different charged states of the self-assembly.

Table S5. Calculated and observed species of the $[Pd_{12}(\mathbf{L^{4ProMeH}})_{24}]^{48+}$ assembly.

Composition	Calculated	Observed
$[Pd_{12}(\mathbf{L^{4ProMeH}})_{24}(OTf)_{42}]^{6+}$	3174.6211	3174.5887
$[Pd_{12}(\mathbf{L^{4ProMeH}})_{24}(OTf)_{41}]^{7+}$	2699.8247	2699.8092
$[Pd_{12}(\mathbf{L^{4ProMeH}})_{24}(OTf)_{40}]^{8+}$	2343.7277	2343.7213
$[Pd_{12}(\mathbf{L^{4ProMeH}})_{24}(OTf)_{39}]^{9+}$	2066.7631	2066.7613
$[Pd_{12}(\mathbf{L^{4ProMeH}})_{24}(OTf)_{38}]^{10+}$	1845.1917	1845.1909
$[Pd_{12}(\mathbf{L^{4ProMeH}})_{24}(OTf)_{37}]^{11+}$	1663.8150	1663.8157
$[Pd_{12}(\mathbf{L^{4ProMeH}})_{24}(OTf)_{36}]^{12+}$	1512.7510	1512.7522
$[Pd_{12}(\mathbf{L^{4ProMeH}})_{24}(OTf)_{35}]^{13+}$	1384.9275	1384.9308

Table S6. Zoom into different charged species of $[Pd_{12}(\mathbf{L^{4ProMeH}})_{24}]^{n+}$ assembly.

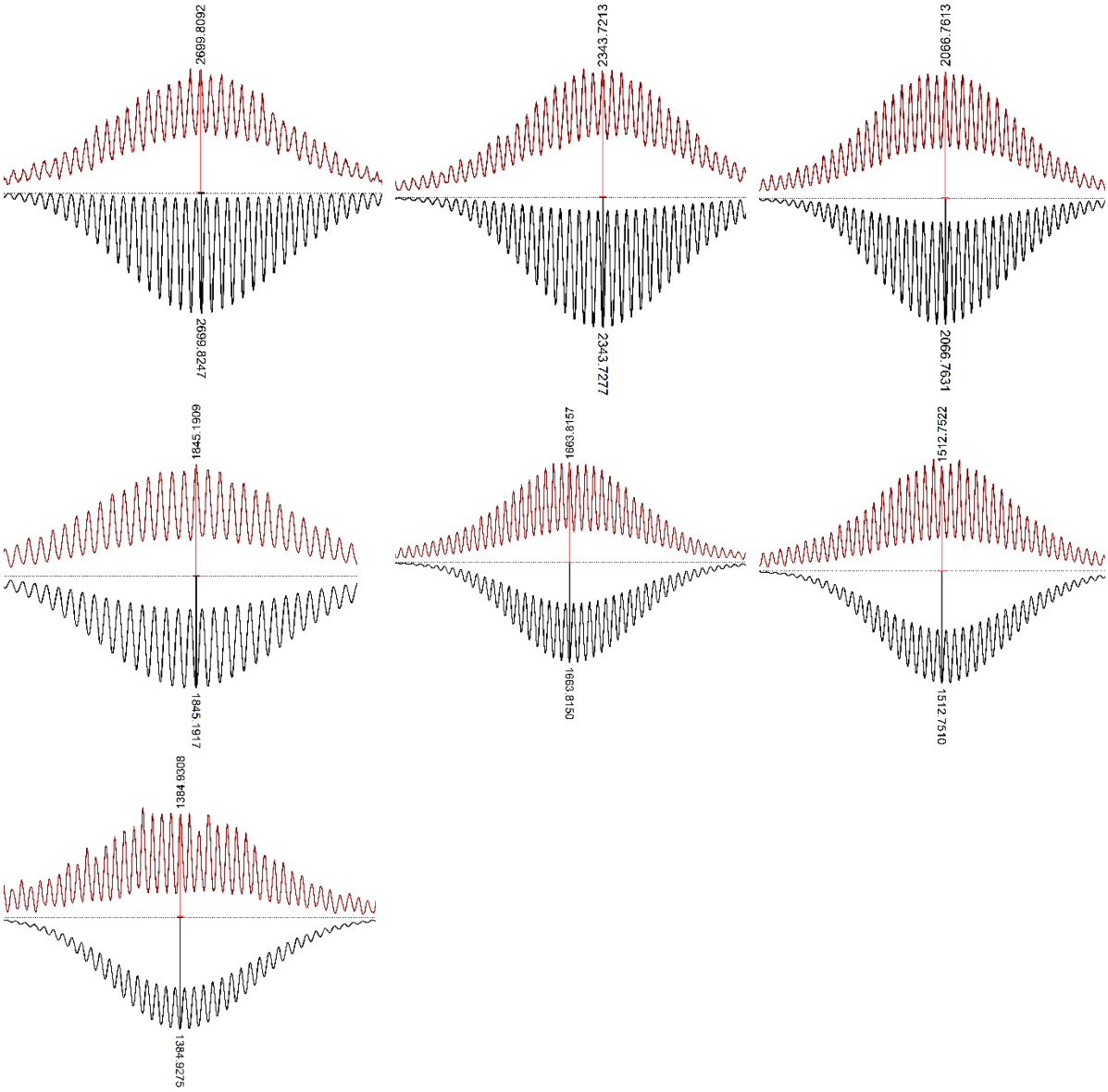

$\underline{Pd_{12}\mathbf{L}^{\mathbf{ProH}}{}_{24}}$

According to the general procedure, 4.36 mg (10 µmol, 1 eq.) $\mathbf{L}^{\mathbf{Pro}}$, 1.83 mg (11 µmol, 1.1 eq.) pyridinium tetrafluoroborate and 2.44 mg (5.5 µmol, 0.55 eq.) $[Pd(BF_4)_2(MeCN)_4]$ were utilized for the preparation of the self-assembly. ^{1}H NMR (400 MHz, Acetonitrile-d_3) δ 9.02 (d, J = 5.7 Hz, 4H), 7.70 (m, 7H), 7.26 (m, 1H), 4.80 (m, 1H), 4.50 (m, 2H), 3.80 (m, 2H), 3.65 (m, 2H), 3.29 (m, 1H). *log D* (300 K; Acetonitrile-d_3) = -9.52; d = 4.4 nm.

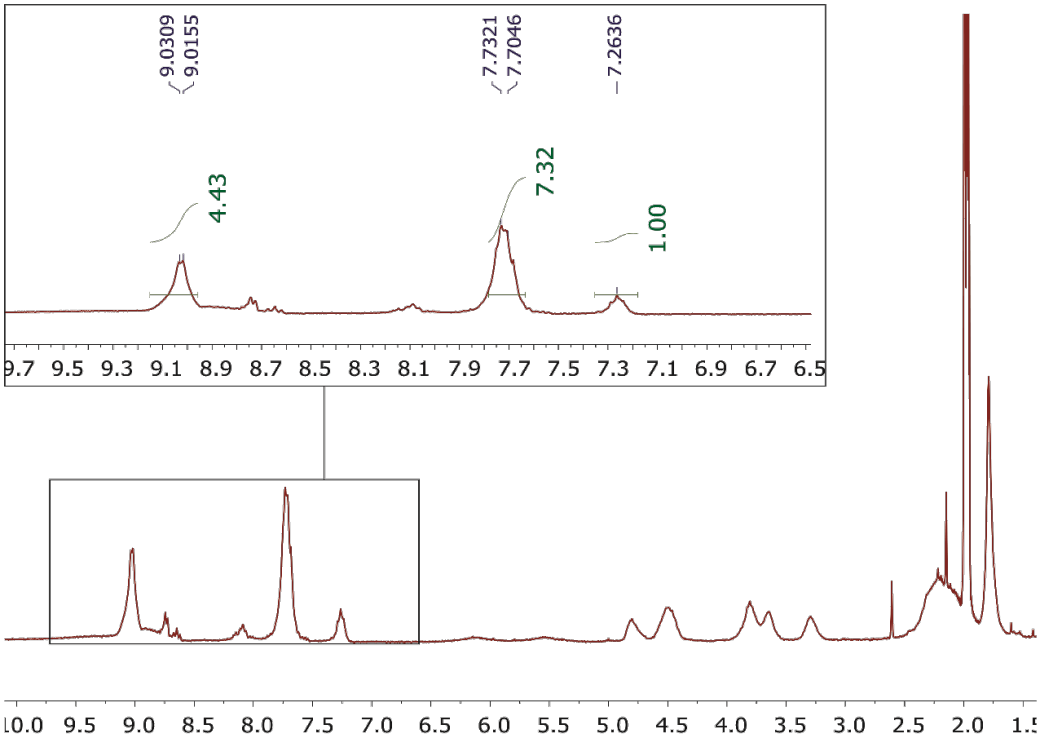

Figure S39. $[Pd_{12}L^{ProH}{}_{24}]$ assembly, ^{1}H NMR in MeCN-d_3.

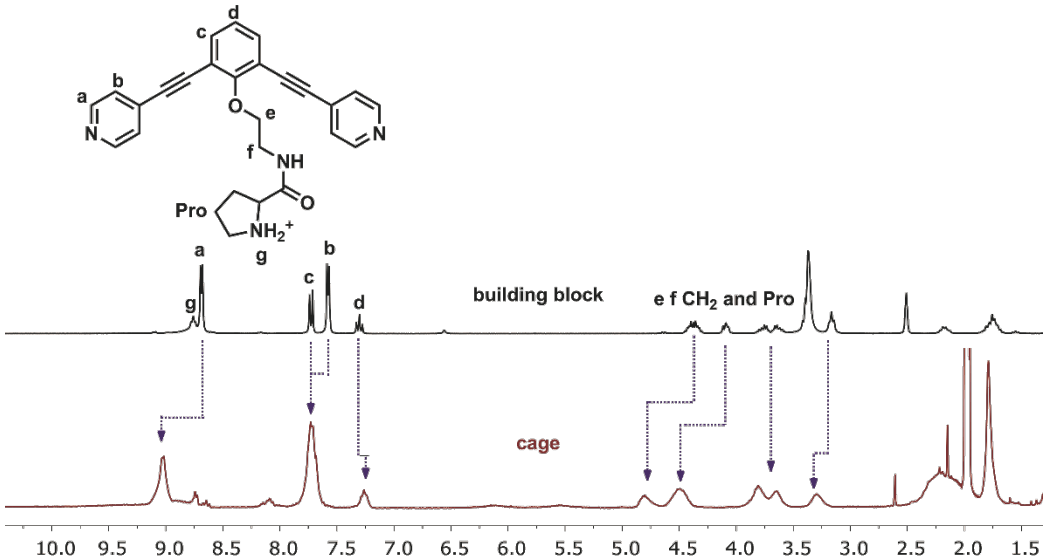

Figure S40. $[Pd_{12}L^{ProH}{}_{24}]$ assembly (bottom) and L^{ProH} building block (top).

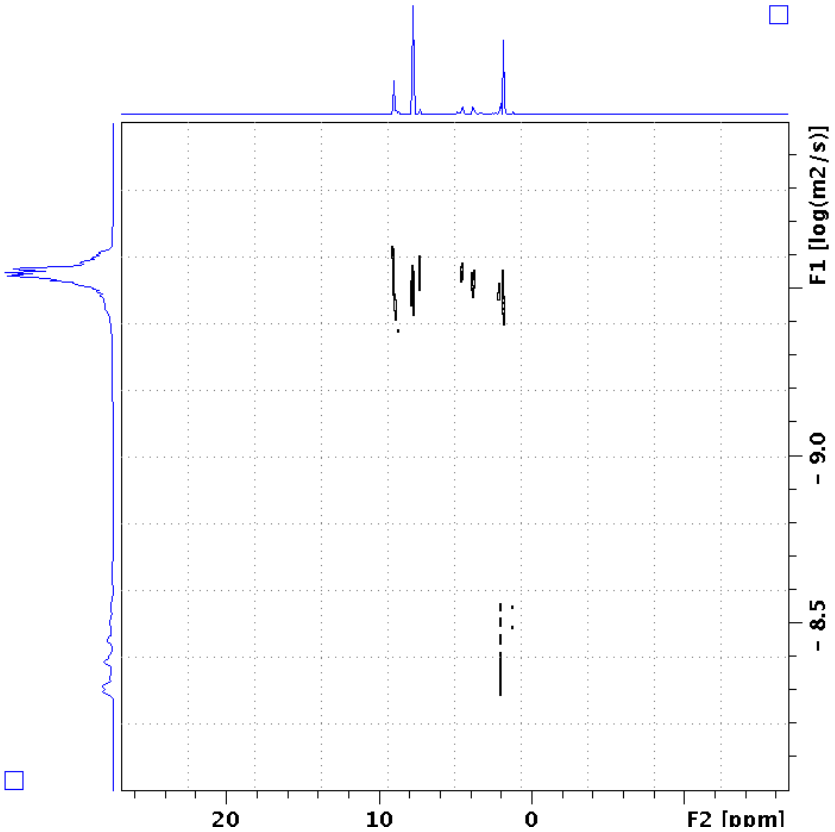

Figure S41. $[Pd_{12}\mathbf{L}^{\mathbf{ProH}}{}_{24}]$ assembly, DOSY NMR in MeCN-d_3 at 300K.

$\underline{Pd_{12}\mathbf{L}^{\mathbf{NMeH}}{}_{24}}$

According to the general procedure, 4.41 mg (10 µmol, 1 eq.) $\mathbf{L}^{\mathbf{NMeH}}$ and 2.44 mg (5.5 µmol, 0.55 eq.) $[Pd(BF_4)_2(MeCN)_4]$ were utilized for the preparation of the self-assembly. ^{1}H NMR (300 MHz, Acetonitrile-d_3) δ 8.94 (m, 4H), 7.73 (m, 6H), 7.31 (t, J = 7.7 Hz, 1H), 7.03 (s_{br}, 2H), 4.51 (s_{br}, 2H), 3.58 (s_{br}, 2H), 3.00 (s, 3H). *log D* (300 K; Acetonitrile-d_3) = -9.50; d = 4.21 nm.

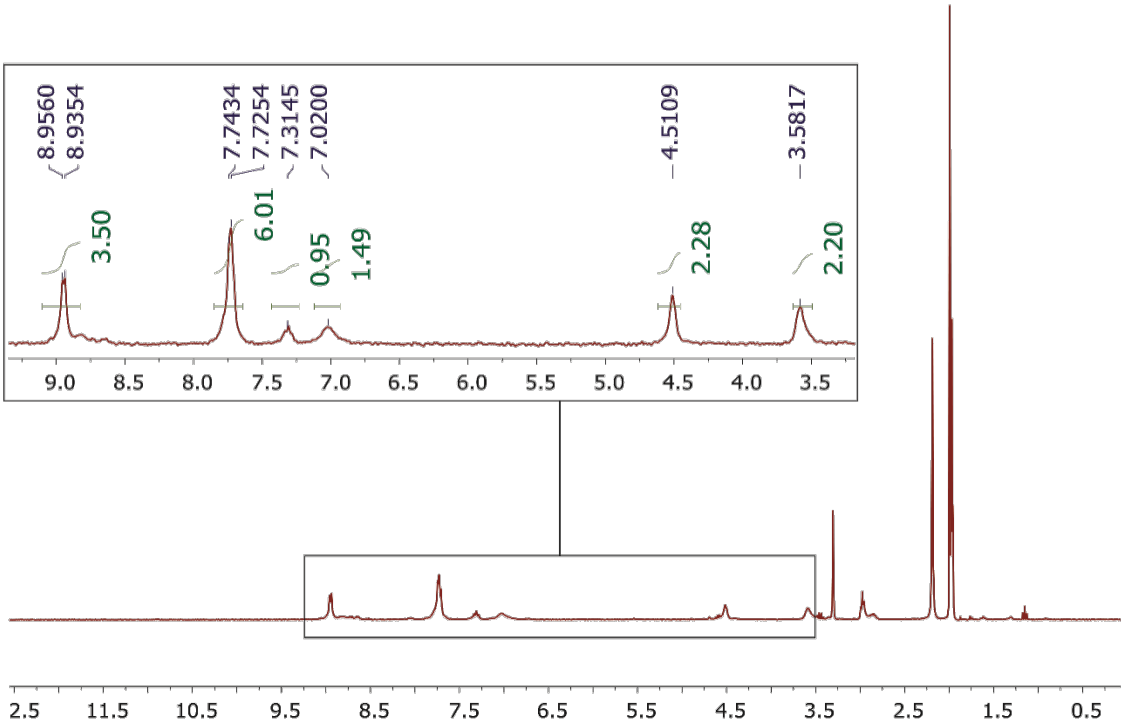

Figure S42. $[Pd_{12}L^{NMeH}{}_{24}]$ assembly, ^{1}H NMR in MeCN-d_3.

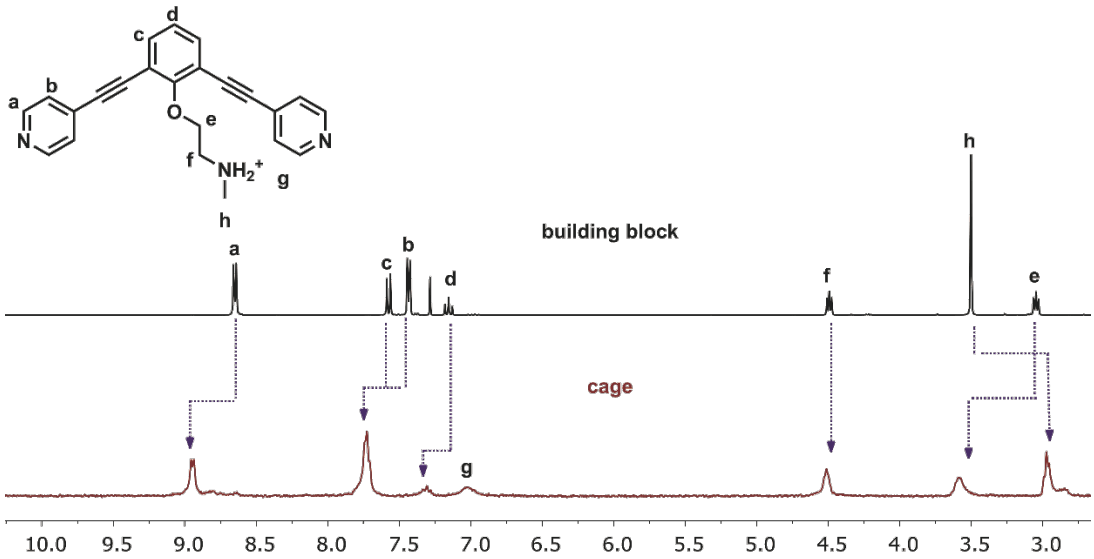

Figure S43. $[Pd_{12}L^{NMeH}{}_{24}]$ assembly (bottom) and L^{NMe} building block (top).

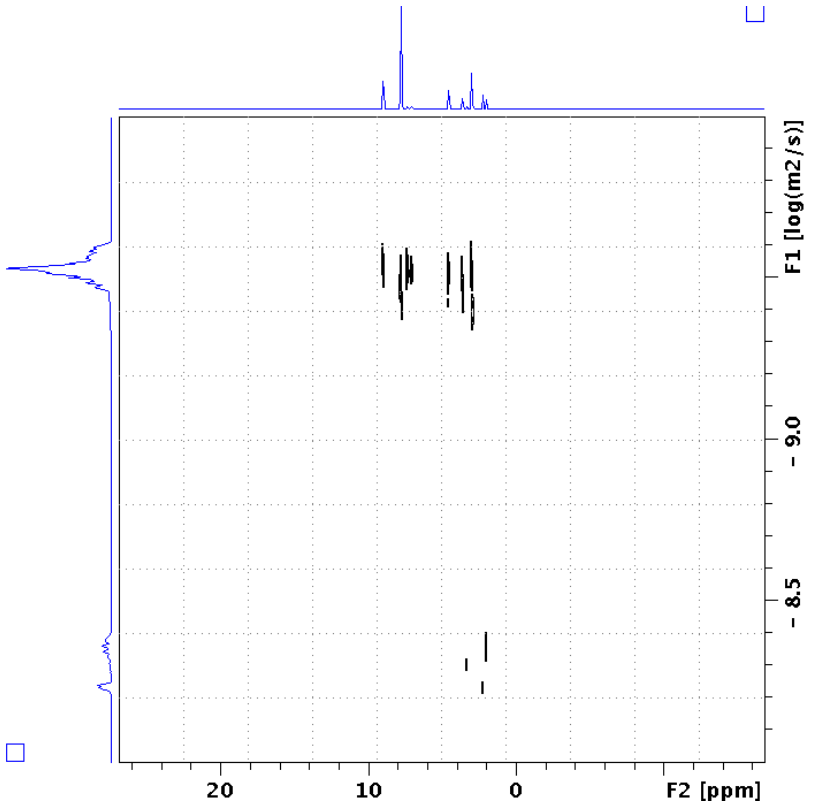

Figure S44. $[Pd_{12}\mathbf{L}^{\mathbf{NMeH}}{}_{24}]$ assembly, DOSY NMR in MeCN-d_3 at 300K.

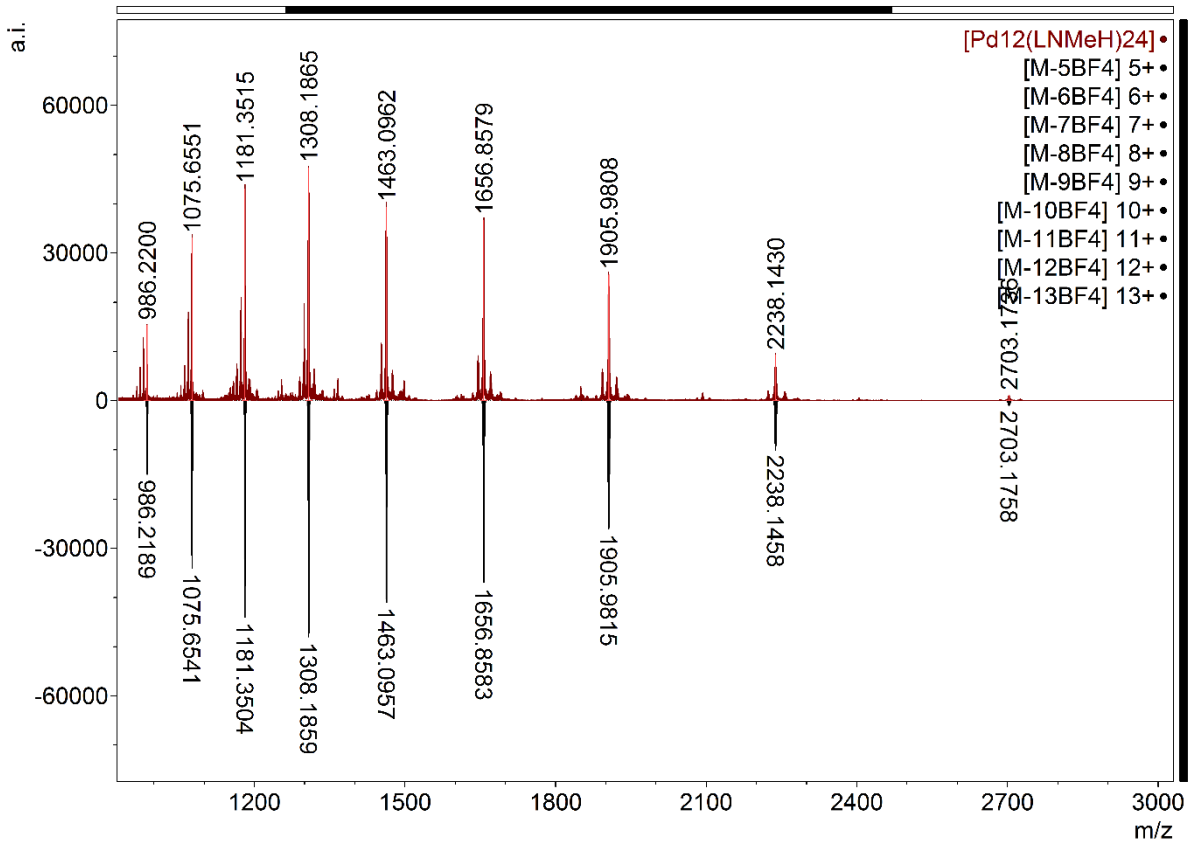

Figure S45. $[Pd_{12}\mathbf{L}^{\mathbf{NMeH}}{}_{24}]$ assembly, full HR-ESI MS spectrum, top measured; bottom, simulated spectra of different charged states of the self-assembly.

Table S7. Calculated and observed species of the $[Pd_{12}(\mathbf{L^{NMeH}})_{24}]^{48+}$ assembly.

Composition	Calculated	Observed
$[Pd_{12}(\mathbf{L^{NMeH}})_{24}(BF_4)_{43}]^{5+}$	2703.1758	2703.1736
$[Pd_{12}(\mathbf{L^{NMeH}})_{24}(BF_4)_{42}]^{6+}$	2238.1458	2238.1430
$[Pd_{12}(\mathbf{L^{NMeH}})_{24}(BF_4)_{41}]^{7+}$	1905.9815	1905.9808
$[Pd_{12}(\mathbf{L^{NMeH}})_{24}(BF_4)_{40}]^{8+}$	1656.8583	1656.8579
$[Pd_{12}(\mathbf{L^{NMeH}})_{24}(BF_4)_{39}]^{9+}$	1463.0957	1463.0962
$[Pd_{12}(\mathbf{L^{NMeH}})_{24}(BF_4)_{38}]^{10+}$	1308.1859	1308.1865
$[Pd_{12}(\mathbf{L^{NMeH}})_{24}(BF_4)_{37}]^{11+}$	1181.3504	1181.3515
$[Pd_{12}(\mathbf{L^{NMeH}})_{24}(BF_4)_{36}]^{12+}$	1075.6541	1075.6551
$[Pd_{12}(\mathbf{L^{NMeH}})_{24}(BF_4)_{35}]^{13+}$	986.2189	986.2200

Table S8. Zoom into different charged species of $[Pd_{12}(\mathbf{L^{ProH}})_{24}]^{n+}$ assembly.

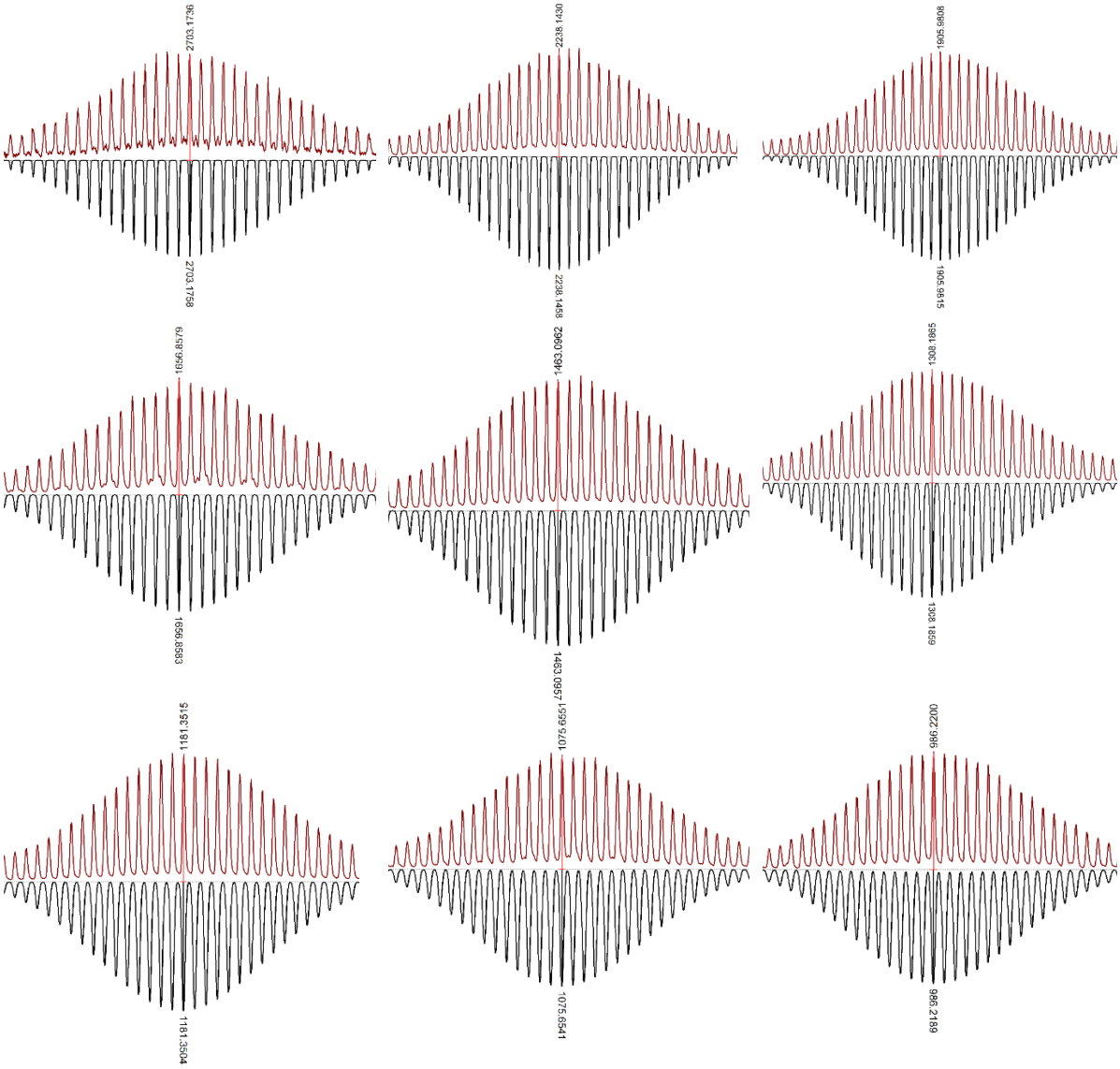

Coordinative post-modification (SI3)

The post-modification approach relies on deprotonation of protonated interior ligand and coordination to a second TSM. We first attempted to perform the post-synthetic modification step wise (i.e., first deprotonation and thereafter coordination). Deprotonation performed at room temperature led to ill-defined materials. Deprotonation at -36°C and heating up the solution to room temperature leads also to decomposition of the nanosphere. Exemplary, ^{1}H-NMR and ESI-MS of "deprotonated" $Pd_{12}\mathbf{L}^{\mathbf{DMAP}}{}_{24}$ were recorded immediately after deprotonation and heating up to room temperature. ^{1}H-NMR displays ill-defined species Fig. S46 (similar to nanosphere formation when non-protonated building block is used, compare Fig. S27). ESI-MS shows no nanosphere present and only oligomeric little charged materials (charge = 2^+ for most species). Although the step wise procedure does not work, it demonstrates that the interior can be successfully deprotonated. For the selective post-assembly modification, we followed a one pot procedure described below.

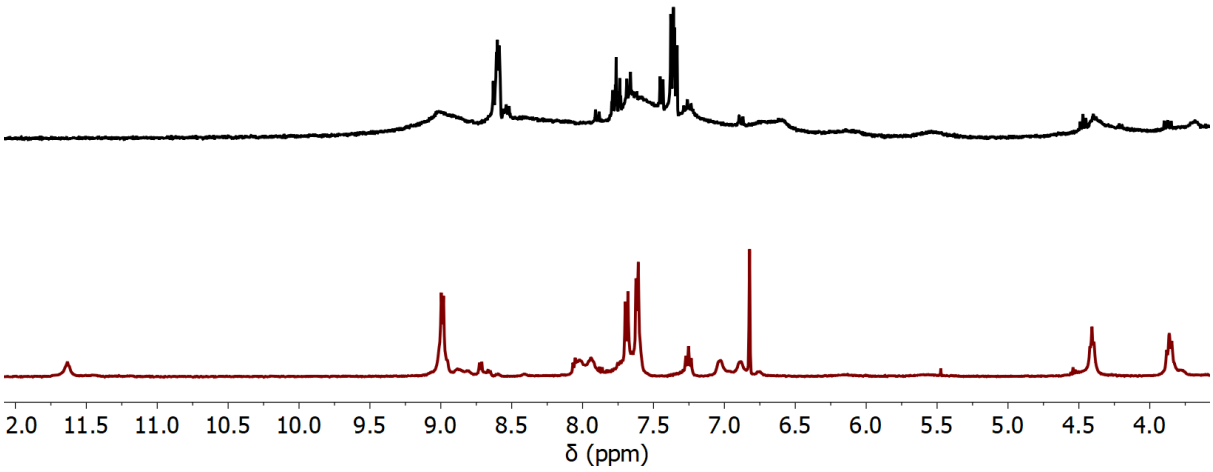

Figure S46. $[Pd_{12}\mathbf{L}^{\mathbf{DMAPH}}{}_{24}]$ assembly (bottom), attempted deprotonation of $[Pd_{12}\mathbf{L}^{\mathbf{DMAPH}}{}_{24}]$ (top) after deprotonation -36°C and room temperature (ca. 15 min) showing no presence of nanosphere anymore, ^{1}H NMR in MeCN-d_3.

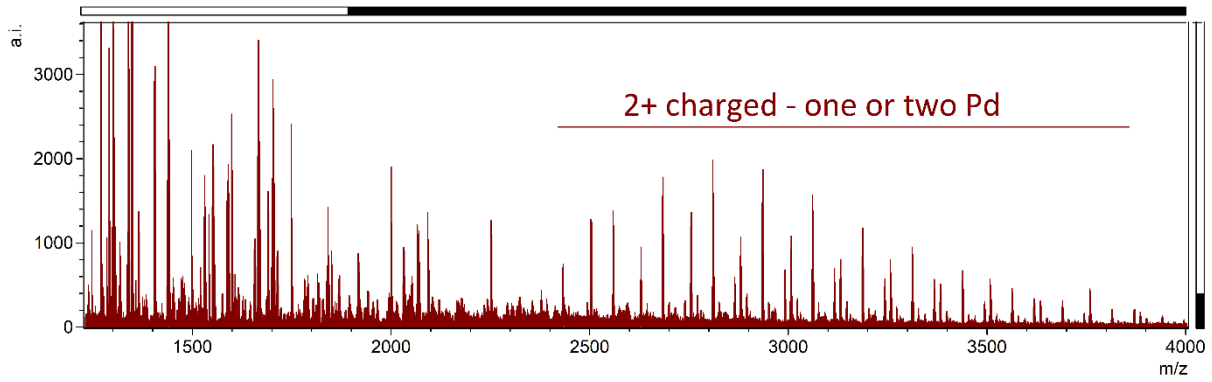

Figure S47. $[Pd_{12}\mathbf{L}^{\mathbf{DMAPH}}{}_{24}]$ assembly after deprotonation, full HR-ESI MS spectrum showing no presence of nanosphere anymore.

All self-assemblies were post-functionalized according to the following procedure: To a cooled 1mL solution (-36°C, dry ice, Methanol:H_2O; 4:6) of 0.416 µmol of sphere, 2.6 µmol of the required metal precursor (6 eq. per sphere for DMAP) or 3.5 µmol (8 eq. per sphere for Proline) were added. The solutions were stirred for 20 min before 1.1 eq. triethylamine per building block was added. The resulting solutions were stirred for 1h at -36°C, then at room temperature for 1h before being analyzed. Due to the paramagnetic nature of some of the applied transition metals, ^{1}H NMR and DOSY NMR can be shifted or broadened. The expected change in relaxation time furthermore complicates analysis with DOSY. MS analysis was especially hampered when different coordination modes are applicable or extra solvent/water coordination is allowed especially in case of **L^{Pro}** (since random loss/association of solvent is observed causing a tremendous broadening and splitting of the signals).

$Pd_{12}Cd_6$**L^{DMAP}**$_{24}$

According to the general procedure, 1.1 mg (2.6 µmol) $Cd(OTf)_2$ were utilized for the post-modification of the self-assembly. ^{1}H NMR (300 MHz, Acetonitrile-d_3) δ 9.03 (d, J = 6.1 Hz, 4H), 8.19 (d, J = 6.1 Hz, 2H), 7.70 (d, J = 7.8 Hz, 2H), 7.61 (d, J = 6.3 Hz, 4H), 7.25 (t, J = 7.8 Hz, 1H), 6.77 (d, J = 6.3 Hz, 2H), 4.39 (s, 2H), 3.85 (s, 2H). *log D* (300 K; Acetonitrile-d_3) = -9.54; d = 4.6 nm.

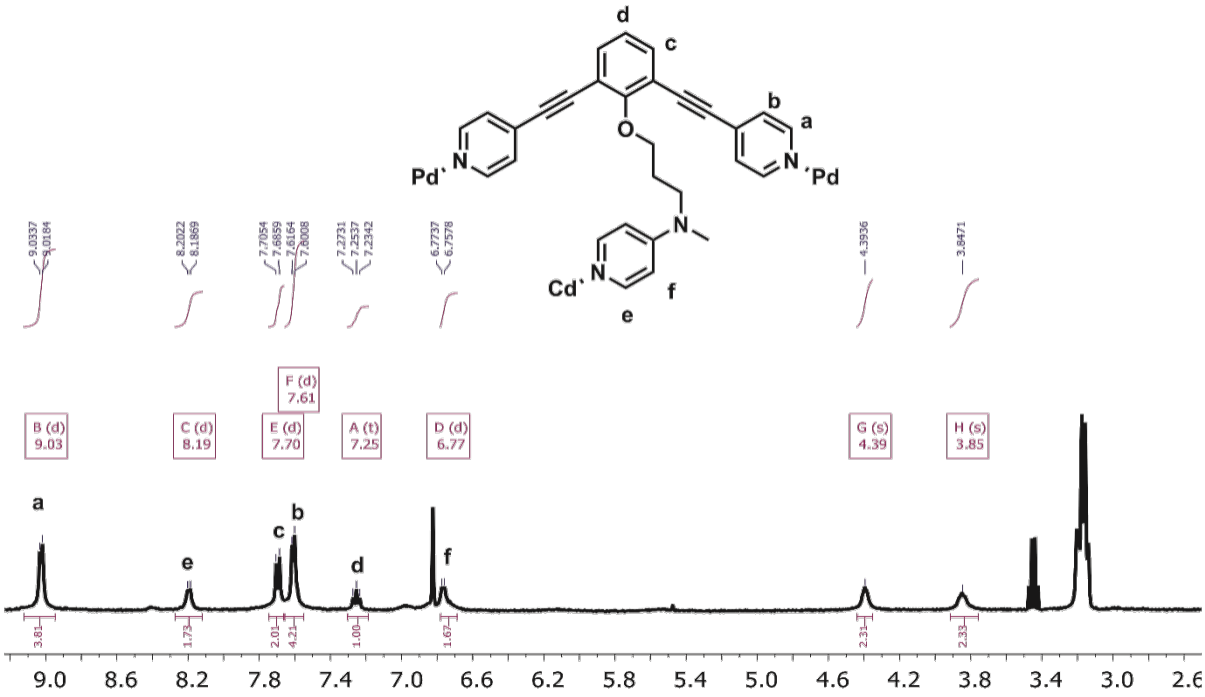

Figure S48. [Pd_{12}**L^{DMAP}**$_{24}Cd_6$] assembly, ^{1}H NMR in MeCN-d_3.

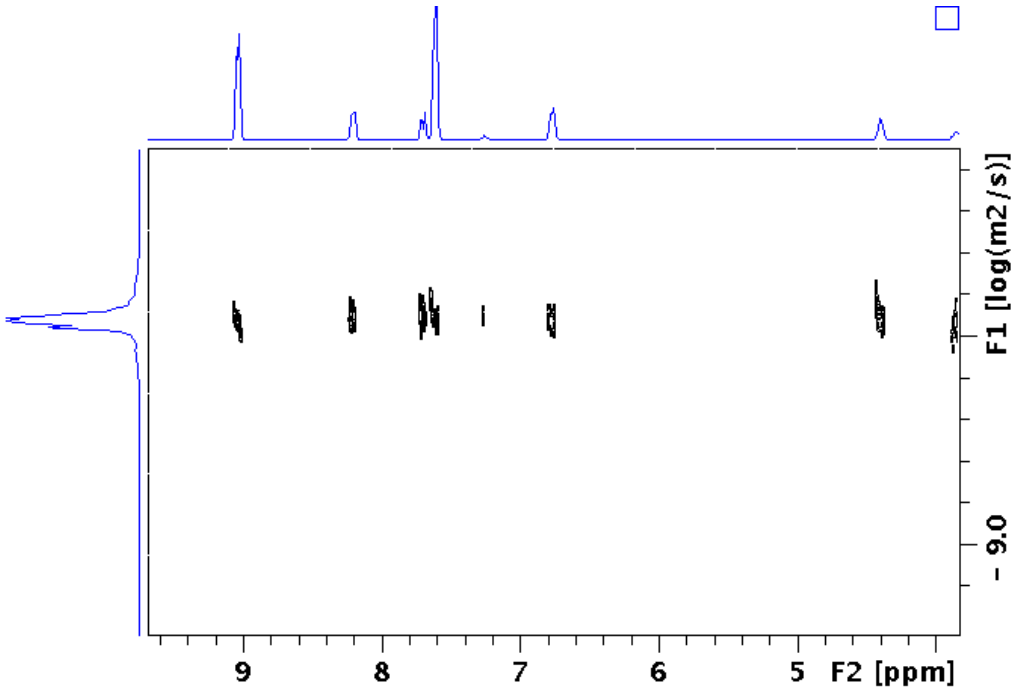

Figure S49. $[Pd_{12}\mathbf{L}^{\mathbf{DMAP}}{}_{24}Cd_6]$ assembly, DOSY NMR in MeCN-d_3 at 300K.

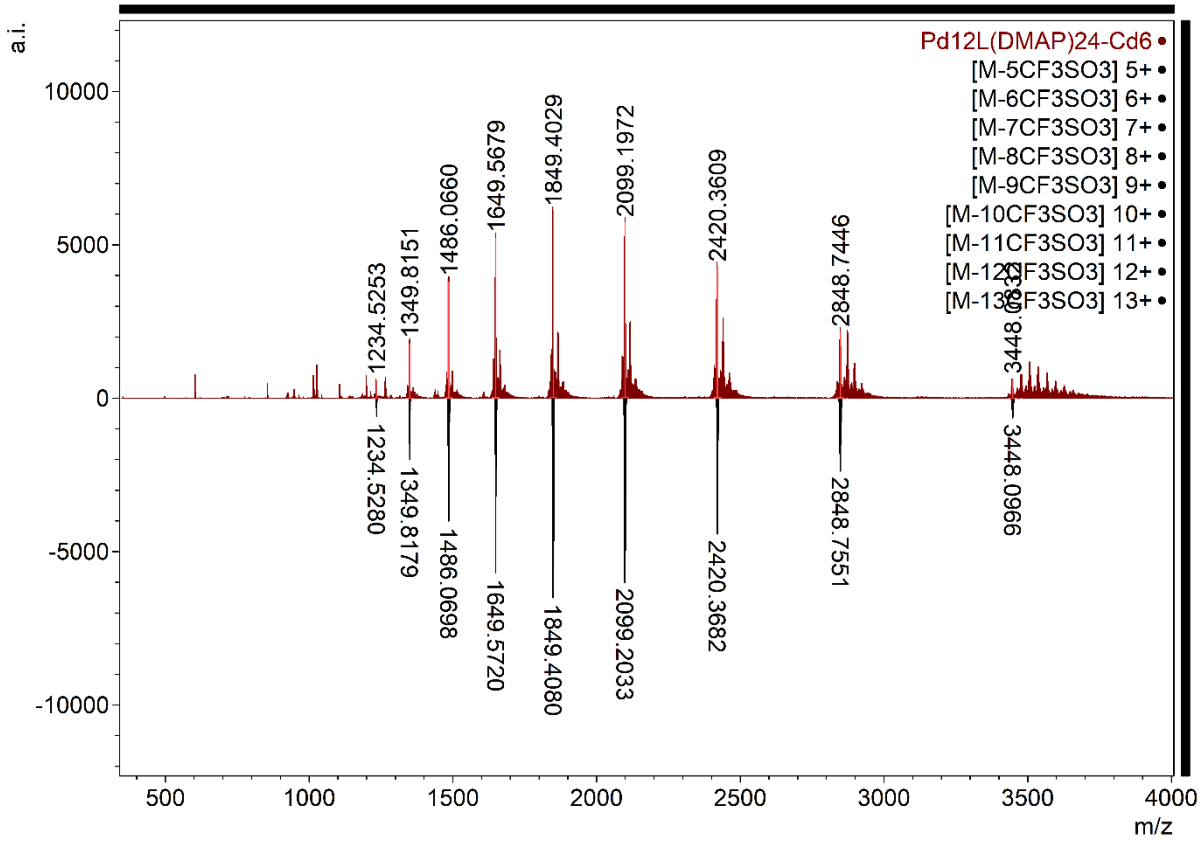

Figure S50. $[Pd_{12}\mathbf{L}^{\mathbf{DMAP}}{}_{24}Cd_6]$ assembly, full HR-ESI MS spectrum, top measured; bottom, simulated spectra of different charged states of the self-assembly.

Table S9. Calculated and observed species of the $[Pd_{12}\mathbf{L}^{\mathbf{DMAP}}{}_{24}Cd_6]^{36+}$ assembly.

Composition	Calculated	Observed
$[Pd_{12}\mathbf{L}^{\mathbf{DMAP}}{}_{24}Cd_6(OTf)_{31}]^{5+}$	3448.0966	3448.0832
$[Pd_{12}\mathbf{L}^{\mathbf{DMAP}}{}_{24}Cd_6(OTf)_{30}]^{6+}$	2848.7551	2848.7446
$[Pd_{12}\mathbf{L}^{\mathbf{DMAP}}{}_{24}Cd_6(OTf)_{29}]^{7+}$	2420.3682	2420.3609
$[Pd_{12}\mathbf{L}^{\mathbf{DMAP}}{}_{24}Cd_6(OTf)_{28}]^{8+}$	2099.2033	2099.1972
$[Pd_{12}\mathbf{L}^{\mathbf{DMAP}}{}_{24}Cd_6(OTf)_{27}]^{9+}$	1849.4080	1849.4029
$[Pd_{12}\mathbf{L}^{\mathbf{DMAP}}{}_{24}Cd_6(OTf)_{26}]^{10+}$	1649.5720	1649.5679
$[Pd_{12}\mathbf{L}^{\mathbf{DMAP}}{}_{24}Cd_6(OTf)_{25}]^{11+}$	1486.0698	1486.0660

Table S10. Zoom into different charged species of $[Pd_{12}\mathbf{L}^{\mathbf{DMAP}}{}_{24}Cd_6]^{n+}$ assembly.

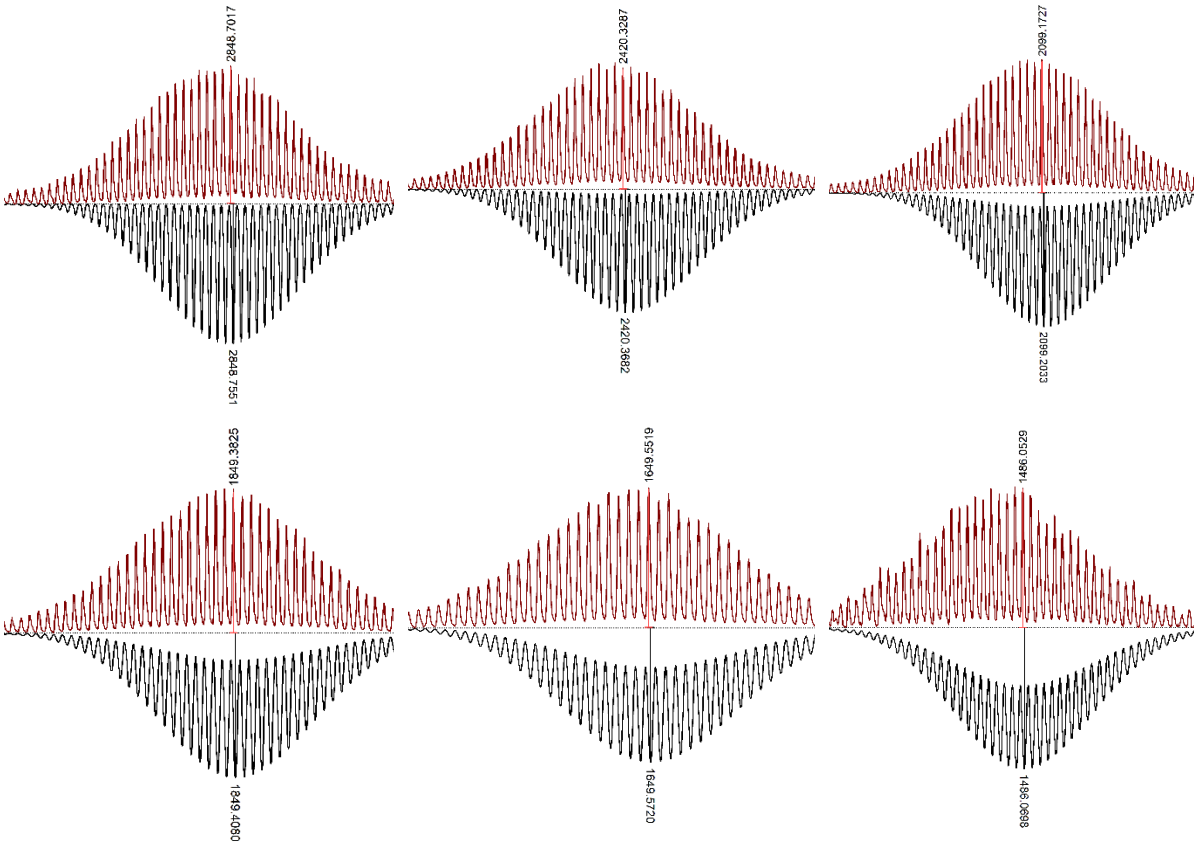

$\underline{Pd_{12}Ni_6\mathbf{L}^{\mathbf{DMAP}}{}_{24}}$

According to the general procedure, 1 mg (2.6 μmol) $Ni(BF_4)_2(MeCN)_4$ were utilized for the post-modification of the self-assembly. ^1H NMR (300 MHz, Acetonitrile-d_3) δ 9.18 (s, 3H), 7.76 (s, 6H), 7.29 (s, 1H), 4.43 (s, 2H). *log D* (300 K; Acetonitrile-d_3) = -9.60; *d* = 5.2 nm (paramagnetic species).

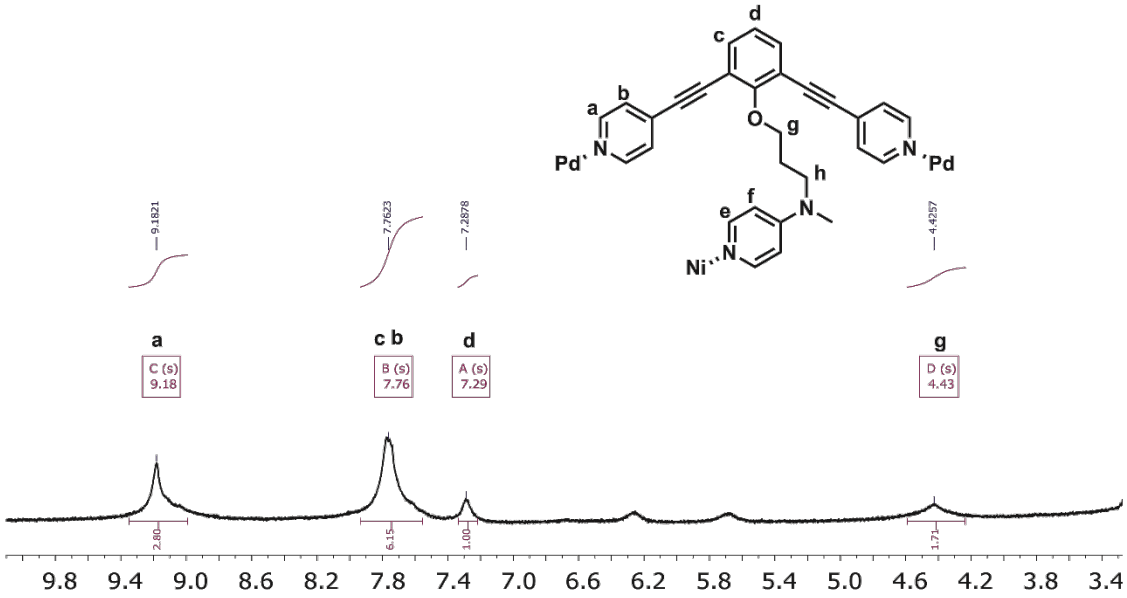

Figure S51. $[Pd_{12}\mathbf{L}^{\mathbf{DMAP}}{}_{24}Ni_6]$ assembly, ^1H NMR in MeCN-d_3.

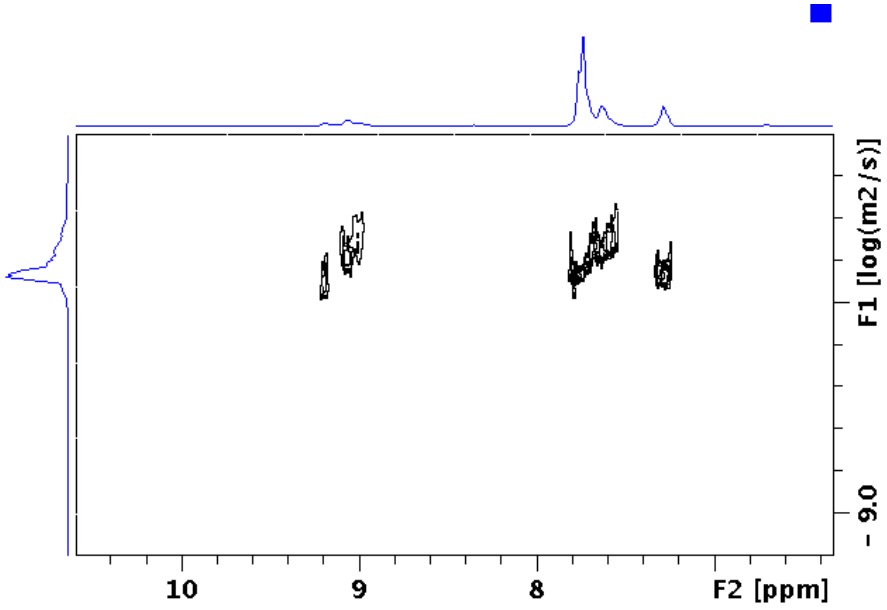

Figure S52. $[Pd_{12}\mathbf{L}^{\mathbf{DMAP}}{}_{24}Ni_6]$ assembly, DOSY NMR in MeCN-d_3 at 300K.

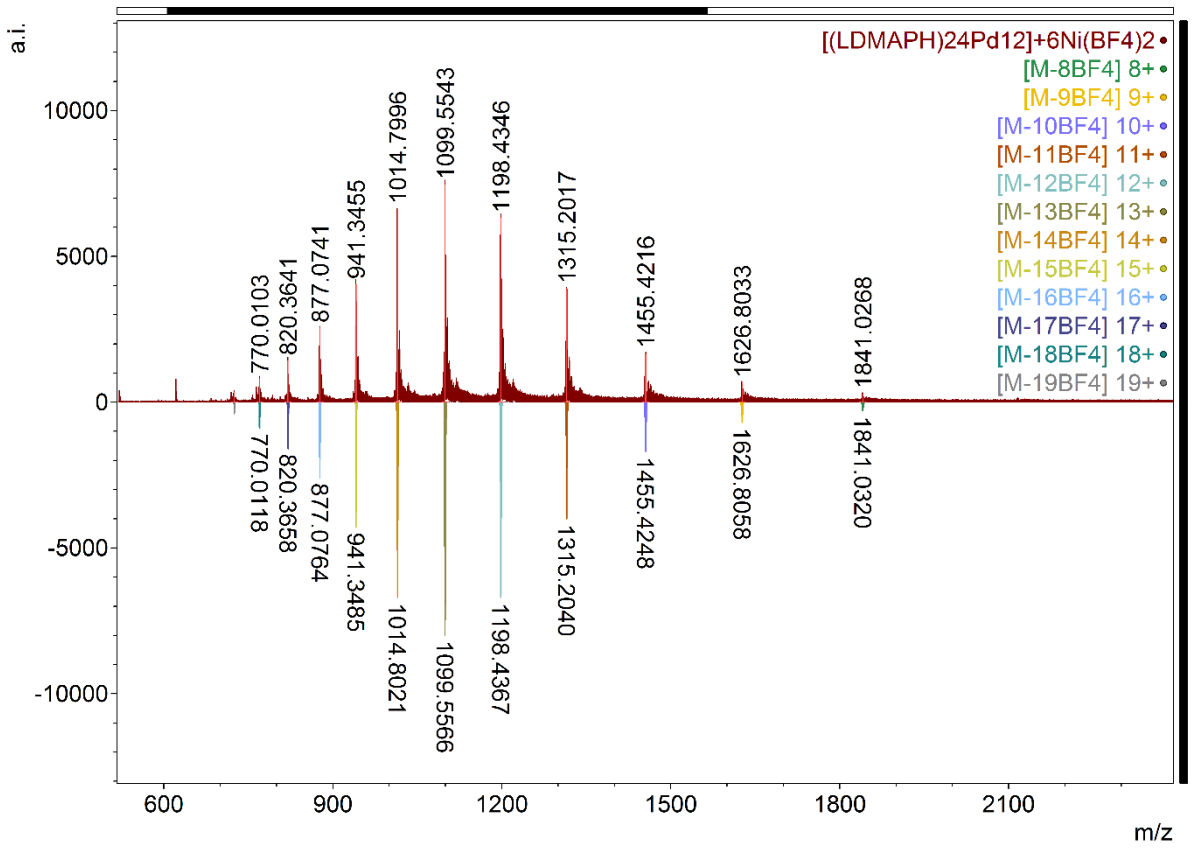

Figure S53. $[Pd_{12}\mathbf{L}^{\mathbf{DMAP}}{}_{24}Ni_6]$ assembly, full HR-ESI MS spectrum, top measured; bottom, simulated spectra of different charged states of the self-assembly.

Table S11. Calculated and observed species of the $[Pd_{12}\mathbf{L}^{\mathbf{DMAP}}{}_{24}Ni_6]^{36+}$ assembly.

Composition	Calculated	Observed
$[Pd_{12}\mathbf{L}^{\mathbf{DMAP}}{}_{24}Ni_6(BF_4)_{28}]^{8+}$	1841.0320	1841.0268
$[Pd_{12}\mathbf{L}^{\mathbf{DMAP}}{}_{24}Ni_6(BF_4)_{27}]^{9+}$	1626.8058	1626.8033
$[Pd_{12}\mathbf{L}^{\mathbf{DMAP}}{}_{24}Ni_6(BF_4)_{26}]^{10+}$	1455.4248	1455.4216
$[Pd_{12}\mathbf{L}^{\mathbf{DMAP}}{}_{24}Ni_6(BF_4)_{25}]^{11+}$	1315.2040	1315.2017
$[Pd_{12}\mathbf{L}^{\mathbf{DMAP}}{}_{24}Ni_6(BF_4)_{24}]^{12+}$	1198.4367	1198.4346
$[Pd_{12}\mathbf{L}^{\mathbf{DMAP}}{}_{24}Ni_6(BF_4)_{23}]^{13+}$	1099.5566	1099.5543
$[Pd_{12}\mathbf{L}^{\mathbf{DMAP}}{}_{24}Ni_6(BF_4)_{22}]^{14+}$	1014.8021	1014.7996
$[Pd_{12}\mathbf{L}^{\mathbf{DMAP}}{}_{24}Ni_6(BF_4)_{21}]^{15+}$	941.3485	941.3455
$[Pd_{12}\mathbf{L}^{\mathbf{DMAP}}{}_{24}Ni_6(BF_4)_{20}]^{16+}$	877.0764	877.0741
$[Pd_{12}\mathbf{L}^{\mathbf{DMAP}}{}_{24}Ni_6(BF_4)_{19}]^{17+}$	820.3658	820.3641
$[Pd_{12}\mathbf{L}^{\mathbf{DMAP}}{}_{24}Ni_6(BF_4)_{18}]^{18+}$	770.0118	770.0103
$[Pd_{12}\mathbf{L}^{\mathbf{DMAP}}{}_{24}Ni_6(BF_4)_{17}]^{19+}$	724.9058	724.9059

Table S12. Zoom into different charged species of $[Pd_{12}\mathbf{L}^{\mathbf{DMAP}}{}_{24}Ni_6]^{n+}$ assembly.

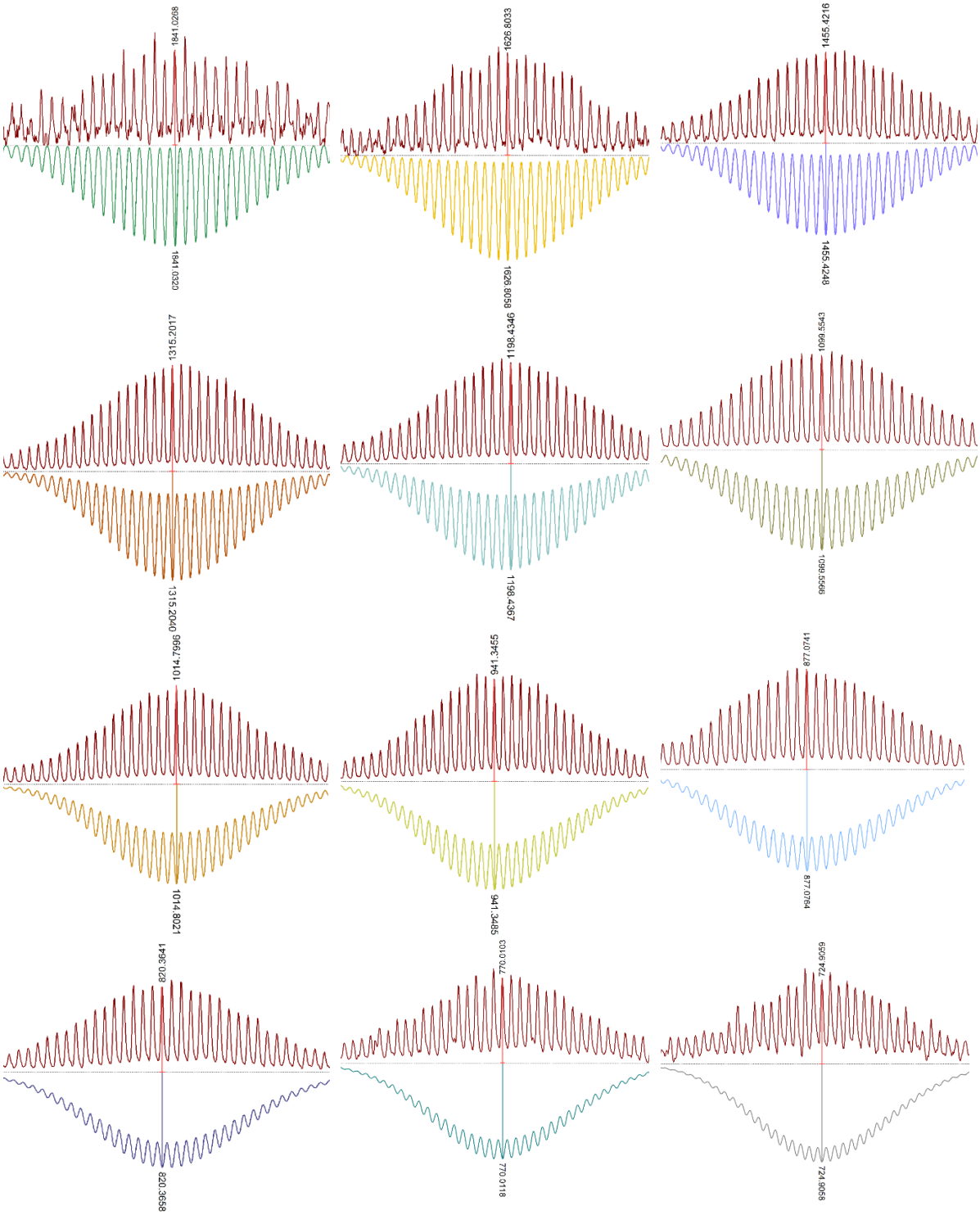

$\underline{Pd_{12}Cu_6\mathbf{L}^{\mathbf{DMAP}}{}_{24}}$

According to the general procedure, 0.64 mg (2.5 μmol) $Cu(BF_4)_2$ was utilized for the post-modification of the self-assembly. ^{1}H NMR (300 MHz, Acetonitrile-d_3) δ 9.13 (m, 3H), 7.76 (m, 6H), 7.29 (m, 1H). *log D* (300 K; Acetonitrile-d_3) = -9.25; *d* = 2.4 nm (paramagnetic species).

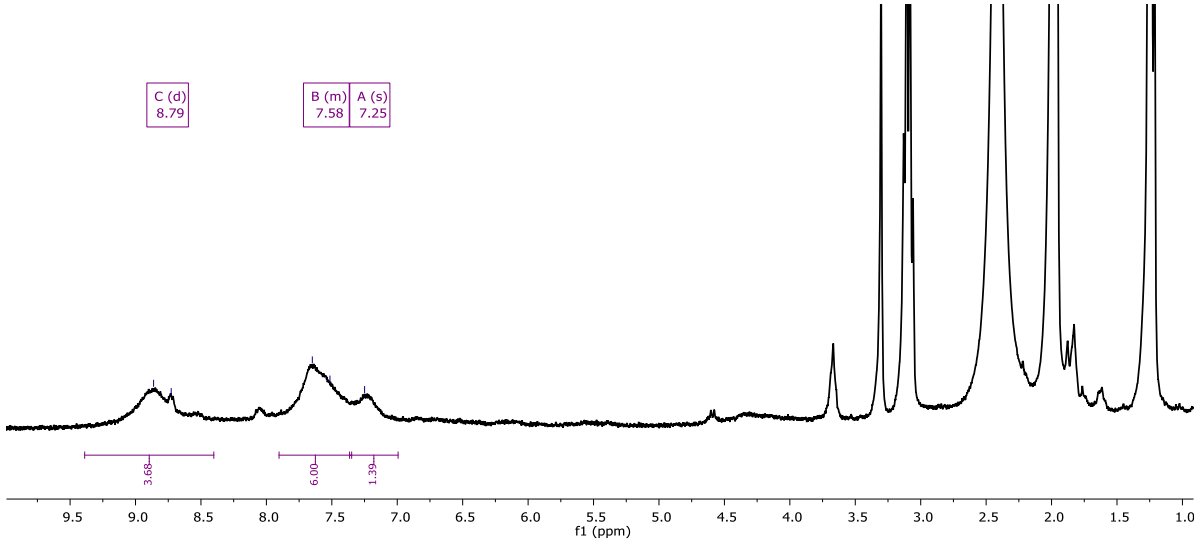

Figure S54. [$Pd_{12}\mathbf{L}^{\mathbf{DMAP}}{}_{24}Cu_6$] assembly, ^{1}H NMR in MeCN-d_3.

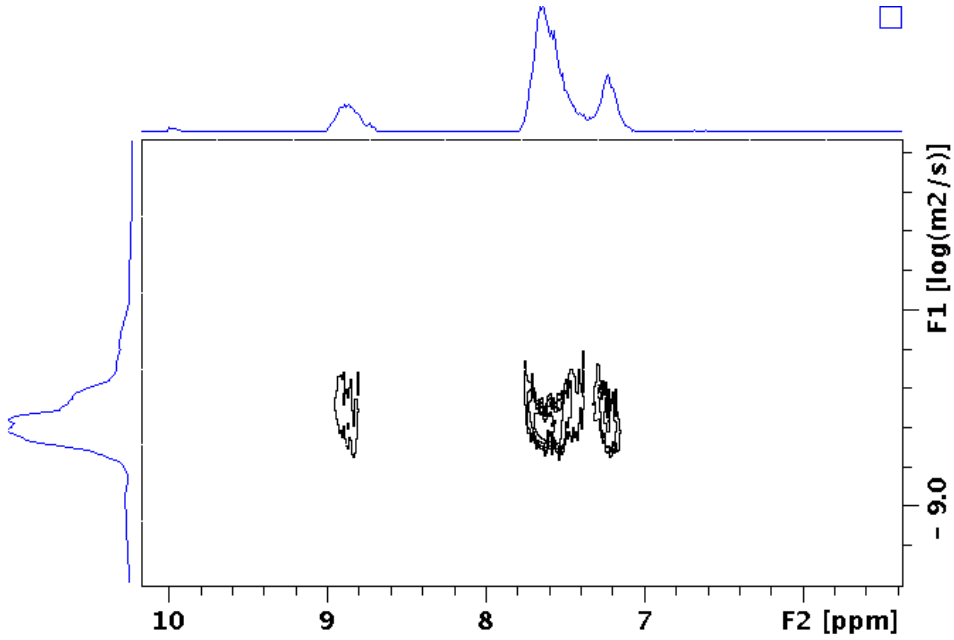

Figure S55. [$Pd_{12}\mathbf{L}^{\mathbf{DMAP}}{}_{24}Cu_6$] assembly, DOSY NMR in MeCN-d_3 at 300K.

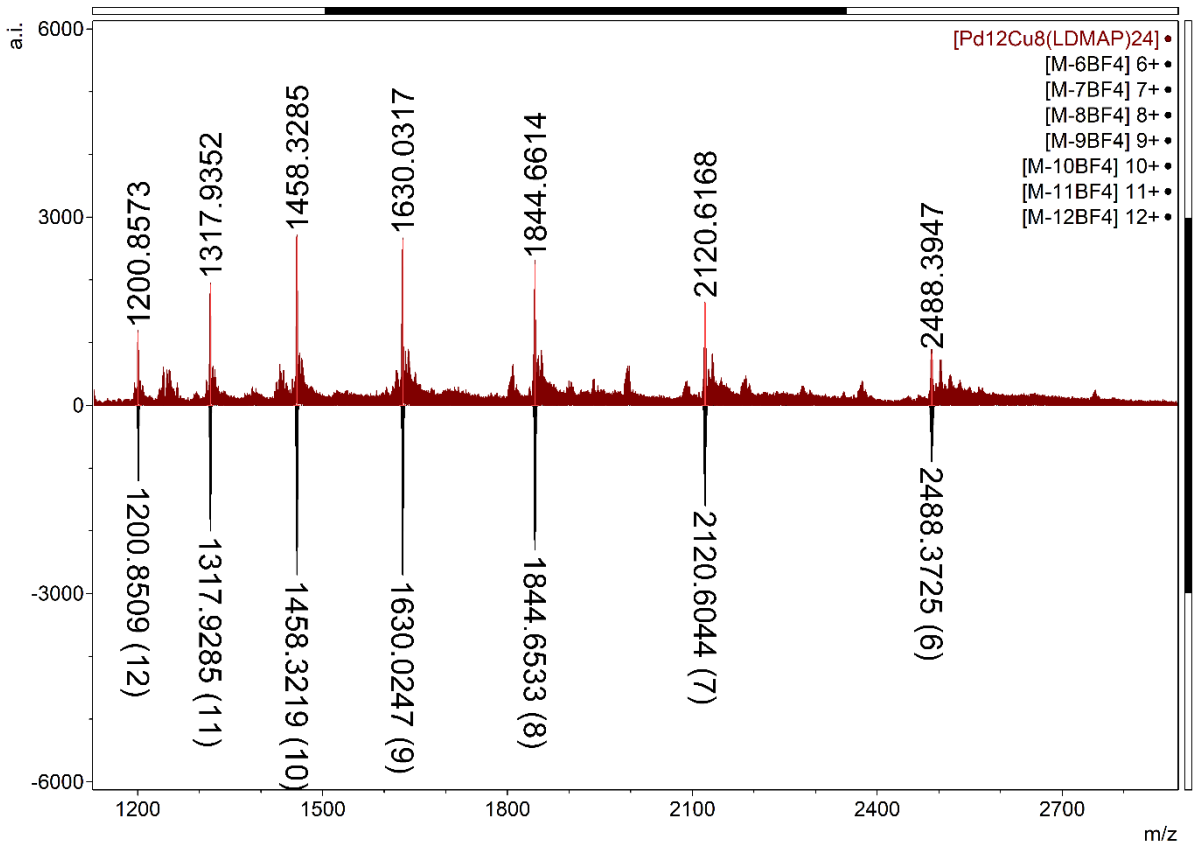

Figure S56. $[Pd_{12}\mathbf{L}^{\mathbf{DMAP}}{}_{24}Cu_6]$ assembly, full HR-ESI MS spectrum, top measured; bottom, simulated spectra of different charged states of the self-assembly.

Table S13. Calculated and observed species of the $[Pd_{12}\mathbf{L}^{\mathbf{DMAP}}{}_{24}Cu_6]^{36+}$ assembly.

Composition	Calculated	Observed
$[Pd_{12}\mathbf{L}^{\mathbf{DMAP}}{}_{24}Cu_6(BF_4)_{28}]^{6+}$	2488.3725	2488.3947
$[Pd_{12}\mathbf{L}^{\mathbf{DMAP}}{}_{24}Cu_6(BF_4)_{27}]^{7+}$	2120.6044	2120.6168
$[Pd_{12}\mathbf{L}^{\mathbf{DMAP}}{}_{24}Cu_6(BF_4)_{26}]^{8+}$	1844.6533	1844.6614
$[Pd_{12}\mathbf{L}^{\mathbf{DMAP}}{}_{24}Cu_6(BF_4)_{25}]^{9+}$	1630.0247	1630.0317
$[Pd_{12}\mathbf{L}^{\mathbf{DMAP}}{}_{24}Cu_6(BF_4)_{24}]^{10+}$	1458.3219	1458.3285
$[Pd_{12}\mathbf{L}^{\mathbf{DMAP}}{}_{24}Cu_6(BF_4)_{23}]^{11+}$	1317.9285	1317.9356
$[Pd_{12}\mathbf{L}^{\mathbf{DMAP}}{}_{24}Cu_6(BF_4)_{22}]^{12+}$	1200.8509	1200.8573

Table S14. Zoom into different charged species of $[Pd_{12}\mathbf{L}^{\mathbf{DMAP}}{}_{24}Cu_6]^{n+}$ assembly.

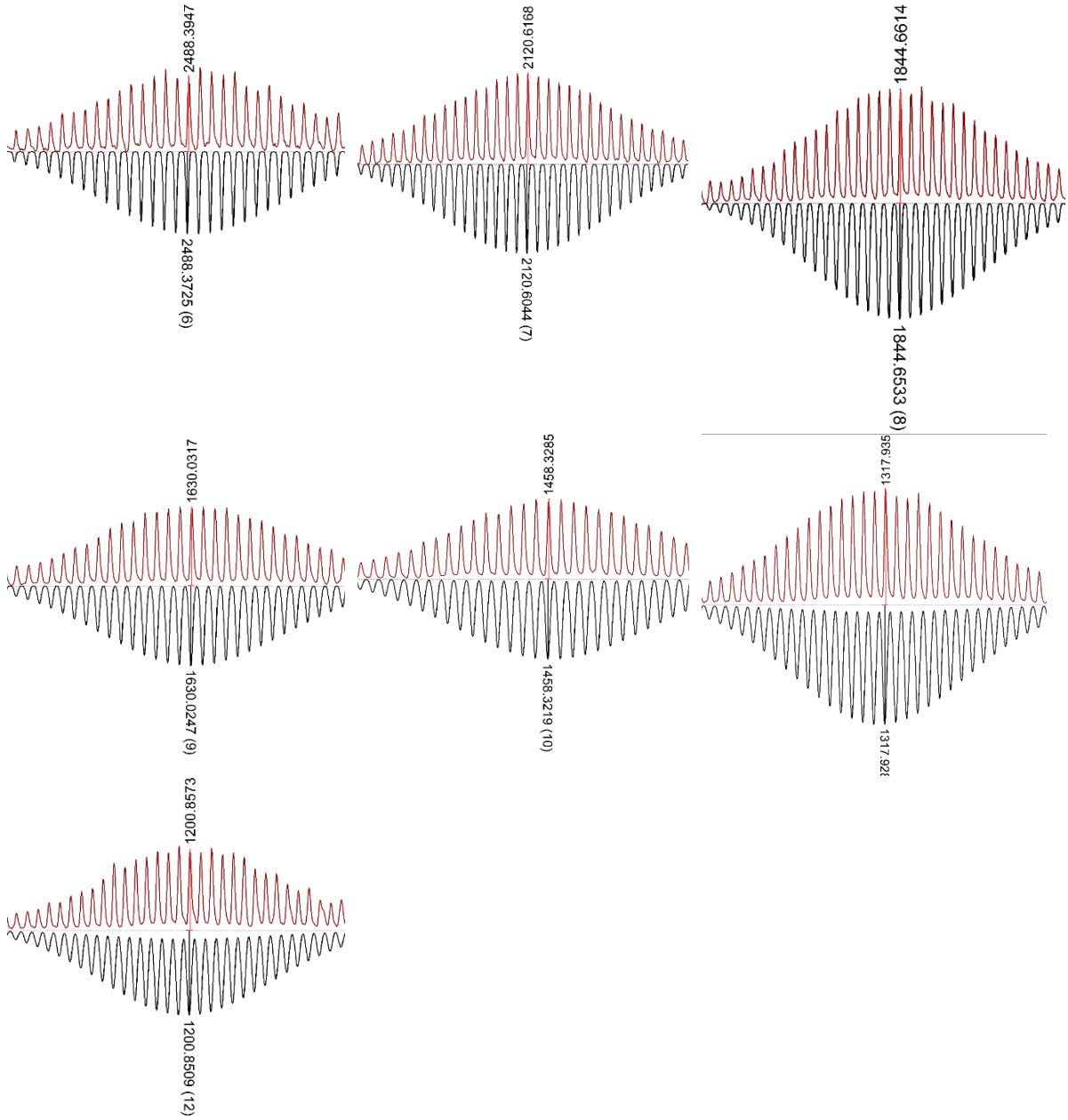

$\underline{Pd_{12}Co_6\mathbf{L}^{\mathbf{DMAP}}{}_{24}}$

According to the general procedure, 0.85 mg (2.5 µmol) $Co(BF_4)_2(H_2O)_6$ was utilized for the post-modification of the self-assembly. Due to the paramagnetic nature of Co^{II}, no detailed information was obtained using ^{1}H-NMR or DOSY analysis. Instead, MS analysis turned out fruitful.

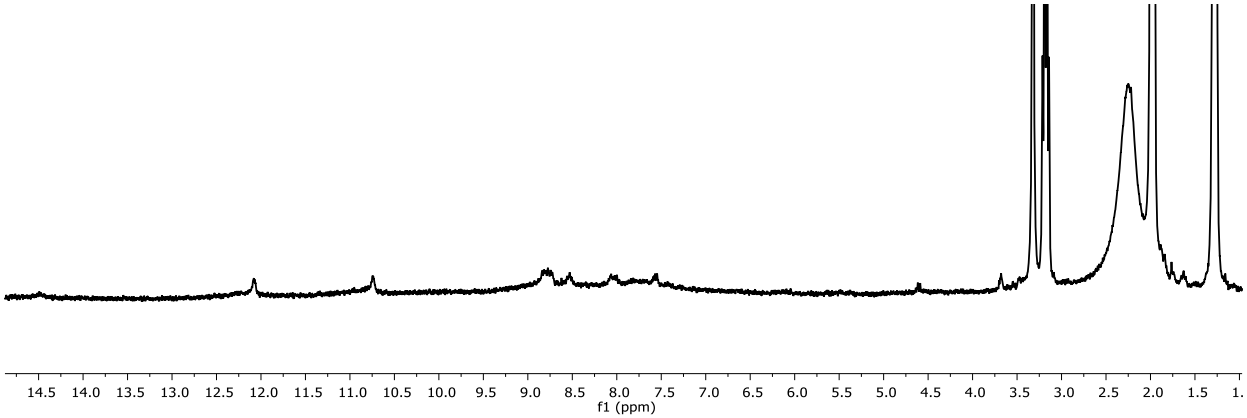

Figure S57. $[Pd_{12}\mathbf{L}^{\mathbf{DMAP}}{}_{24}Co_6]$ assembly, ^{1}H NMR in MeCN-d_3.

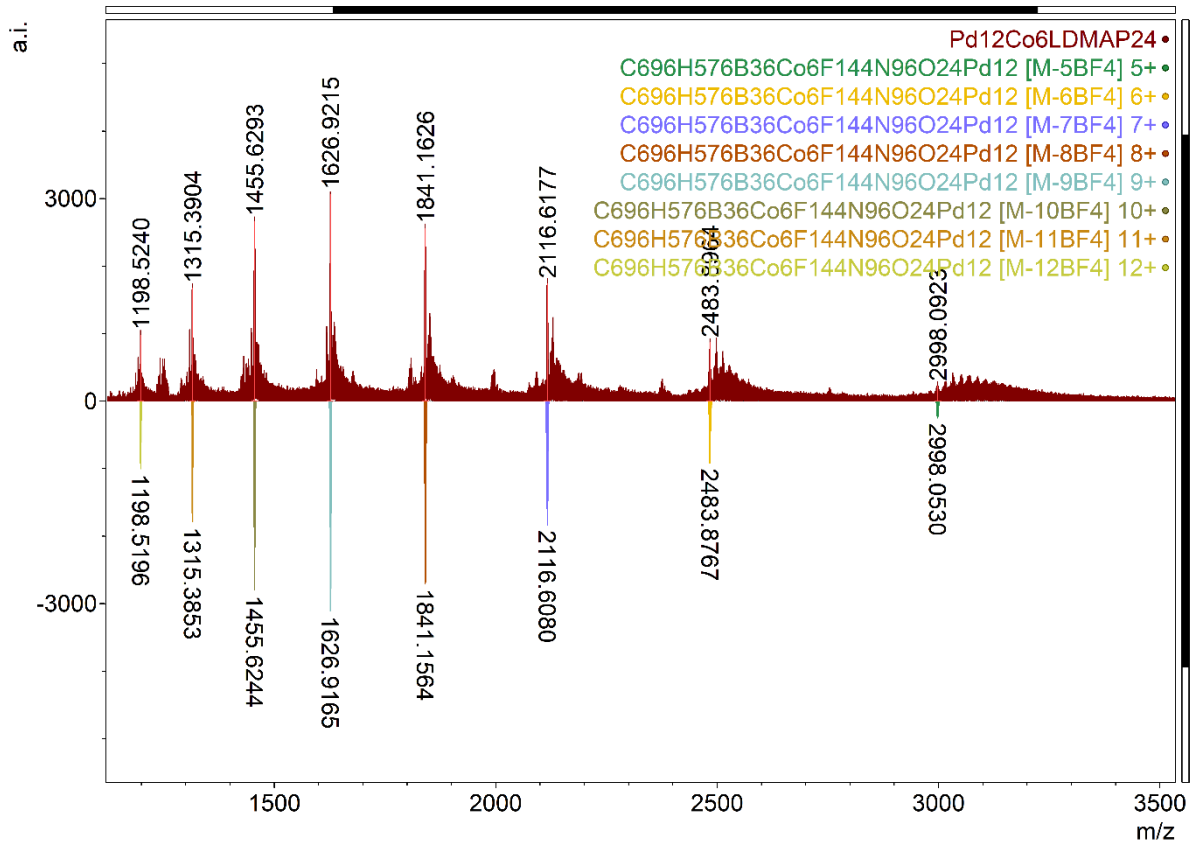

Figure S58. $[Pd_{12}\mathbf{L}^{\mathbf{DMAP}}{}_{24}Co_6]$ assembly, full HR-ESI MS spectrum, top measured; bottom, simulated spectra of different charged states of the self-assembly.

Table S15. Calculated and observed species of the $[Pd_{12}\mathbf{L}^{\mathbf{DMAP}}{}_{24}Co_6]^{36+}$ assembly.

Composition	Calculated	Observed
$[Pd_{12}\mathbf{L}^{\mathbf{DMAP}}{}_{24}Co_6(BF_4)_{29}]^{5+}$	2998.0530	2998.0923
$[Pd_{12}\mathbf{L}^{\mathbf{DMAP}}{}_{24}Co_6(BF_4)_{28}]^{6+}$	2483.8767	2483.8964
$[Pd_{12}\mathbf{L}^{\mathbf{DMAP}}{}_{24}Co_6(BF_4)_{27}]^{7+}$	2116.6080	2116.6177
$[Pd_{12}\mathbf{L}^{\mathbf{DMAP}}{}_{24}Co_6(BF_4)_{26}]^{8+}$	1841.1564	1841.1626
$[Pd_{12}\mathbf{L}^{\mathbf{DMAP}}{}_{24}Co_6(BF_4)_{25}]^{9+}$	1626.9165	1626.9215
$[Pd_{12}\mathbf{L}^{\mathbf{DMAP}}{}_{24}Co_6(BF_4)_{24}]^{10+}$	1455.6244	1455.6293
$[Pd_{12}\mathbf{L}^{\mathbf{DMAP}}{}_{24}Co_6(BF_4)_{23}]^{11+}$	1315.3853	1315.3904
$[Pd_{12}\mathbf{L}^{\mathbf{DMAP}}{}_{24}Co_6(BF_4)_{22}]^{12+}$	1198.5196	1198.5240

Table S16. Zoom into different charged species of $[Pd_{12}\mathbf{L}^{\mathbf{DMAP}}{}_{24}Co_6]^{n+}$ assembly.

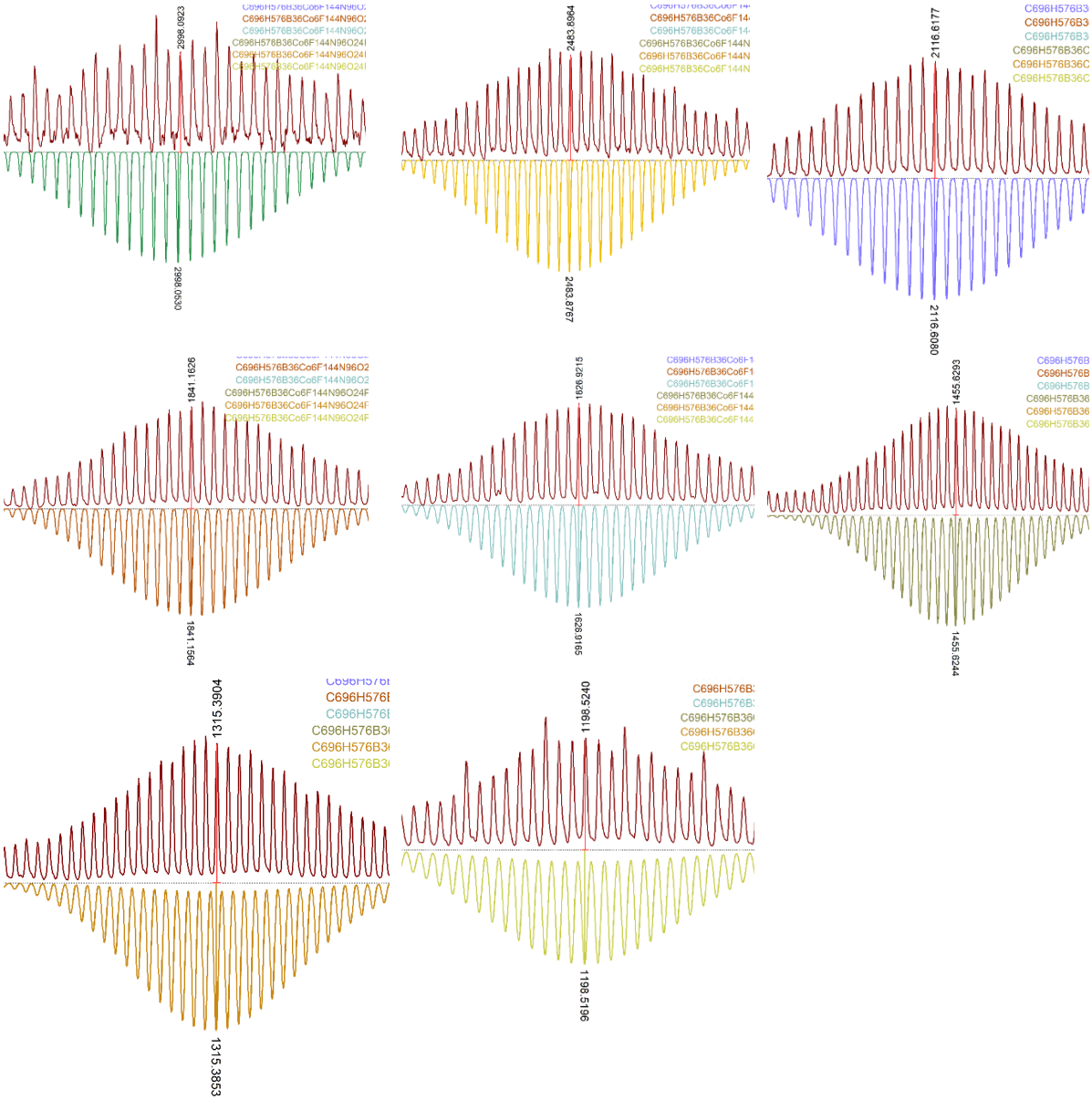

$\underline{Pd_{12}Rh_{12}\mathbf{L}^{\mathbf{DMAP}}{}_{24}}$

According to the general procedure, 1.9 mg (5 µmol) $[Rh(BF_4)(MeCN)_2(COD)]$ was utilized for the post-modification of the self-assembly. ^{1}H NMR (300 MHz, Acetonitrile-d_3) δ 8.97 (s, 4H), 8.06 (s, 2H), 7.65 (d, J = 23.2 Hz, 6H), 7.26 (s, 1H), 6.64 (s, 2H), 4.39 (s, 3H), 2.61 (d, J = 61.0 Hz, 11H). *log D* (300 K; Acetonitrile-d_3) = -9.34; d = 2.9 nm. MS analysis showed a more complicated pattern due to possible loss of the COD ligand during ionization.

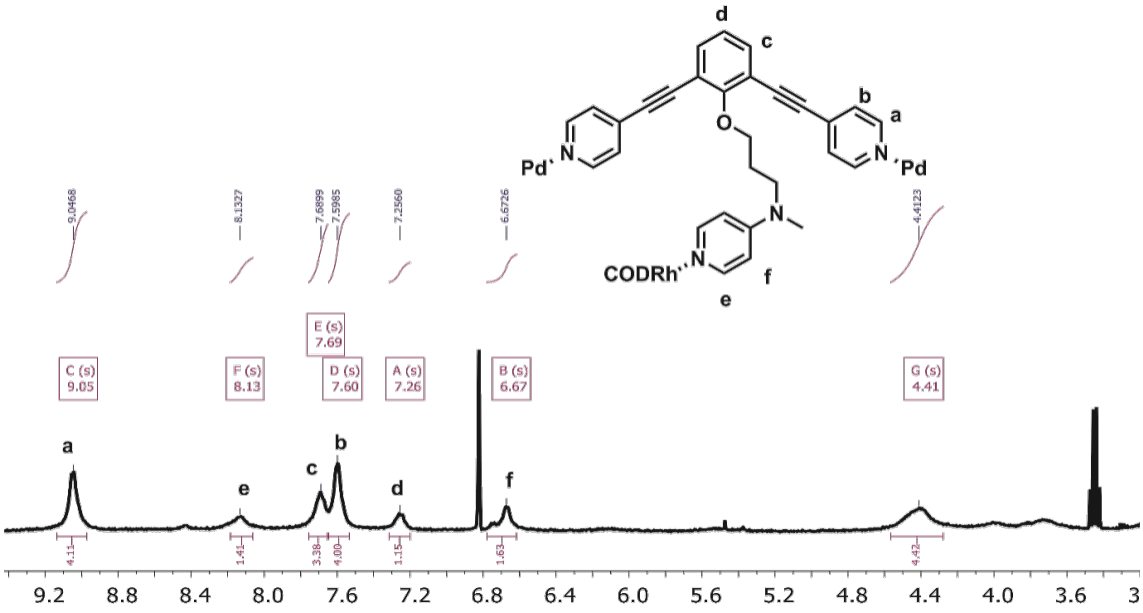

Figure S59. $[Pd_{12}\mathbf{L}^{\mathbf{DMAP}}{}_{24}Rh_{12}]$ assembly, ^{1}H NMR in MeCN-d_3.

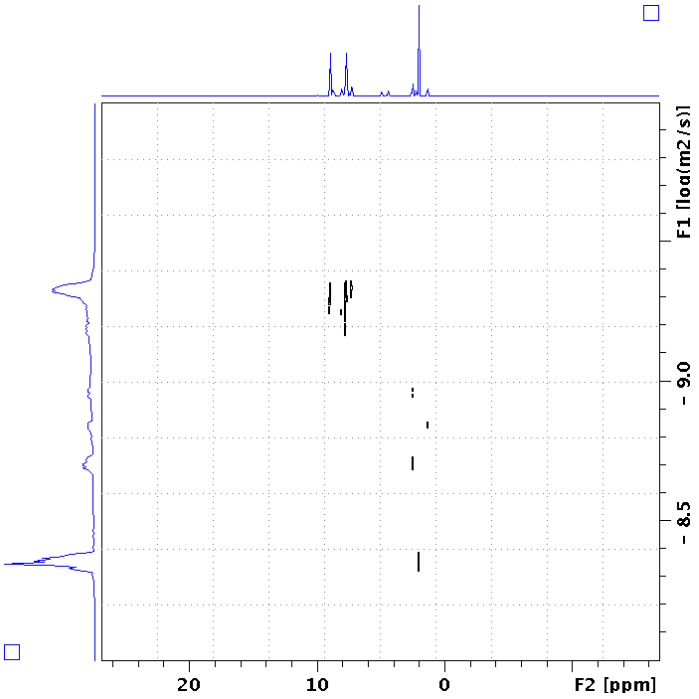

Figure S60. $[Pd_{12}\mathbf{L}^{\mathbf{DMAP}}{}_{24}Rh_{12}]$ assembly, DOSY NMR in MeCN-d_3 at 300K.

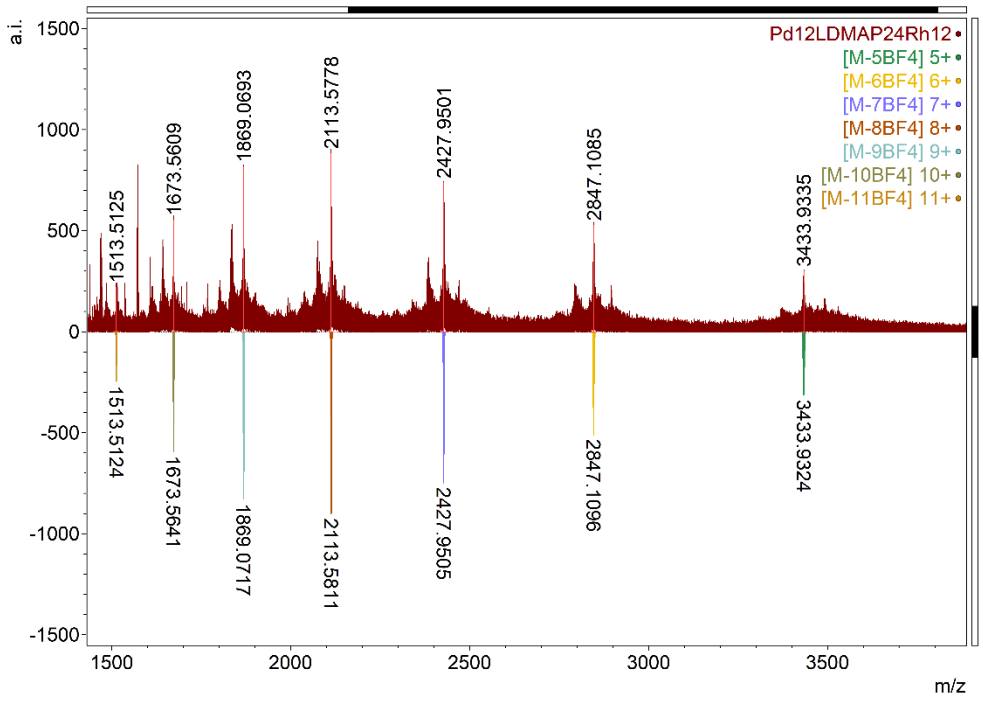

Figure S61. $[Pd_{12}\mathbf{L}^{\mathbf{DMAP}}{}_{24}Rh_{12}]$ assembly, full HR-ESI MS spectrum, top measured; bottom, simulated spectra of different charged states of the self-assembly.

Table S17. Calculated and observed species of the $[Pd_{12}\mathbf{L}^{\mathbf{DMAP}}{}_{24}Rh_{12}]^{36+}$ assembly.

Composition	Calculated	Observed
$[Pd_{12}\mathbf{L}^{\mathbf{DMAP}}{}_{24}Rh_{12}(BF_4)_{29}]^{5+}$	3433.9324	3433.9335
$[Pd_{12}\mathbf{L}^{\mathbf{DMAP}}{}_{24}\ Rh_{12}(BF_4)_{28}]^{6+}$	2847.1096	2847.1085
$[Pd_{12}\mathbf{L}^{\mathbf{DMAP}}{}_{24}\ Rh_{12}(BF_4)_{27}]^{7+}$	2427.9505	2427.9501
$[Pd_{12}\mathbf{L}^{\mathbf{DMAP}}{}_{24}\ Rh_{12}(BF_4)_{26}]^{8+}$	2113.5811	2113.5778
$[Pd_{12}\mathbf{L}^{\mathbf{DMAP}}{}_{24}\ Rh_{12}(BF_4)_{25}]^{9+}$	1869.0717	1869.0693
$[Pd_{12}\mathbf{L}^{\mathbf{DMAP}}{}_{24}\ Rh_{12}(BF_4)_{24}]^{10+}$	1673.5641	1673.5609
$[Pd_{12}\mathbf{L}^{\mathbf{DMAP}}{}_{24}\ Rh_{12}(BF_4)_{23}]^{11+}$	1513.5124	1513.5125

Table S18. Zoom into different charged species of $[Pd_{12}\mathbf{L}^{\mathbf{DMAP}}{}_{24}Rh_{12}]^{n+}$ assembly.

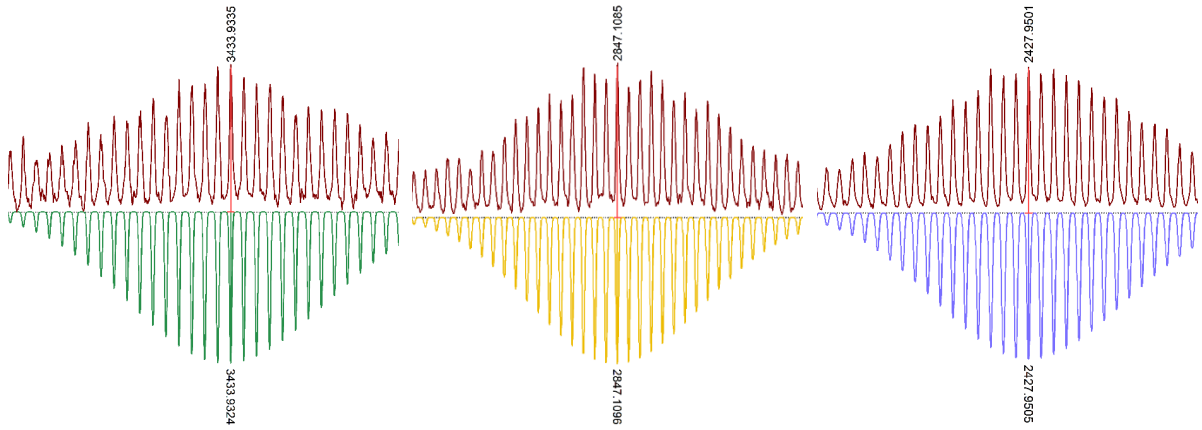

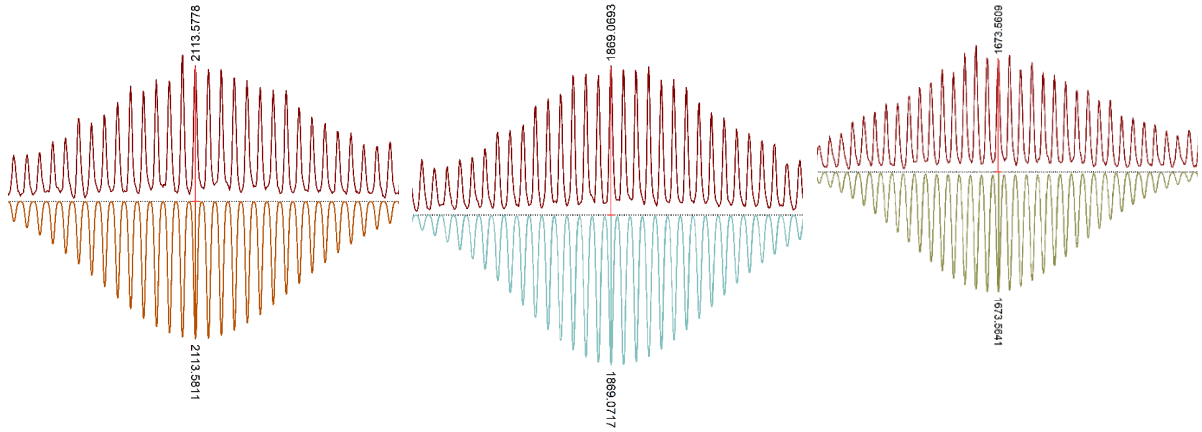

$\underline{Pd_{12}Cd_8\mathbf{L^{Pro}}_{24}}$

According to the general procedure, 1.4 mg (3.4 µmol) $Cd(OTf)_2$ were utilized for the post-modification of the self-assembly. Both, MS analysis of the proline sphere precursor and of the formed product were unsuccessful. ^{1}H NMR (300 MHz, Acetonitrile-d_3) δ 9.06 (d, J = 6.2 Hz, 4H), 7.73 (m, 6H), 7.24 (m, 1H), 4.40 (s, 2H), 3.76 (m, 2H), 3.54 (m, 1H), 2.78 (m, 1H). *log D* (300 K; Acetonitrile-d_3) = -9.52; *d* = 4.4 nm.

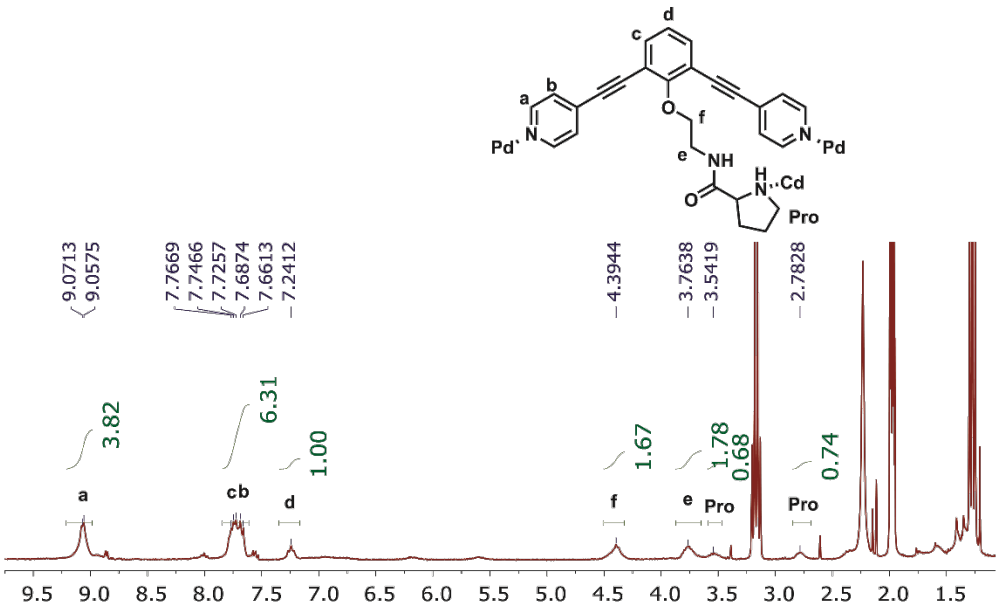

Figure S62. [$Pd_{12}\mathbf{L^{Pro}}_{24}Cd_8$] assembly, ^{1}H NMR in MeCN-d_3.

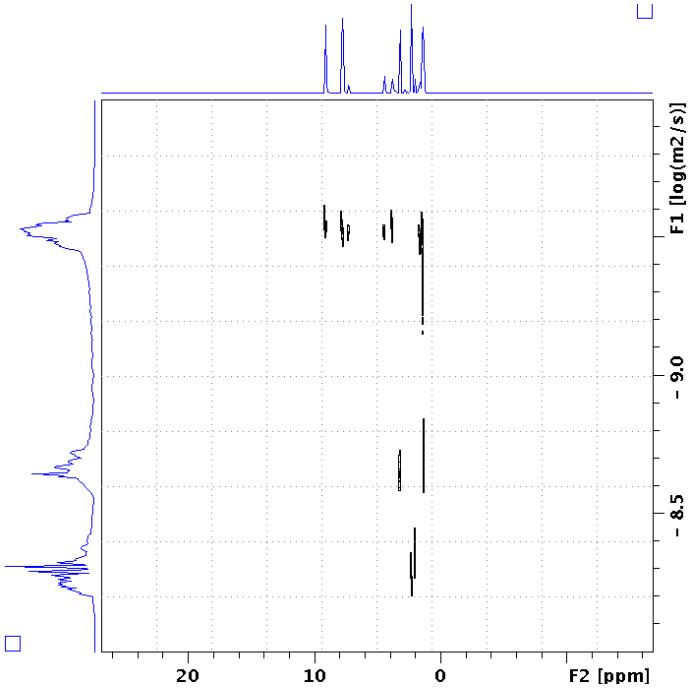

Figure S63. [Pd_{12}**L**$^{Pro}{}_{24}Cd_8$] assembly, DOSY NMR in MeCN-d_3 at 300K.

$\underline{Pd_{12}Cd_8\mathbf{L}^{ProMe}{}_{24}}$

According to the general procedure, 1.4 mg (3.4 µmol) $Cd(OTf)_2$ were utilized for the post-modification of the self-assembly. ^{1}H NMR (300 MHz, Acetonitrile-d_3) δ 9.11 (s, 4H), 7.68 (d, J = 10.5 Hz, 6H), 7.27 (d, J = 9.3 Hz, 1H). *log D* (300 K; Acetonitrile-d_3) = -9.40; *d* = 3.3 nm.

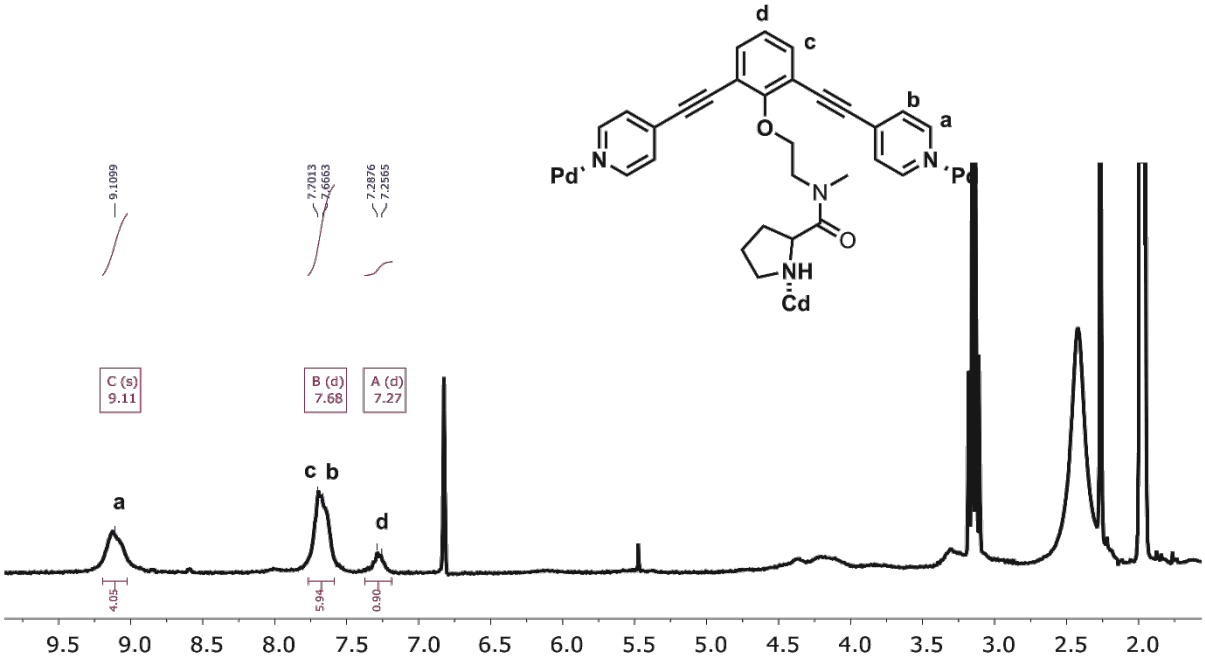

Figure S64. [Pd_{12}**L**$^{ProMe}{}_{24}Cd_8$] assembly, ^{1}H NMR in MeCN-d_3.

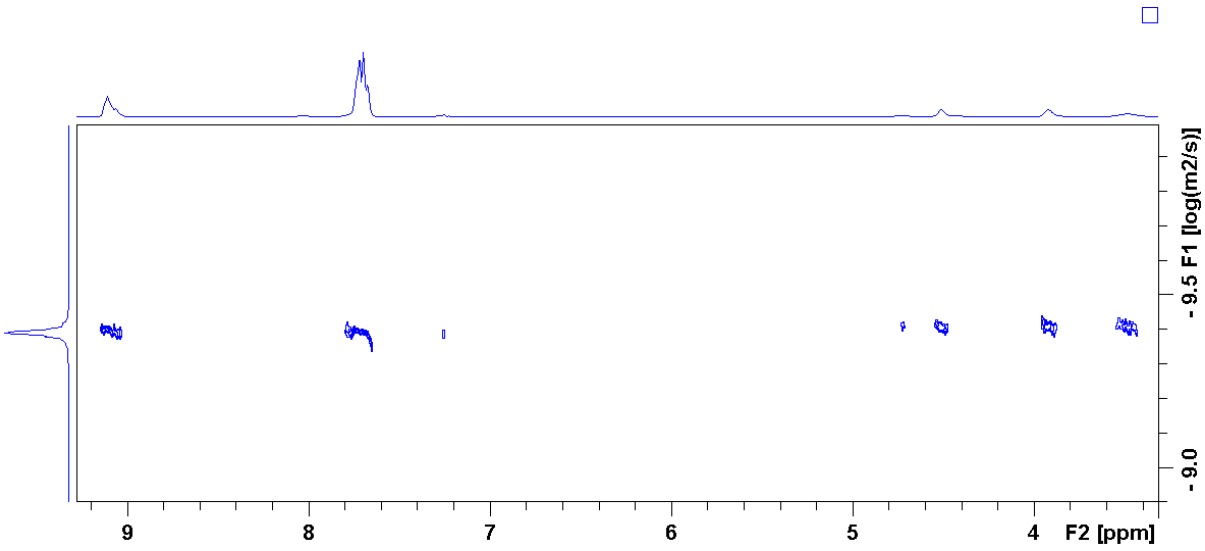

Figure S65. [$Pd_{12}\mathbf{L}^{\mathbf{ProMe}}{}_{24}Cd_8$] assembly, DOSY NMR in MeCN-d_3 at 300K.

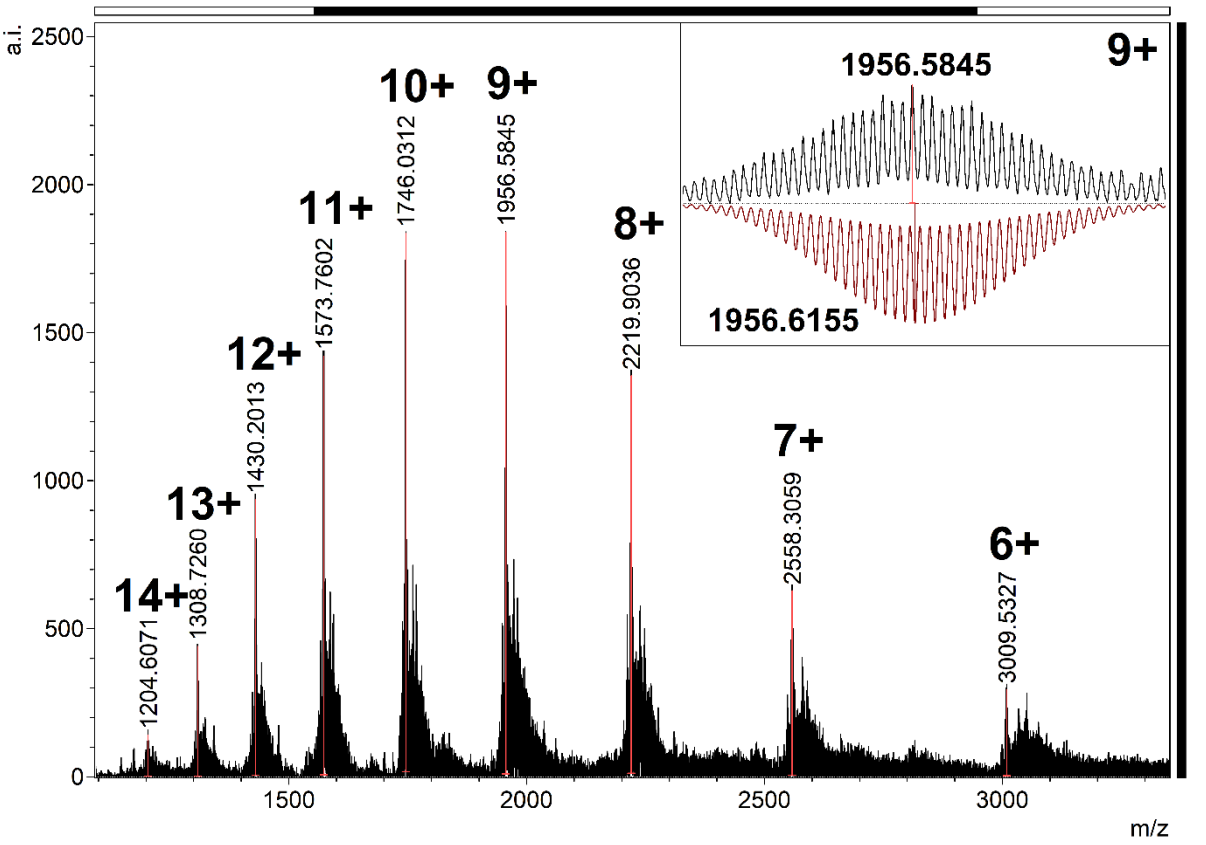

Figure S66. [$Pd_{12}\mathbf{L}^{\mathbf{ProMe}}{}_{24}Cd_8$] assembly, full HR-ESI MS spectrum of different charged states of the self-assembly.

Table S19. Calculated and observed species of the $[Pd_{12}\mathbf{L}^{\mathbf{ProMe}}{}_{24}Cd_8]^{40+}$ assembly.

Composition	Calculated	Observed
$[Pd_{12}\mathbf{L}^{\mathbf{ProMe}}{}_{24}Cd_8(OTf)_{34}]^{6+}$	3009.5664	3009.5327
$[Pd_{12}\mathbf{L}^{\mathbf{ProMe}}{}_{24}Cd_8(OTf)_{33}]^{7+}$	2558.3493	2558.3059
$[Pd_{12}\mathbf{L}^{\mathbf{ProMe}}{}_{24}Cd_8(OTf)_{32}]^{8+}$	2219.9366	2219.9036
$[Pd_{12}\mathbf{L}^{\mathbf{ProMe}}{}_{24}Cd_8(OTf)_{31}]^{9+}$	1956.6155	1956.5845
$[Pd_{12}\mathbf{L}^{\mathbf{ProMe}}{}_{24}Cd_8(OTf)_{30}]^{10+}$	1746.0590	1746.0312
$[Pd_{12}\mathbf{L}^{\mathbf{ProMe}}{}_{24}Cd_8(OTf)_{29}]^{11+}$	1573.7852	1573.7602
$[Pd_{12}\mathbf{L}^{\mathbf{ProMe}}{}_{24}Cd_8(OTf)_{28}]^{12+}$	1430.2237	1430.2013
$[Pd_{12}\mathbf{L}^{\mathbf{ProMe}}{}_{24}Cd_8(OTf)_{27}]^{13+}$	1308.7434	1308.7260
$[Pd_{12}\mathbf{L}^{\mathbf{ProMe}}{}_{24}Cd_8(OTf)_{26}]^{14+}$	1204.6271	1204.6071

Table S20. Zoom into different charged species of $[Pd_{12}\mathbf{L}^{\mathbf{ProMe}}{}_{24}Cd_8]^{n+}$ assembly.

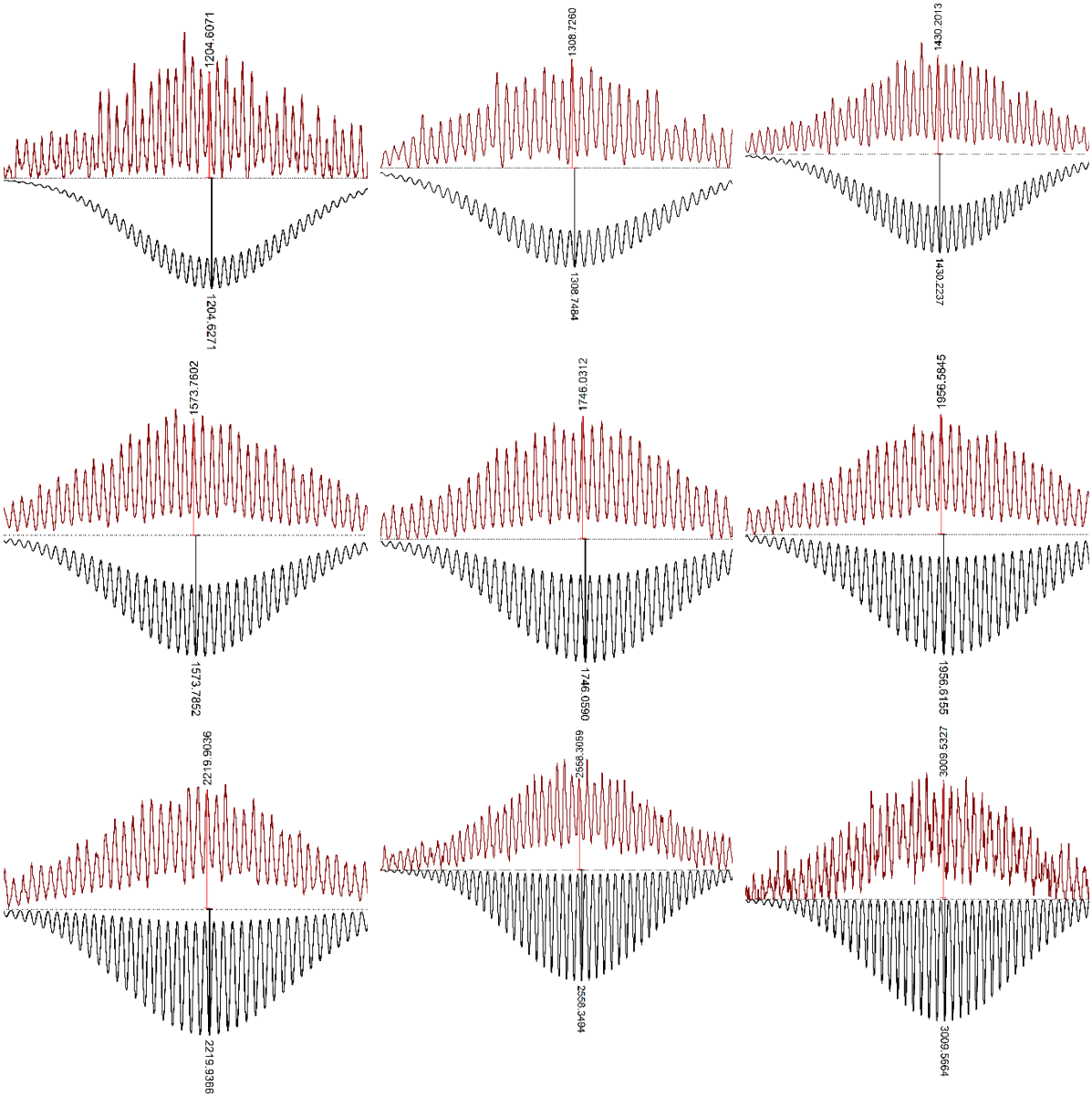

$\underline{Pd_{12}Ni_8\mathbf{L}^{\mathbf{ProMe}}{}_{24}}$

According to the general procedure, 1.33 mg (3.3 µmol) $Ni(BF_4)_2(MeCN)_4$ and 1.6 µl NEt_3 were utilized for the post-modification of the $[Pd_{12}\mathbf{L}^{\mathbf{ProMeH}}{}_{24}]$ self-assembly. Due to the paramagnetic nature of Ni^{II} and closer proximity to the sphere framework in comparison to the DMAP building block, no detailed information was obtained using ^{1}H-NMR or DOSY analysis. Instead, MS analysis turned out fruitful.

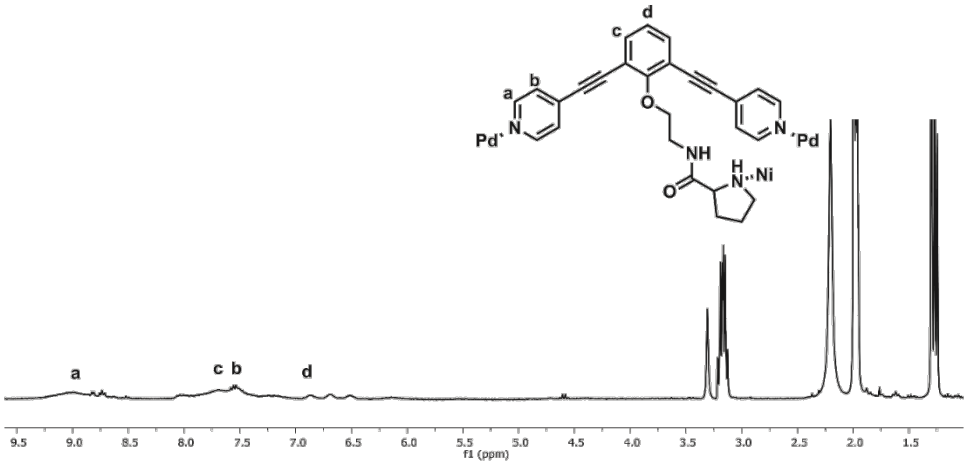

Figure S67. $[Pd_{12}\mathbf{L}^{\mathbf{ProMe}}{}_{24}Ni_8]$ assembly, ^{1}H NMR in MeCN-d_3.

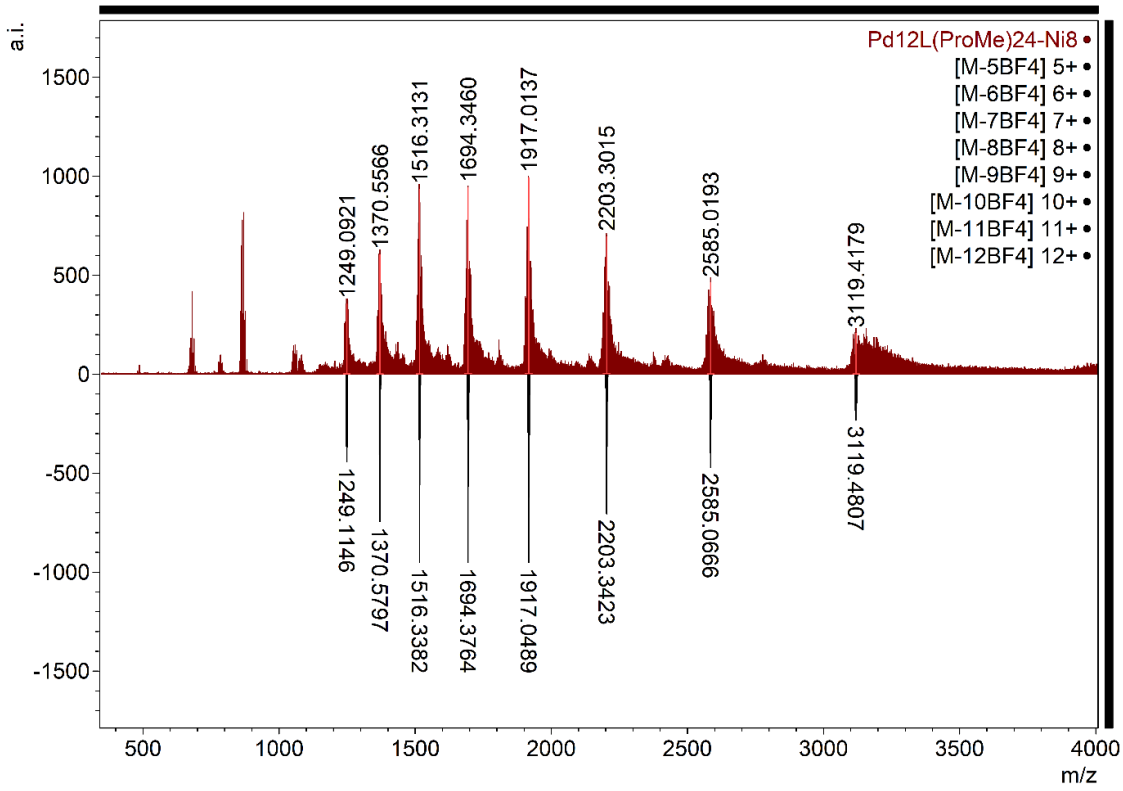

Figure S68. $[Pd_{12}\mathbf{L}^{\mathbf{ProMe}}{}_{24}Ni_8]$ assembly, full HR-ESI MS spectrum, top measured; bottom, simulated spectra of different charged states of the self-assembly.

Table S21. Calculated and observed species of the $[Pd_{12}\mathbf{L}^{\mathbf{ProMe}}{}_{24}Ni_8]^{40+}$ assembly.

Composition	Calculated	Observed
$[Pd_{12}\mathbf{L}^{\mathbf{ProMe}}{}_{24}Ni_8(BF_4)_{35}]^{5+}$	3119.4807	3119.4179
$[Pd_{12}\mathbf{L}^{\mathbf{ProMe}}{}_{24}Ni_8(BF_4)_{34}]^{6+}$	2585.0666	2585.0193
$[Pd_{12}\mathbf{L}^{\mathbf{ProMe}}{}_{24}Ni_8(BF_4)_{33}]^{7+}$	2203.3423	2203.3015
$[Pd_{12}\mathbf{L}^{\mathbf{ProMe}}{}_{24}Ni_8(BF_4)_{32}]^{8+}$	1917.0489	1917.0137
$[Pd_{12}\mathbf{L}^{\mathbf{ProMe}}{}_{24}Ni_8(BF_4)_{31}]^{9+}$	1694.3764	1694.3460
$[Pd_{12}\mathbf{L}^{\mathbf{ProMe}}{}_{24}Ni_8(BF_4)_{30}]^{10+}$	1516.3382	1516.3131
$[Pd_{12}\mathbf{L}^{\mathbf{ProMe}}{}_{24}Ni_8(BF_4)_{29}]^{11+}$	1370.5797	1370.5566
$[Pd_{12}\mathbf{L}^{\mathbf{ProMe}}{}_{24}Ni_8(BF_4)_{28}]^{12+}$	1249.1146	1249.0921

Table S22. Zoom into different charged species of $[Pd_{12}\mathbf{L}^{\mathbf{ProMe}}{}_{24}Ni_8]^{n+}$ assembly.

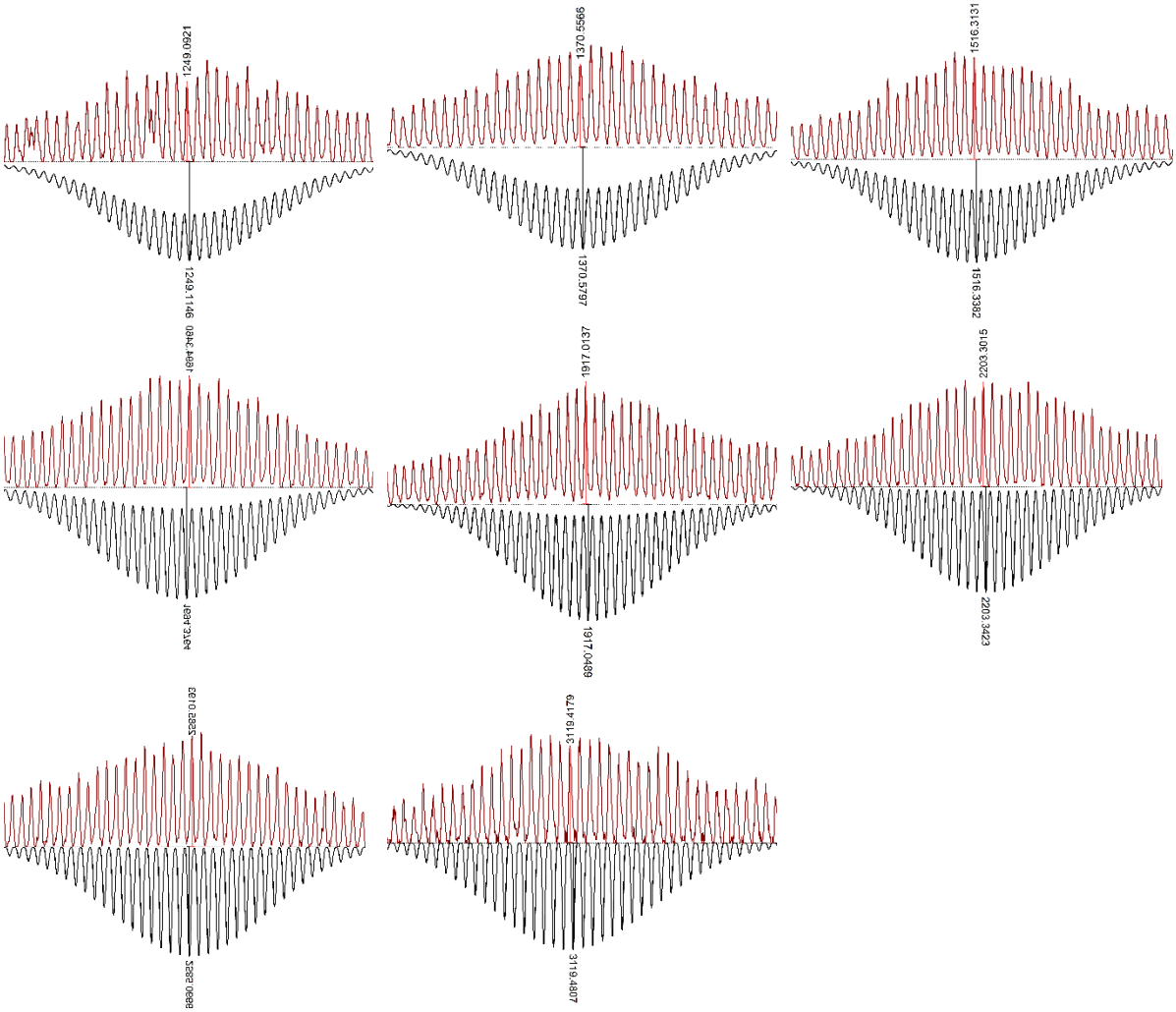

$Pd_{12}Cd_8\mathbf{L}^{\mathbf{4ProMe}}{}_{24}$

According to the general procedure, 1.4 mg (3.4 µmol) $Cd(OTf)_2$ were utilized for the post-modification of the self-assembly. ^{1}H NMR (300 MHz, Acetonitrile-d_3) δ 9.13 (s, 4H), 7.67 (d, J = 10.5 Hz, 5H), 7.24 (s, 1H), 4.24 (s, 3H). *log D* (300 K; Acetonitrile-d_3) = -9.22; *d* = 2.3 nm.

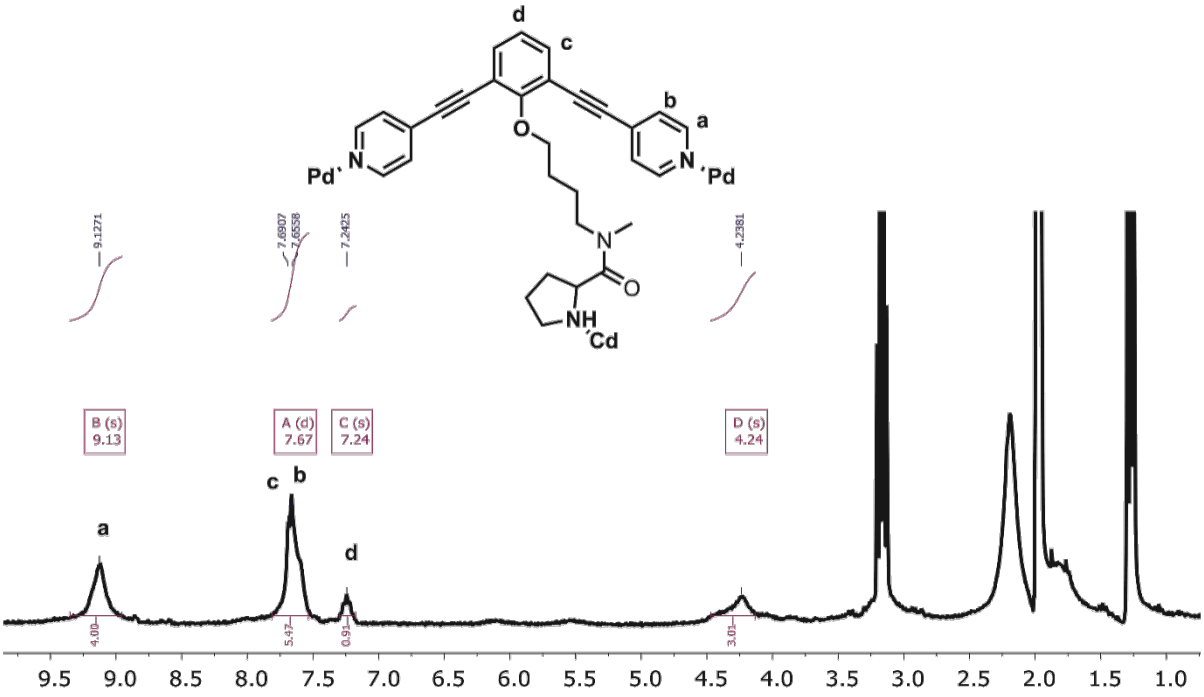

Figure S69. [$Pd_{12}\mathbf{L}^{\mathbf{ProMe}}{}_{24}Cd_8$] assembly, ^{1}H NMR in MeCN-d_3.

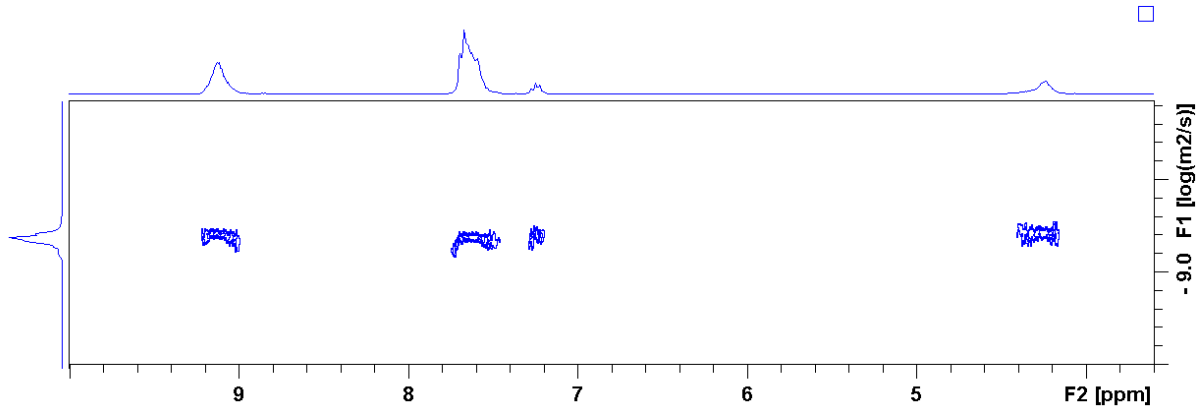

Figure S70. [$Pd_{12}\mathbf{L}^{\mathbf{4ProMe}}{}_{24}Cd_8$] assembly, DOSY NMR in MeCN-d_3 at 300K.

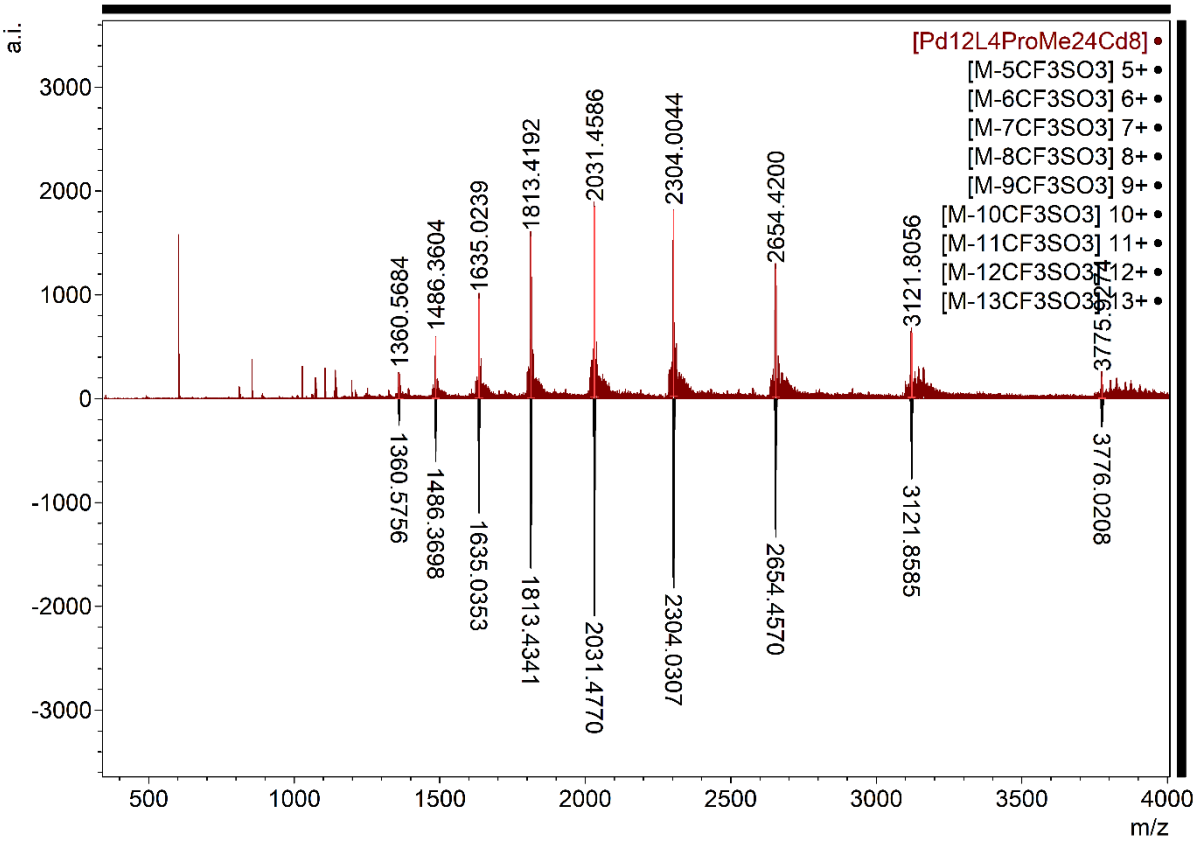

Figure S71. $[Pd_{12}\mathbf{L}^{\mathbf{4ProMe}}{}_{24}Cd_8]$ assembly, full HR-ESI MS spectrum of different charged states of the self-assembly.

Table S23. Calculated and observed species of the $[Pd_{12}\mathbf{L}^{\mathbf{4ProMe}}{}_{24}Cd_8]^{40+}$ assembly.

Composition	Calculated	Observed
$[Pd_{12}\mathbf{L}^{\mathbf{4ProMe}}{}_{24}Cd_8(OTf)_{34}]^{6+}$	3121.8585	3121.8056
$[Pd_{12}\mathbf{L}^{\mathbf{4ProMe}}{}_{24}Cd_8(OTf)_{33}]^{7+}$	2654.4570	2654.4200
$[Pd_{12}\mathbf{L}^{\mathbf{4ProMe}}{}_{24}Cd_8(OTf)_{32}]^{8+}$	2304.0307	2304.0044
$[Pd_{12}\mathbf{L}^{\mathbf{4ProMe}}{}_{24}Cd_8(OTf)_{31}]^{9+}$	2031.4770	2031.4586
$[Pd_{12}\mathbf{L}^{\mathbf{4ProMe}}{}_{24}Cd_8(OTf)_{30}]^{10+}$	1813.4341	1813.4192
$[Pd_{12}\mathbf{L}^{\mathbf{4ProMe}}{}_{24}Cd_8(OTf)_{29}]^{11+}$	1635.0353	1635.0239
$[Pd_{12}\mathbf{L}^{\mathbf{4ProMe}}{}_{24}Cd_8(OTf)_{28}]^{12+}$	1486.3698	1486.3604
$[Pd_{12}\mathbf{L}^{\mathbf{4ProMe}}{}_{24}Cd_8(OTf)_{27}]^{13+}$	1360.5756	1360.5684

Table S24. Zoom into different charged species of $[Pd_{12}\mathbf{L^{4ProMe}}_{24}Cd_8]^{n+}$ assembly.

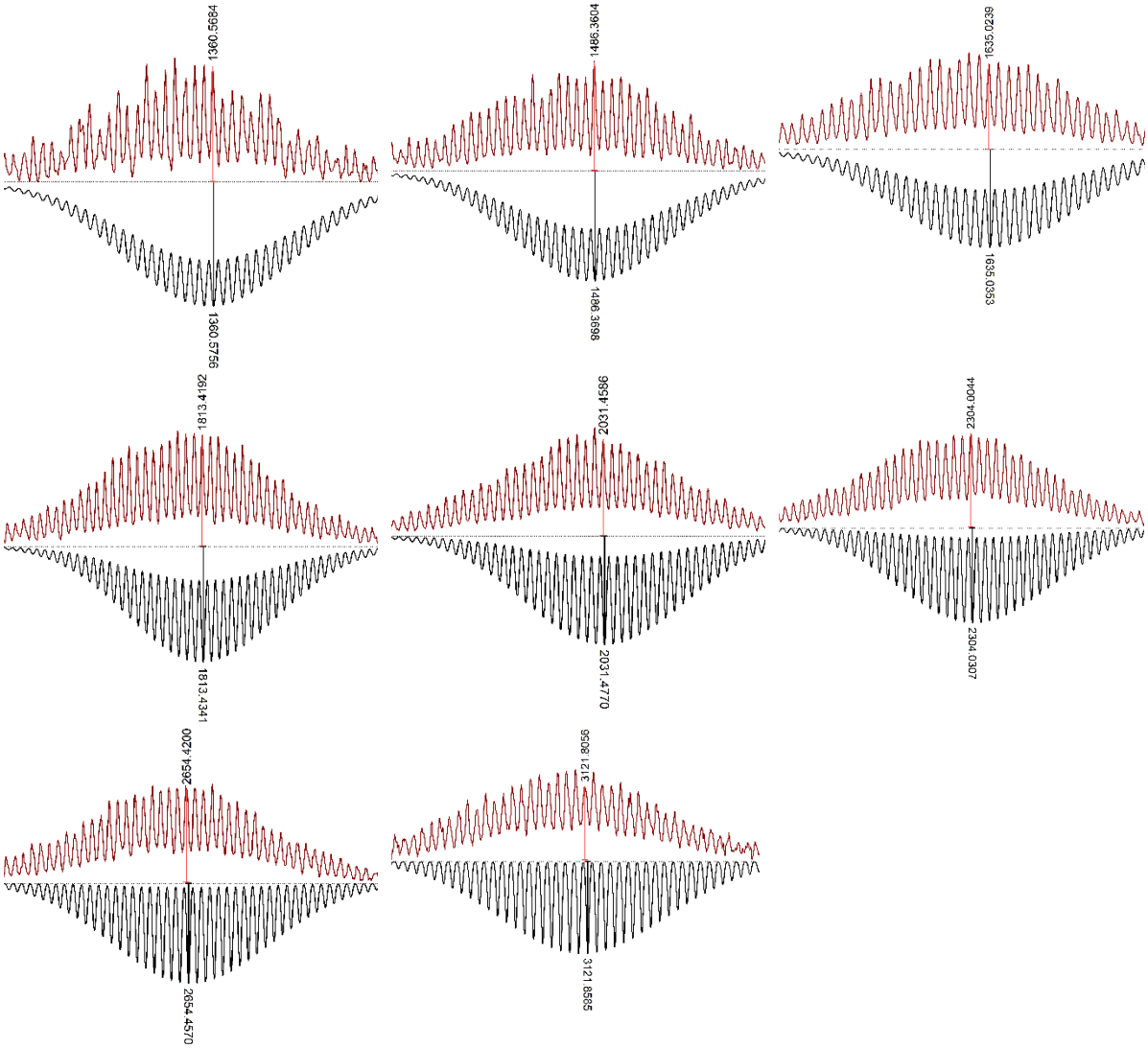

$Pd_{12}Cu_8\mathbf{L^{Pro}}_{24}$

According to the general procedure, 0.8 mg (3.3 µmol) $Cu(BF_4)_2(MeCN)_4$ were utilized for the post-modification of the self-assembly. Due to the paramagnetic nature of Cu^{II}, no detailed information was obtained using ^{1}H-NMR or DOSY analysis. Instead, MS analysis turned out fruitful.

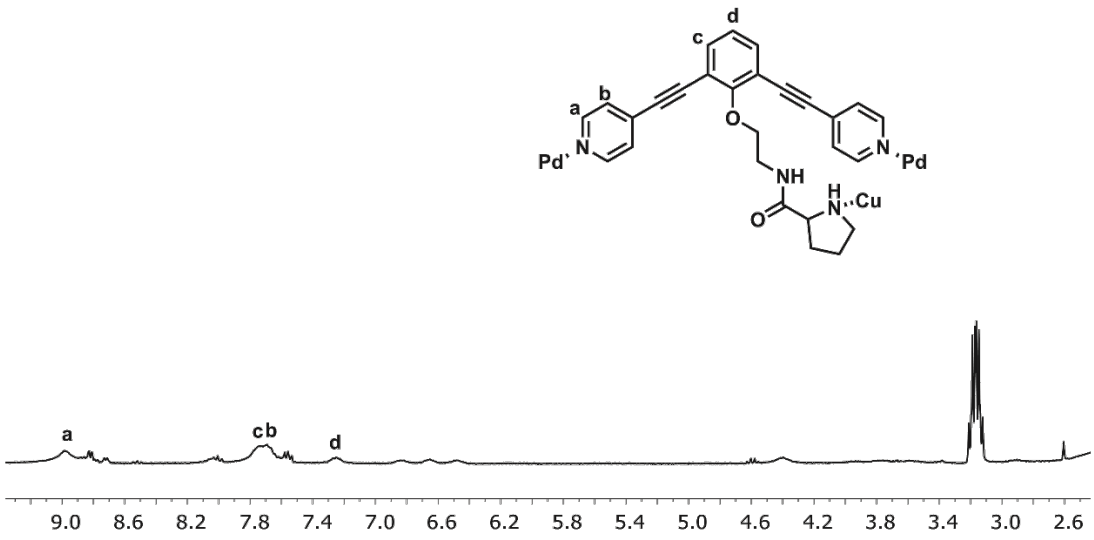

Figure S72. $[Pd_{12}\mathbf{L^{Pro}}_{24}Cu_8]$ assembly, ^{1}H NMR in MeCN-d_3.

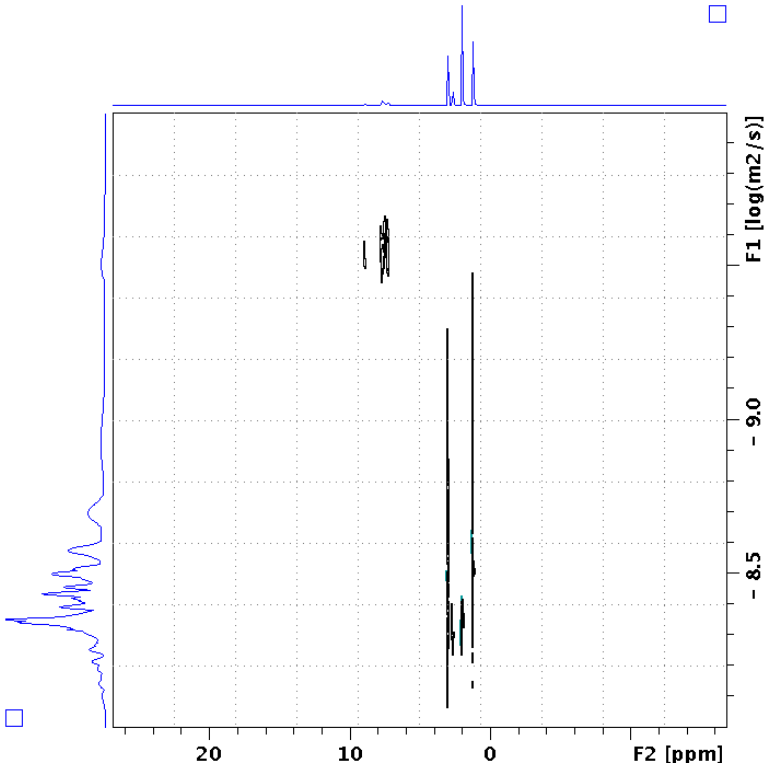

Figure S73. $[Pd_{12}\mathbf{L^{Pro}}_{24}Cu_8]$ assembly, DOSY NMR in MeCN-d_3 at 300K.

$\underline{Pd_{12}\mathbf{L}^{\mathbf{NMe}}{}_{24}+Ni}$

According to the general procedure, 2 mg (5 μmol) $Ni(BF_4)_2(MeCN)_4$ were utilized for the post-modification of the self-assembly. ^1H NMR and DOSY displayed intact self-assembly. MS analysis only revealed signals corresponding to the sphere with protonated and deprotonated building blocks. No in cooperation of nickel was observed *via* MS.

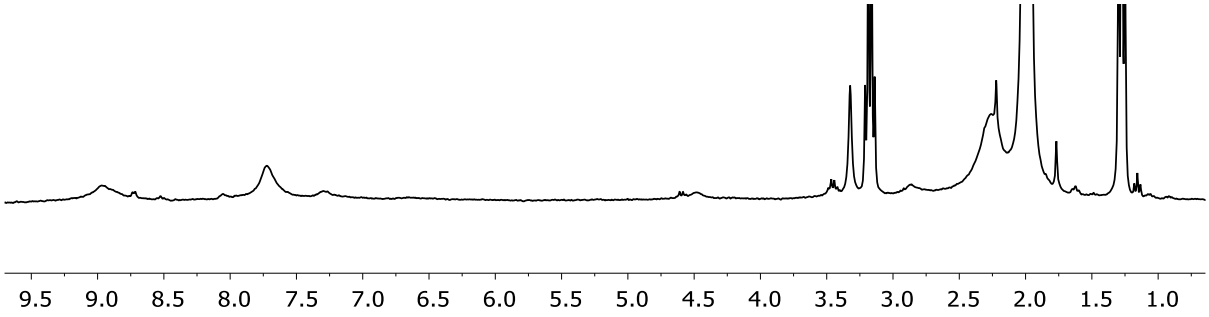

Figure S74. $[Pd_{12}\mathbf{L}^{\mathbf{NMeH}}{}_{24}]$ assembly with added nickel precursor and base, ^1H NMR in MeCN-d_3.

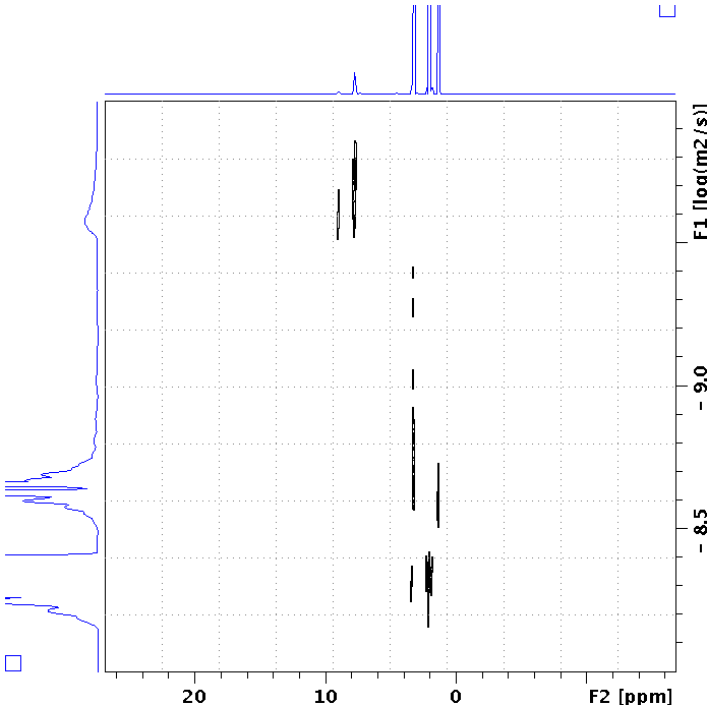

Figure S75. $[Pd_{12}\mathbf{L}^{\mathbf{NMe}}{}_{24}]$+ Ni^{II} assembly, DOSY NMR in MeCN-d_3 at 300K.

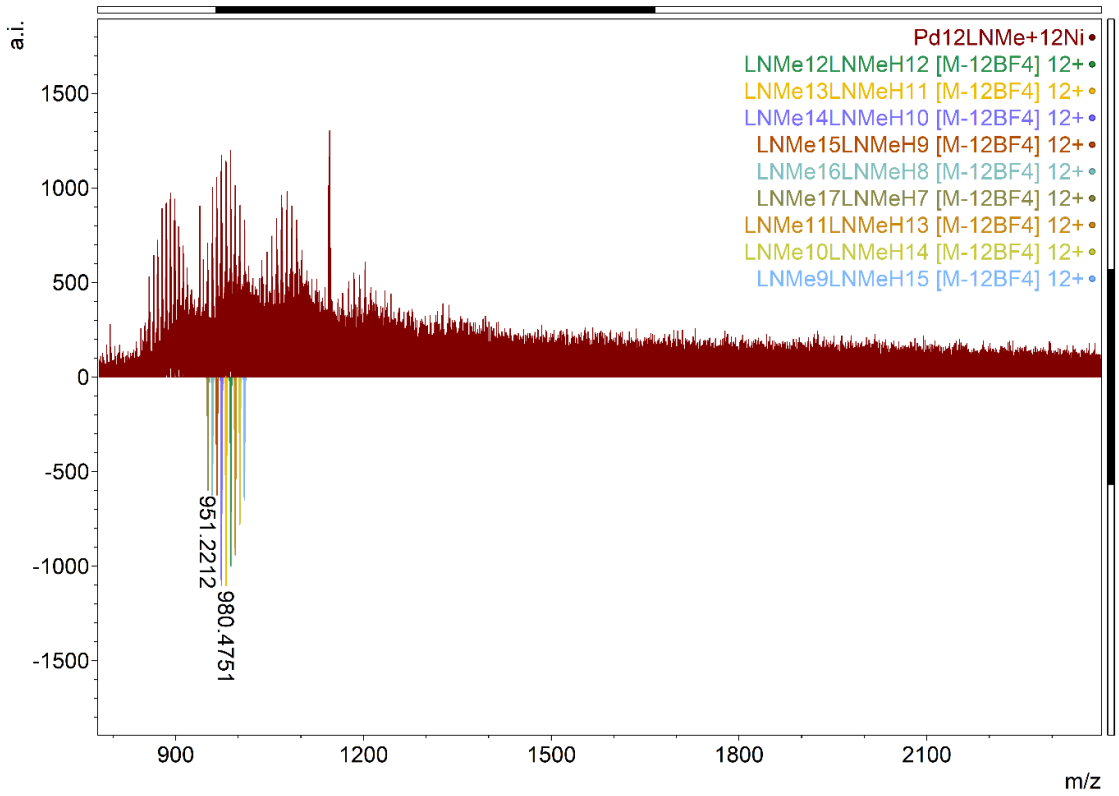

Figure S76. $[Pd_{12}L^{NMeH}{}_{24}]$ assembly with added nickel precursor and base, full HR-ESI MS spectrum, top measured; bottom, simulated spectra of different charged states of the self-assembly. Only signals corresponding to the protonated and deprotonated form of the ligand were detected. No nickel coordination was observed based on MS studies.

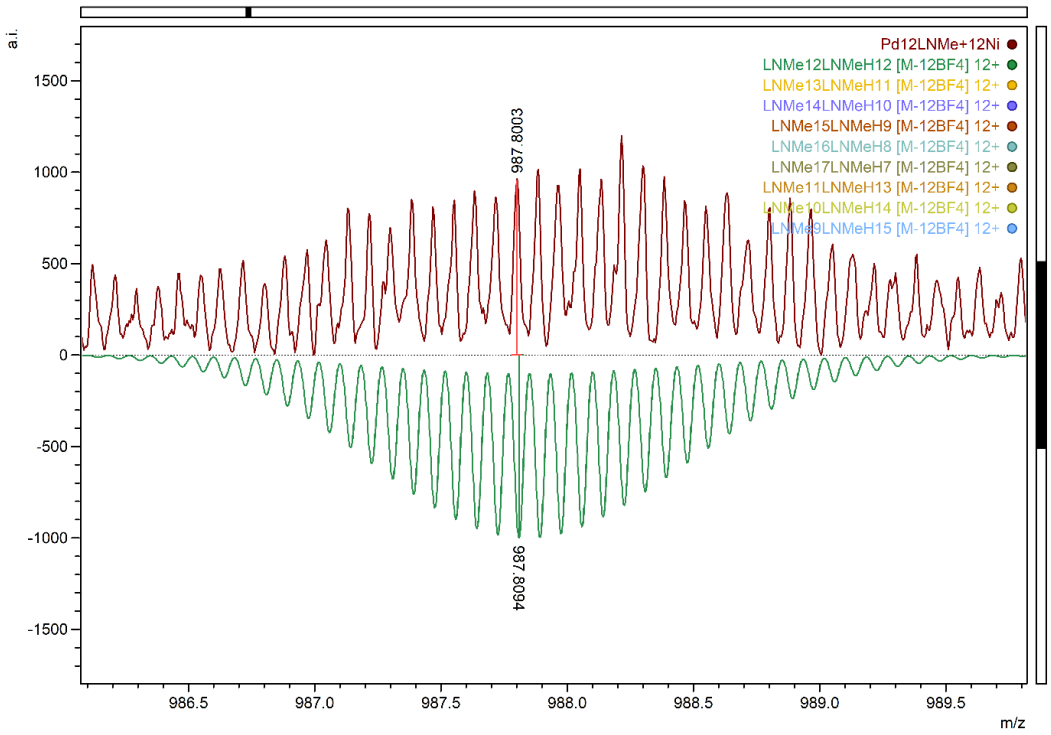

Figure S77. Zoom into $[Pd_{12}L^{NMe}{}_{12}L^{NMeH}{}_{12}]^{12+}$ species, bottom simulated spectra, top obtained.

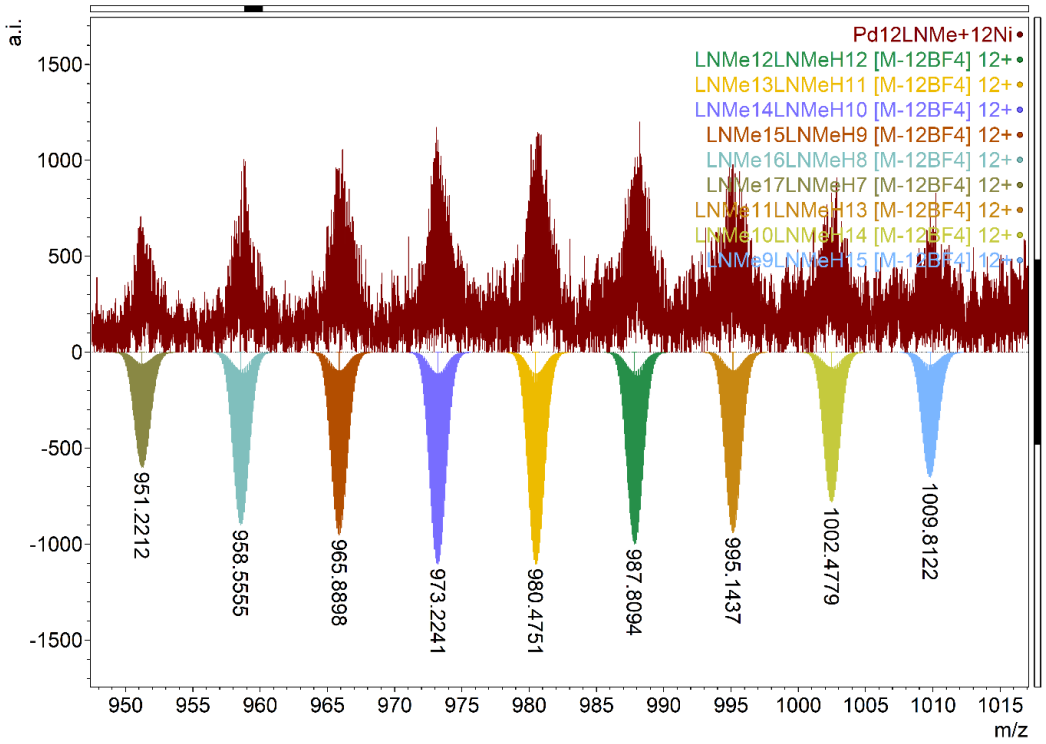

Figure S78. Zoom into $[Pd_{12}\mathbf{L}^{\mathbf{NMe}}{}_{x}\mathbf{L}^{\mathbf{NMeH}}{}_{y}]^{12+}$ species, bottom simulated spectra, top obtained, showing a distribution of building blocks being protonated and deprotonated within the assembly.

Trimetallic $Pd_{12}\mathbf{L}^{\mathbf{DMAP}}{}_{24}Ni_nCd_{6-n}$ for n = 0-4

According to the general procedure, 0.5 mg (1.3 µmol) $Ni(OTf)_2$ and 0.6 mg (1.3 µmol) $Cd(OTf)_2$ were added to a solution of 1 mL (correspond to 10 µmol $\mathbf{L}^{\mathbf{DMAPH}}$) $Pd_{12}\mathbf{L}^{\mathbf{DMAPH}}{}_{24}$ at -36°C and stirred for 15 minutes. To the cold solution, 2 ml (13 mmol) triethylamine was added and the solution was stirred at -36°C for 30 minutes and at room temperature for 1 h before being analyzed. MS analysis only revealed signals corresponding to the sphere with 6 M2 (M2 being Cd and Ni). Cd and Ni show a statistical distribution with favour towards more Cd incorporation (which is anticipated due to the low solubility of $Ni(OTf)_2$ in MeCN). Although further optimization is required for the incorporation of different metals into the nanosphere, this experiment demonstrates that it is possible. ^{1}H NMR (300 MHz, Acetonitrile-d_3) δ 9.08 (s_{br}, 4H), 8.60 (s_{br}, 1H), 8.19 (s_{br}, 1H), 7.88 – 7.49 (m, 7H), 7.39 (s_{br}, J = 5.8 Hz, 1H), 7.26 (s_{br}, 1H), 6.76 (s_{br}, 2H).

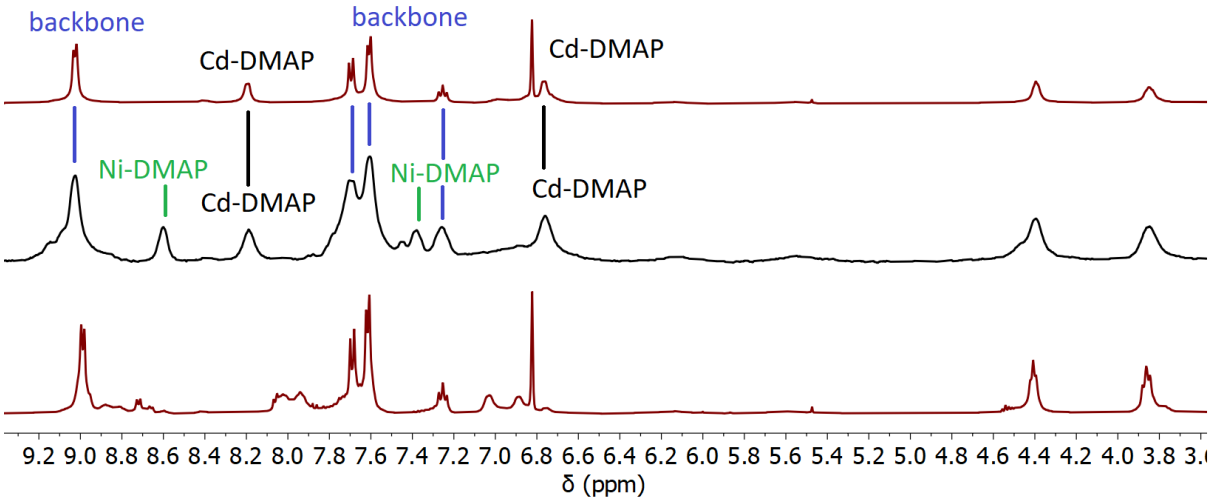

Figure S79. $[Pd_{12}\mathbf{L}^{\mathbf{DMAPH}}{}_{24}]$ nanosphere (bottom), $[Pd_{12}\mathbf{L}^{\mathbf{DMAP}}{}_{24}Cd_6]$ nanosphere (top) and mixed metal $[Pd_{12}\mathbf{L}^{\mathbf{DMAP}}{}_{24}Cd_{6-n}Ni_n]$ (for n = 0-4) with annotation of the NMR signals, ^{1}H NMR in MeCN-d_3.

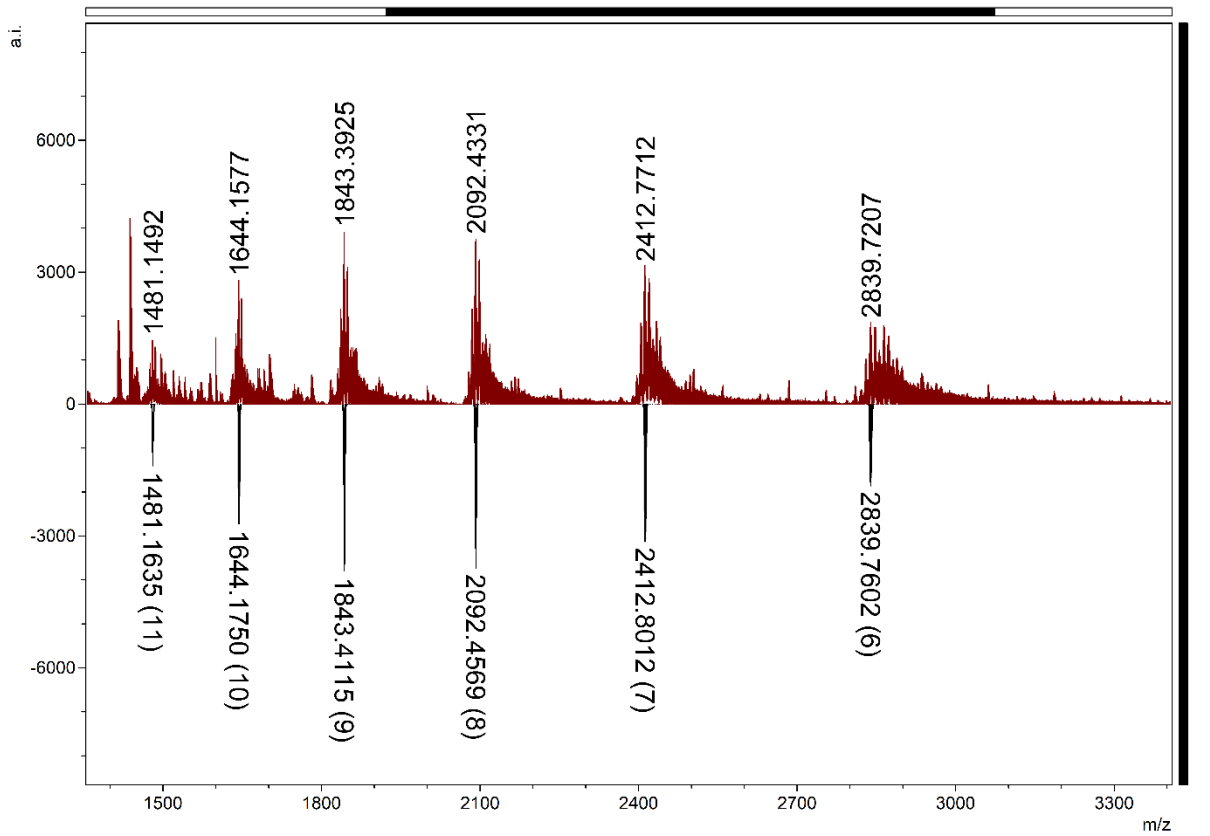

Figure S80. $[Pd_{12}\mathbf{L}^{\mathbf{DMAP}}{}_{24}Cd_{6-n}Ni_n]$ (for n = 0-4) assembly, full HR-ESI MS spectrum, top measured; bottom, simulated spectra of different charged states of the self-assembly for n = 1 (i.e., 1 Ni and 5 Cd).

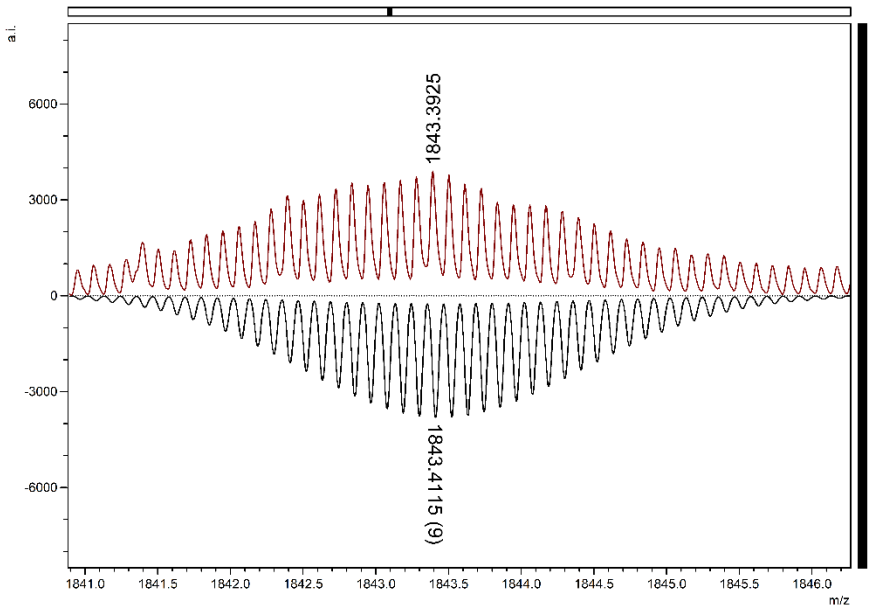

Figure S81. Zoom into $[Pd_{12}\mathbf{L}^{\mathbf{DMAP}}{}_{24}Cd_5Ni_1]^{9+}$ species, bottom simulated spectra, top obtained.

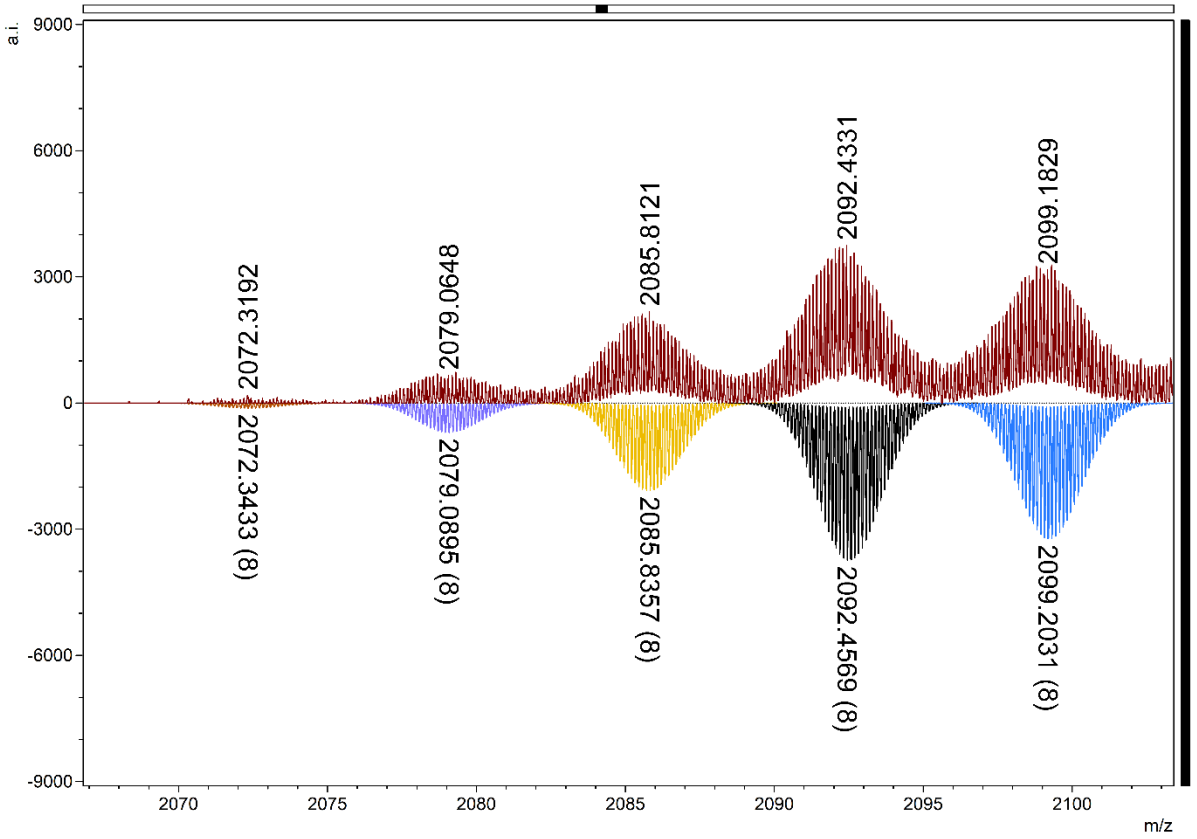

Figure S82. Zoom into $[Pd_{12}\mathbf{L}^{\mathbf{DMAP}}{}_{24}Cd_{6-n}Ni_n]^{8+}$ species, bottom simulated spectra, top obtained, showing a distribution of different amounts of Ni and Cd in the nanosphere (for: Cd_6Ni_0 (light blue); Cd_5Ni_1 (black); Cd_4Ni_2 (yellow); Cd_3Ni_3 (purple) and Cd_2Ni_4 (brown)).

CW-EPR measurements (SI4)

MWFQ	**9.6501 GHz**
CenterField	**3300.00 G**
SweepWidth	**2000 G**
SweepTime	**120 s**
Timeconst	**0.01 ms**
PowerAtten	**15.0 dB**
ModAmp	**8.000 G**

The CW X-band EPR spectrum was recorded at 70K in a 3:1 n-butylnitrile : acetonitrile glass, displaying an characteristic axial Cu^{II} spectrum. Using the EasySpin software program package, simulation of the observed spectrum of $[Pd_{12}\mathbf{L}^{\mathbf{Pro}}{}_{24}Cu_8]$ to a S=1/2 system provided the nearly axial g tensor = [2.26 2.053 2.049], with a resolved copper hyperfine coupling of A^{Cu}=507 MHz to the axial component. Simulation of the observed spectrum of $[Pd_{12}\mathbf{L}^{\mathbf{DMAP}}{}_{24}Cu_6]$ to a S=1/2 system similarly provides an identical nearly axial g tensor = [2.26 2.053 2.049] and a resolved copper hyperfine coupling of A^{Cu}=537 MHz to the axial component, and also superhyperfine coupling to four nitrogen atoms with A^{N}=43 MHz to the non-axial component.

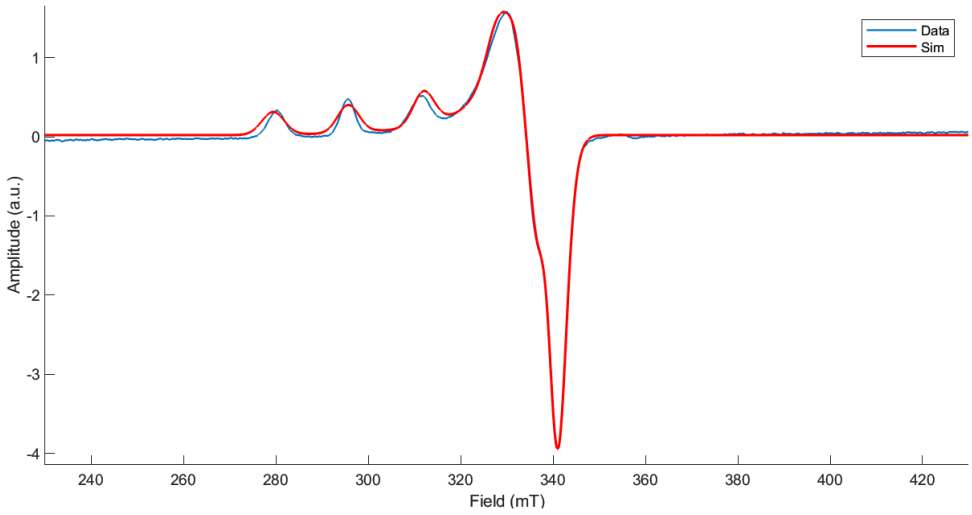

Figure S83. EPR spectrum of $[Pd_{12}\mathbf{L}^{\mathbf{Pro}}{}_{24}Cu_8]$ (blue) and simulated spectrum (red).

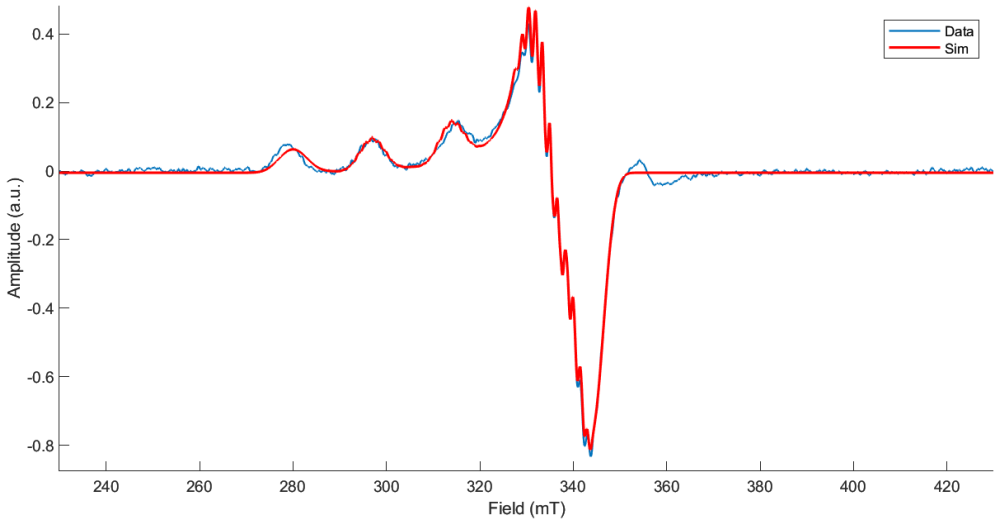

Figure S84. EPR spectrum of [$Pd_{12}\mathbf{L}^{\mathbf{DMAP}}{}_{24}Cu_6$] (blue) and simulated spectrum (red).

Pulse EPR (SI5)

Pulsed EPR measurements were performed at 9 GHz on an Elexsys E680 spectrometer (Bruker) using a 3 mm ER 4118 X-MD-3-W1 splitring resonator. The cryogenic temperature was obtained with helium gas in a CF935 (Oxford Instruments) cryostat with an ITC502 temperature controller (Oxford Instruments). Samples were prepared in 3 mm outer-diameter quartz tubes and frozen and stored in liquid nitrogen before insertion into the precooled helium gas-flow cryostat.

PARAMETERS FOR RELAXATION MEASUREMENTS

The T_m relaxation was measured with the two-pulse sequence $(\pi/2)$-τ- (π)- τ-[echo] with an initial τ of 200 ns and 4 ns step increments. The T_1 relaxation was measured with the inversion-recovery sequence (π)- T-$(\pi/2)$-τ- (π)- τ-[echo]. The τ values was kept constant at 200 ns, starting T value was 400 ns with 40 ns step increments. 16 ns length for $\pi/2$ pulses and 32ns for π pulses were used. The T_m and T_2 time constants were obtained through exponential fitting.

PARAMETERS FOR DEER EXPERIMENTS

The four-pulse DEER [6, 7] sequence $(\pi/2)_1$-τ_1- $(\pi)_1$–$(\tau_1 + t)$-$(\pi)_2$–$(\tau_2$-$t)$-$(\pi)_1$–τ_2-[echo] was employed, where subscripts 1 and 2 indicate events occurring at the observer and pump frequency, respectively. The pump and observer frequencies were separated by 75 MHz. The power of the pump pulse was adjusted to invert the echo maximally. The lengths of the pulses at the observer frequency were 16 and 32 ns for the π /2 and π pulses,

respectively. The length of the pump pulse was 16 ns. In the measurements the τ time was incremented with 8 ns steps starting at τ = 140 ns to suppress nuclear modulation. The slices were added to obtain hyperfine-modulation-free time traces and phase corrected.

The DEER data were analyzed using the DeerAnalysis2019 program [8], which is available from http://www.epr.ethz.ch/ software/index. Contribution of a known instrumentation artifact at 1940 ns could not be completely eliminated from the real part, therefore all traces were truncated to 1932 ns. Zero time of the traces was 88 ns. After background correction of the data using a three-dimensional background, the distance distribution was determined by Tikhonov regularization, with a regularization parameter of 125. The validation was performed using the validation tool in DeerAnalysis. For $Pd_{12}Cu_6\mathbf{L}^{\mathbf{DMAP}}{}_{24}$ the white-noise contribution was varied between 0.02 and 1.5 with 10 steps, and the background start from 372 ns to 1000 ns with 20 steps. For $Pd_{12}Cu_8\mathbf{L}^{\mathbf{Pro}}{}_{24}$ the white-noise contribution was varied between 0.03 and 1.5 with 10 steps, and the background start from 232 ns to 612 ns with 20 steps. The shaded areas in the distance distribution plots show, for a given distance, the lower and upper error bounds (two times the standard deviation) calculated over all the validation steps. The modulation depth was around 20 %. This depth is relatively large compared to conventional 9 GHz DEER of Cu(II)-Cu(II) interactions [9, 10] where modulation depths up to 14 % are reported. As modulation depths are strongly dependent on instrumentation and pulse parameters, e.g. [11], for a proper interpretation of the modulation depth, reference measurements of genuine two Cu(II)-systems would be needed, which we plan in the future. As only one spectral position was probed, possible effects of orientation selection cannot be assessed.

DEER RESULTS

The DEER experiments were performed with the pump pulse at the maximum of the EPR spectrum and the observer pulse displaced towards lower fields, see insert Fig. S85. The total evolution time was limited by the short phase memory times of these samples, see Table S25. Both traces in Fig. S85 a have a fast initial decay, suggesting short distances around 2 nm. In the trace of $Pd_{12}Cu_6\mathbf{L}^{\mathbf{DMAP}}{}_{24}$, a modulation is visible with a maximum at 360 ns. The modulation depth is around 20 % for both complexes, see Table S25. The traces have been processed as reported in "SI5 – Parameters for DEER Experiments". Superposition of the two raw DEER traces shows that they differ from each other.

The traces are analyzed using DeerAnalysis, see details in "SI5 – Parameters for DEER Experiments", assuming that they derive from spin-pair interactions, thus neglecting the influence of possible multi-spin interactions in these complexes. Below we show that the influence of such multi-spin effects is expected to be small for our system.

Fig. S85c shows that $Pd_{12}Cu_6\mathbf{L}^{\mathbf{DMAP}}{}_{24}$ has two distances. A shorter distance, r_1, at 1.9 nm and a longer one, r_2, at 2.5 nm (Table. S26). The intensity of the peak at r_2 is smaller than

that of r_1. Validation with DeerAnalysis (Fig. S85c) shows that both peaks are significant, because also the peak at 2.5 nm is visible for the entire confidence range.

The distance distribution of $Pd_{12}Cu_8\mathbf{L^{Pro}}_{24}$ (Fig. S85d) has one broad peak centered at 1.8 nm, with a tail in the distribution that extends to approximately 3 nm. Because of the short evolution times, that derive from the short T_m times in these complexes (see Table S25), for distances above 2.8 nm the shape of features in the distance distribution is not reliable [8, 12]. This is particularly evident for $Pd_{12}Cu_8\mathbf{L^{Pro}}_{24}$, where a broad distribution of distances seems to extend from 2.2 nm to longer distances, although validation shows that this part if the distance distribution is non reliable.

DISTANCES

In Table S25, the observed distances are compared to those expected from PM3 modeling of the structure of $Pd_{12}Cu_6\mathbf{L^{DMAP}}_{24}$ and $Pd_{12}Cu_8\mathbf{L^{Pro}}_{24}$. For $Pd_{12}Cu_6\mathbf{L^{DMAP}}_{24}$, the observed distances match the ones from the PM3 model (see main text). For $Pd_{12}Cu_8\mathbf{L^{Pro}}_{24}$, in addition to a distance of 2.0 nm (expected), 1.8 nm (observed), also two longer distances at 2.8 and 3.4 nm are expected. Although the distribution (Fig. S85d) shows some intensity in this distance region, such distances cannot be reliably determined, given the short evolution time of the DEER traces. Also, given the width of the experimental distance-distribution peaks it is likely that the two distances (2.8 and 3.4 nm) overlap as one broad peak, making the detection even more difficult. We therefore consider that the distance distributions are consistent with the expectations from the model.

OVERVIEW OF ARRANGEMENT OF CU IONS IN $Pd_{12}Cu_6\mathbf{L^{DMAP}}_{24}$ AND $Pd_{12}Cu_8\mathbf{L^{Pro}}_{24}$

For the $Pd_{12}Cu_8\mathbf{L^{Pro}}_{24}$ complex, the relative arrangement of the Cu(II) ions can be visualized as a cube, Fig. S87. In $Pd_{12}Cu_8\mathbf{L^{Pro}}_{24}$, each Cu ion has three neighboring Cu ions at a distance r_1, the edges of the cube, three along the diagonal of the faces (r_2) and one along the space diagonal (r_3). The pairwise interactions should therefore occur as 3:3:1 in intensity for the distances r_1, r_2 and r_3 respectively. Table S26 gives these distances for the PM3 model of the complexes. For the $Pd_{12}Cu_6\mathbf{L^{DMAP}}_{24}$ complex, the Cu(II) ions form a regular octahedron, with four pairwise interactions along the edges and another along the diagonal with an expected ratio of 4:1 in the distance distribution, Fig. S87. Comparison with the distance distributions (Fig. S85 c and d) shows that for $Pd_{12}Cu_6\mathbf{L^{DMAP}}_{24}$ indeed the peak at r_1 has a higher intensity than the peak at r_2, however, less than the ratio of 4:1 suggests. For In $Pd_{12}Cu_8\mathbf{L^{Pro}}_{24}$, the two longer distances are in the range that is difficult to detect given the evolution times, but they may explain the broad tail of the main peak in Fig. S85d.

MULTISPIN INTERACTIONS

In principle, all Cu(II) spins in the complex, i.e. six in $Pd_{12}Cu_6\mathbf{L}^{\mathbf{DMAP}}{}_{24}$ and eight in $Pd_{12}Cu_8\mathbf{L}^{\mathbf{Pro}}{}_{24}$, could contribute to the sum/difference-combination frequencies that have been described for DEER on multi-spin systems before [13, 14], because all their respective distances are within the sensitive range of the DEER experiment as performed here. Interpretation of such combination frequencies as pair distances could lead to "ghost peaks" in the distance distributions. Jeschke et al. [13] showed that the excitation of combination frequencies scales with the modulation depth. Most of the cases analyzed for multi-spin effects refers to nitroxide-based systems, where multi-spin effects are expected to be stronger than for Cu(II)[15, 16]. For Cu(II)-Cu(II) interactions, the modulation depth is intrinsically smaller than for nitroxides because of the broader width of the Cu(II) EPR spectrum, leading to less prominent ghost features for Cu(II).

To test for possible ghost features, we used the ghost suppression tool in DEER analysis. Fig. S86 shows distance distributions for different numbers of interacting spins. Suppression is performed for three to six spins ($Pd_{12}Cu_6\mathbf{L}^{\mathbf{DMAP}}{}_{24}$) and three to eight spins ($Pd_{12}Cu_8\mathbf{L}^{\mathbf{Pro}}{}_{24}$). The relative distance-peak intensity changes only slightly with respect to the pair interactions, suggesting that the distributions are dominated by pairwise interactions.

Table S25. Measured relaxation time constants, and modulation depth (Δ) in DEER experiments for $Pd_{12}Cu_6\mathbf{L}^{\mathbf{DMAP}}{}_{24}$ and $Pd_{12}Cu_8\mathbf{L}^{\mathbf{Pro}}{}_{24}$. T_m: phase-memory time, T_1: spin-lattice-relaxation time. Relaxation times: Temperature 30 K.

	T_m (ns)	**T_1(µs)**	**Δ (%)**
$Pd_{12}Cu_6\mathbf{L}^{\mathbf{DMAP}}{}_{24}$	522 ± 11	8.7 ± 0.4	21 ± 3
$Pd_{12}Cu_8\mathbf{L}^{\mathbf{Pro}}{}_{24}$	302 ± 7	15.4 ± 0.5	18.5 ± 1.2

Table S26. Experimental and PM3 model-derived distance parameters obtained for $Pd_{12}Cu_6\mathbf{L}^{\mathbf{DMAP}}{}_{24}$ and $Pd_{12}Cu_8\mathbf{L}^{\mathbf{Pro}}{}_{24}$. The DEER data were analyzed by means of Tikhonov regularization. <r> is the center of the distance distribution in nm, S(r) the width.

$Pd_{12}Cu_6\mathbf{L}^{\mathbf{DMAP}}{}_{24}$ distances from DEER		**$Pd_{12}Cu_6\mathbf{L}^{\mathbf{DMAP}}{}_{24}$ MODEL**	**$Pd_{12}Cu_8\mathbf{L}^{\mathbf{Pro}}{}_{24}$d istances from DEER**		**$Pd_{12}Cu_8\mathbf{L}^{\mathbf{Pro}}{}_{24}$ MODEL**
<r> (nm)	S(r)	r (nm)	<r> (nm)	S(r)	r (nm)
1.9 2.5	0.18 0.12	1.9 2.7	1.8	0.18	2.0 2.8 3.4

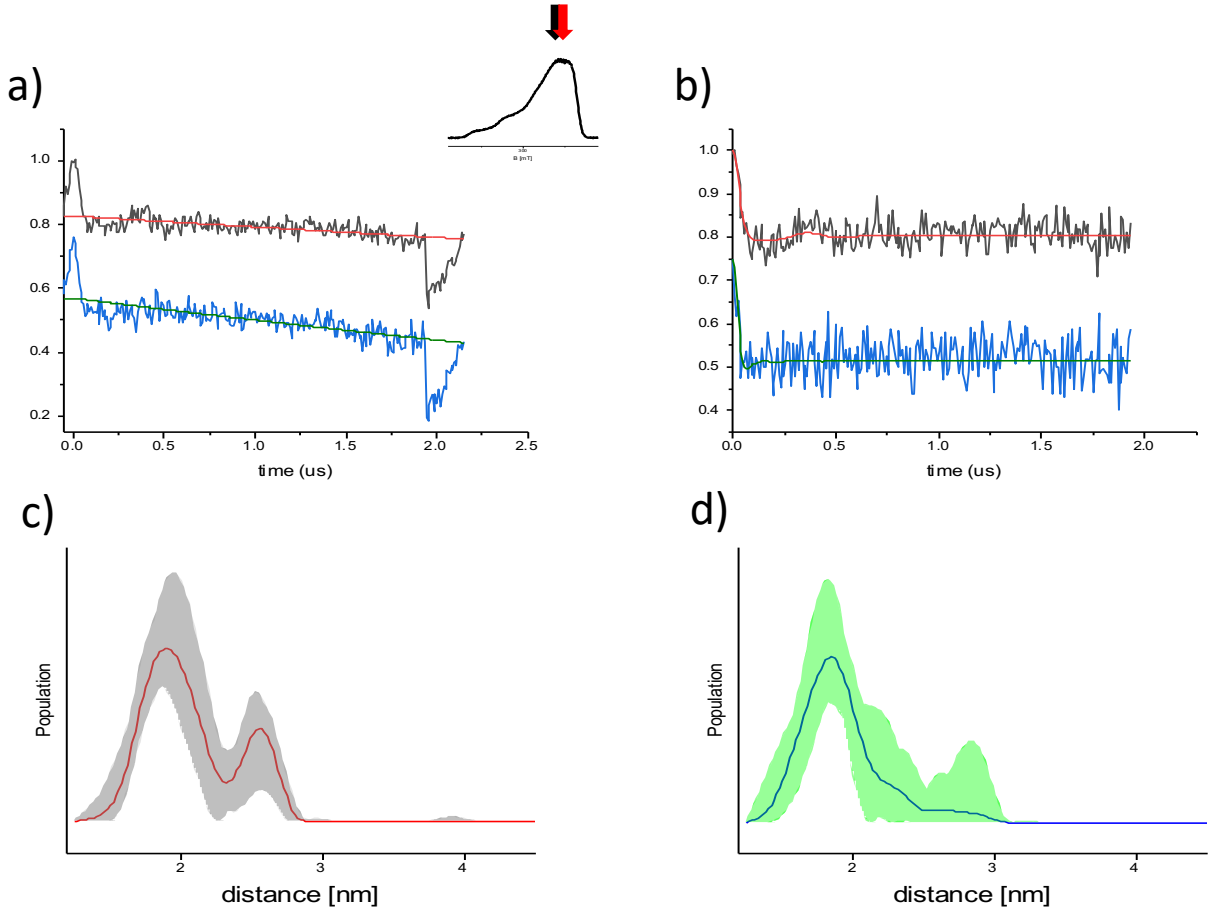

Figure S85. Determination of the distances between the copper ions in the $Pd_{12}Cu_6\mathbf{L}^{\mathbf{DMAP}}{}_{24}$ and $Pd_{12}Cu_8\mathbf{L}^{\mathbf{Pro}}{}_{24}$ complexes. (a) Experimental DEER traces and baseline, $Pd_{12}Cu_6\mathbf{L}^{\mathbf{DMAP}}{}_{24}$: black, baseline: red. $Pd_{12}Cu_8\mathbf{L}^{\mathbf{Pro}}{}_{24}$: blue, baseline: green. Inset: field swept echo EPR spectrum of $Pd_{12}Cu_6\mathbf{L}^{\mathbf{DMAP}}{}_{24}$. Arrows indicate position of pump (red) and observer (black) pulses. (b) Background corrected traces with fits, corresponding to distance distributions (c and d). $Pd_{12}Cu_6\mathbf{L}^{\mathbf{DMAP}}{}_{24}$ trace: black, fit: red. $Pd_{12}Cu_8\mathbf{L}^{\mathbf{Pro}}{}_{24}$ trace: blue, fit: green. Distance distributions for $Pd_{12}Cu_6\mathbf{L}^{\mathbf{DMAP}}{}_{24}$ (c) and $Pd_{12}Cu_8\mathbf{L}^{\mathbf{Pro}}{}_{24}$ (d). DEER time traces (a, b) are normalized to 1 and $Pd_{12}Cu_8\mathbf{L}^{\mathbf{Pro}}{}_{24}$ traces are down-shifted for clarity. Accumulation time: 23 hours for $Pd_{12}Cu_6\mathbf{L}^{\mathbf{DMAP}}{}_{24}$; 17 hours for $Pd_{12}Cu_8\mathbf{L}^{\mathbf{Pro}}{}_{24}$. Temperature: 20K. Artifact at 1940 ns: see "S8 – Parameters for DEER Experiments".

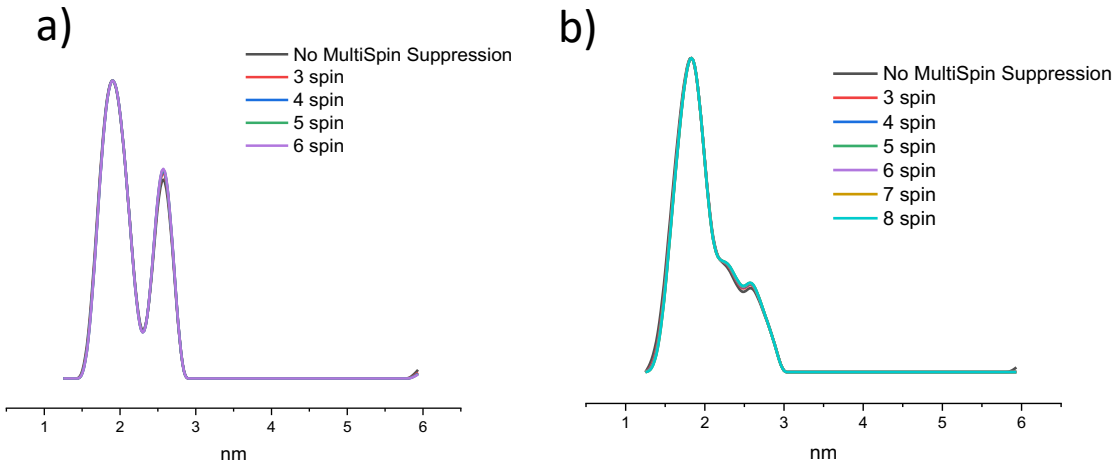

Figure S86. Effect of ghost suppression on the distance distributions. Number of spins: from 2 to the number of paramagnetic centers in the complexes, (a) 6 for for $Pd_{12}Cu_6\mathbf{L}^{\mathbf{DMAP}}{}_{24}$, (b) 8 for $Pd_{12}Cu_8\mathbf{L}^{\mathbf{Pro}}{}_{24}$. Plots are normalized to maximum.

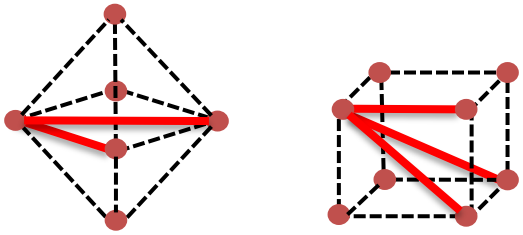

Figure S87. Sketch of relative positions of the copper ions in the $Pd_{12}Cu_6\mathbf{L}^{\mathbf{DMAP}}{}_{24}$ (left) and $Pd_{12}Cu_8\mathbf{L}^{\mathbf{Pro}}{}_{24}$ (right) complexes. $Pd_{12}Cu_6\mathbf{L}^{\mathbf{DMAP}}{}_{24}$: regular octahedron, 4 shorter distances and a longer one. $Pd_{12}Cu_8\mathbf{L}^{\mathbf{Pro}}{}_{24}$: cube, 3 distances in 3:3:1 ratio.

References

[1] S. Stoll, A. Schweiger. EasySpin, a comprehensive software package for spectral simulation and analysis in EPR. *J. Magn. Reson.* **2006**, 178, 42–55.

[2] Thomas Casey (2021). cwEPR (https://www.mathworks.com/matlabcen-tral/fileexchange/73292-cwepr), MATLAB Central File Exchange.

[3] Zeneca Limited; Zeneca Pharma S. A., US6362336, 2002, B1, Location in patent: Example 48.

[4] C. Lang, X. Zhang, Q. Luo, Z. Dong, J. Xu, J. Liu, Eur. J. Org. Chem. 2015, 2015, 6458–6465.

[5] R. Zaffaroni, E. O. Bobylev, R. Plessius, J. I. van der Vlugt, J. N. H. Reek, J. Am. Chem. Soc. 2020, 142, 8837–8847.

[6] M. Pannier, S. Veit, A. Godt, G. Jeschke, H.W. Spiess, 2000, J Magn Reson, 213 (2011) 316-325.

[7] M.P. Rainer E. Martin, François Diederich, Volker Gramlich, Michael Hubrich, and Hans W. Spiess, Angew. Chem. Int. Ed. Engl., 37 (1998) 2834 - 2837.

[8] G. Jeschke, P. Ionita, A. Godt, H. Zimmermann, J. Banham, C. R. Timmel, D. Hilger, and H. Jung, Applied Magnetic Resonance, 30 (2006) 473 - 498.

[9] F.D. Breitgoff, K. Keller, M. Qi, D. Klose, M. Yulikov, A. Godt, G. Jeschke, J Magn Reson, 308 (2019) 106560.

[10] S. Ghosh, M.J. Lawless, H.J. Brubaker, K. Singewald, M.R. Kurpiewski, L. Jen-Jacobson, S. Saxena, Nucleic Acids Res, 48 (2020) e49.

[11] M.J. Lawless, J.L. Sarver, S. Saxena, Angew Chem Int Ed Engl, 56 (2017) 2115-2117.

[12] G. Jeschke, DeerAnalysis User Manual - Version 2019, (2019).

[13] T. von Hagens, Y. Polyhach, M. Sajid, A. Godt, G. Jeschke, Phys Chem Chem Phys, 15 (2013) 5854-5866.

[14] G. Jeschke, Miriam Schulteb and Adelheid Godt, Phys Chem Chem Phys, 11 (2009) 6580-6591.

[15] D.T. Edwards, T. Huber, S. Hussain, K.M. Stone, M. Kinnebrew, I. Kaminker, E. Matalon, M.S. Sherwin, D. Goldfarb, S. Han, Structure, 22 (2014) 1677-1686.

[16] A. Meyer, D. Abdullin, G. Schnakenburg, O. Schiemann, Single and double nitroxide labeled bis(terpyridine)-copper(II): influence of orientation selectivity and multispin effects on PELDOR and RIDME, Phys Chem Chem Phys, 18 (2016) 9262-9271.